CRANFIELD INSTITUTE OF TECHNOLOGY

RADIAL INFLOW TURBINE STUDY

FINAL REPORT

by

Dr S Hamid
Prof R L Elder

JULY 1992

United States Army
EUROPEAN RESEARCH OFFICE OF THE US ARMY
London England

CONTRACT NUMBER: DAJA45-89-C-0006
CRANFIELD REFERENCE: 06/769E

PROJECT START DATE: 1st January 1989
PROJECT COMPLETION DATE: 30th June 1992

Department of Turbomachinery & Engineering Mechanics
School of Mechanical Engineering
Cranfield Institute of Technology
Cranfield, Bedford, MK43 0AL

DAJA45-89-C-0006
ATTACHMENT #1

SECURITY CLASSIFICATION OF THIS PAGE

REPORT DOCUMENTATION PAGE

Form Approved
OMB No. 0704-0188

1a. REPORT SECURITY CLASSIFICATION: Unclassified	1b. RESTRICTIVE MARKINGS
2a. SECURITY CLASSIFICATION AUTHORITY	3. DISTRIBUTION/AVAILABILITY OF REPORT: Distribution unlimited
2b. DECLASSIFICATION/DOWNGRADING SCHEDULE	
4. PERFORMING ORGANIZATION REPORT NUMBER(S): 06/769 - final	5. MONITORING ORGANIZATION REPORT NUMBER(S)
6a. NAME OF PERFORMING ORGANIZATION: Cranfield Institute of Technology; 6b. OFFICE SYMBOL (If applicable)	7a. NAME OF MONITORING ORGANIZATION: European Research Office
6c. ADDRESS (City, State, and ZIP Code): Cranfield, Bedford, MK43 OAL	7b. ADDRESS (City, State, and ZIP Code): 223 Old Marylebone London NW1 5TH
8a. NAME OF FUNDING/SPONSORING ORGANIZATION: USACCE - RCO Burtonwood; 8b. OFFICE SYMBOL (If applicable)	9. PROCUREMENT INSTRUMENT IDENTIFICATION NUMBER: R & D 5824-AN-01
8c. ADDRESS (City, State, and ZIP Code): HQ 47th Area Support Group Burtonwood Road, Great Sankey Warrington, Cheshire, WA5 1UN	10. SOURCE OF FUNDING NUMBERS: PROGRAM ELEMENT NO. / PROJECT NO. / TASK NO. / WORK UNIT ACCESSION NO.

11. TITLE (Include Security Classification): Radial Inflow Turbine Study

12. PERSONAL AUTHOR(S): Dr S Hamid - Professor R L Elder

13a. TYPE OF REPORT	13b. TIME COVERED	14. DATE OF REPORT (Year, Month, Day)	15. PAGE COUNT
FINAL	FROM 1.3.92 TO 30.6.92	July 1992	120

16. SUPPLEMENTARY NOTATION: R7-8.43/IH

COSATI CODES		
FIELD	GROUP	SUB-GROUP

18. SUBJECT TERMS (Continue on reverse if necessary and identify by block number): Radial Turbines; Laser Anemometry

19. ABSTRACT (Continue on reverse if necessary and identify by block number)

This document gives the final report on the project - see attached.

20. DISTRIBUTION/AVAILABILITY OF ABSTRACT ☐ UNCLASSIFIED/UNLIMITED ☐ SAME AS RPT ☐ DTIC USERS	21. ABSTRACT SECURITY CLASSIFICATION
22a. NAME OF RESPONSIBLE INDIVIDUAL	22b. TELEPHONE (Include Area Code) / 22c. OFFICE SYMBOL

DD Form 1473, JUN 86 — Previous editions are obsolete. — SECURITY CLASSIFICATION OF THIS PAGE

ABSTRACT

Small radial inflow turbines have various applications in industry and are successfully being used as a major component of gas turbines and turbochargers. The performance of the turbine is of great importance for the success of these systems. Although the design of radial inflow turbines has improved in the last few years, the detailed aerodynamic study of these components still needs considerable attention. Better understanding of the flow processes involved in these machines will provide a good basis for the design of improved components and for this purpose a joint research programme has been undertaken by Cranfield, the US Army Research Office and Turbomach (San Diego).

The main objective of the study was to investigate the flow processes involved in the radial inflow turbine using experimental methods. The work presented in this report describes the various steps undertaken to perform these studies together with results. The project involved two phases, the first measurements downstream of the rotor and the second measurements between the nozzle guide vanes and rotor inlet. The scope of the study was limited to two man years during which considerable success was achieved in obtaining the desired measurement but more time to further reduce this data and to compare with computational results, which was outside the scope of the present study, would have been advantageous.

The studies using laser anemometry undertaken downstream of the turbine rotor indicated a swirling flow with a region of counter-rotating flow in the centre. A cobra probe was used to compare with the laser anemometry results. Both measuring techniques show similar trends of flow velocity and flow angle at various running conditions. The extent of the region of counter-rotating flow increase with decreasing flow coefficient and was more confined closer to the turbine rotor trailing edge. A strobing unit was used to examine the extent of blade passing effect on the flow at the window located closest to the rotor trailing edge. No noticeable effect could be observed indicating mixing was complete at this station.

Studies upstream of the rotor inlet (again using laser anemometry) showed a largely two-dimensional flow in the area between the nozzle guide vanes and rotor. Strobing was again undertaken to observe the blade passing effect on the flow conditions. Results show that there was hardly any unsteadiness in the flow caused by the passing blades at these positions. Interestingly, this contrasts with similar measurements made on another turbine studied.

The results of this study are velocity measurements obtained from the small internal passages of a high speed turbine. Some conclusions such as those reported are immediately possible but further consideration should be undertaken by comparing results with computations which were outside the scope of this project.

INTRODUCTION

1.1 Radial Inflow Turbine

Small radial inflow turbines have various applications in industry and are successfully being used as a major component of gas turbines and turbochargers. The performance of the turbine is of great importance for the success of these systems. Although the design of radial inflow turbines has improved in the last few years, the detailed aerodynamic study of these components still needs considerable attention. Better understanding of the flow processes involved in these machines will provide a good basis for the design of improved components and for this purpose a joint research programme has been undertaken by Cranfield, the US Army Research Office and Turbomach (San Diego).

1.2 Objectives of the Present Research

The main objective of the study was to investigate the flow processes involved in the radial inflow turbine using experimental methods. The work presented in this report describes the various steps undertaken to perform these studies which were completed in two phases as described below. The scope of the study was limited to two man years during which considerable success was achieved in obtaining the desired measurement but more time to further reduce this data and to compare with computational results, which was outside the scope of the present study, would have been advantageous.

Phase 1 : Flow studies downstream of the turbine rotor

The flow downstream of the rotor (rotor exhaust) has been investigated where the turning of the flow from radial to axial (and the strong inertial forces introduced) has been noted to complicate the flow. Complex mixing processes which occur downstream of the rotor are ill defined and it was proposed to investigate the flow at two different downstream positions. These investigations were undertaken using laser anemometry techniques which are described in Section 5. In addition, conventional measurements with a cobra yawmeter probe were made which could be compared with the laser anemometry results at some locations.

Phase 2 : Flow studies between the nozzle guide vanes and the turbine inlet

The flow has been investigated in the region between the nozzle vanes and the turbine rotor inlet. Uncertainties exist regarding the operation of the guide vanes in this environment and the interaction of rotor and guide vane flow.

2. HARDWARE

Turbomach (San Diego) participated in the programme by providing rig hardware including a rotating assembly, bearing housing, nozzle guide vanes and turbine inlet. The turbine rotor had 16 blades and 19 nozzle guide vanes (no exit guide vanes). Cranfield modified an existing test rig stand onto which this unit was mounted. Details of the rig are provided schematically in fig 1 and pictorially in Plate A. An extensive range of specialist equipment was employed to support the experimental work.

The turbine was powered by plant air compressors from the Department's air plant. The installation included the design and manufacture of an ejector at the outlet of the turbine which was used to reduce the turbine operating density and the braking power required to better match the turbine with the compressor brake. The details of the ejector design have been included in Appendix A.

3. TEST RIG INSTRUMENTATION

Fig 1 gives the details of the instrumented turbine in the test cell. Mass flow information was obtained from the two venturitubes positioned upstream of the turbine inlet. Valves V_1, V_2, V_3, V_4 and V_5 were used to control the range of operating conditions of the machine.

The following instrumentation at the various stations shown in fig 1 were used:

Station 1 - inlet total pressure and temperature
Station 2 - outlet total pressure and temperature
Station 3 - venturi differentials to provide turbine flow
Station 4 - two thermocouples for turbine mass flow measurement

The turbine test cell data collection scheme is shown schematically in fig 2. Located in the control area are the different valves throttle controls and data acquisition system. The turbine performance was continuously monitored and updated on a display monitor. Values for pressures and temperatures at different stations were logged by the rig computer and a programme developed to calculate the desired operating parameters for the turbine. Appendix B gives the details and definition of various parameters used in the program together with an outline of its operation.

After the test rig was installed and the instrumentation completed, the turbine unit was tested. Plate A shows the fully instrumented unit mounted on the test rig. During the initial phase the turbine unit was run for fixed speeds and the turbine flow rate controlled by bleeding flow off upstream of the rig and diverting flow between the turbine and ejector, fig 1.

Variation in the pressure ratio across the turbine was mapped against corrected mass flow using the program described above. Initial results obtained for various speeds were compared with the test running points obtained from the data sheets provided by Turbomach and it was found that the mass flow rate tended to be low. A detailed inspection of each component was carried out. Further investigation suggested that compressibility effects within the mass flow meter caused the problem. Correction of the formulae for these effects then provided good agreement. To simplify the problem, the two venturi mass flow meters were replaced by an orifice plate device which provided much less pressure loss.

4. RUNNING

The turbine was operated at different values of U/V and at different pressure ratios. Fig 3 shows the turbine performance at pressure ratios 3.0 and 3.5. Running conditions to carry out laser anemometry work were discussed with Turbomach (Mr C Rodgers) and it was decided to keep the pressure ratio at 3.0 and 3.5 whilst controlling the velocity ratio (U/V) to be in the range from .55 to .75.

The following running conditions were eventually selected for laser measurements at various positions in the machine.

PR = 3.0 ; U/V = .64. .68. .70. .72
PR = 3.5 ; U/V = .64. .68. .70.

The rig was operated to give the required values of U/V by fixing the pressure ratio and throttling the compressor outlet, the flow through the ejector being controlled to vary the pressure ratio across the turbine. Condition PR = 3.5 ; U/V = .72 was not achievable with the current air supply unit in the test cell.

5. LASER ANEMOMETRY

A Malvern Instruments 4772 Laser Transit Anemometer was used in "time-of-flight" (or 'Transit') mode together with a Malvern digital correlator (processor) to measure the air velocities. An on-line data reduction program was used to reduce the laser anemometry data to gas velocities and turbulence intensities. A lens system providing a 500mm working distance provided sufficient distance between the laser anemometer and the turbine volute. With this configuration, the depth of focus of the measurement volume was theoretically $\pm 225\mu$m but past experience showed that measurements closer than 1mm from the wall surfaces were difficult to achieve. The spot spacing was 450μm. Further details of the system are provided in Ref 1.

The laser system was mounted on a milling machine base providing X, Y, Z movements so that it could be adjusted to any required position.

6. SEEDER

A seeding device is required to 'seed' the flow with small particles which when passing through the measurement volume of the laser anemometer, scatter light which can be detected by the photodetectors. The particles involved must follow the flow and to achieve this they must be sub-micron. Devices for generating liquid seed particles have been in continual use over recent years but liquid 'seed' has temperature limitations associated with the properties of the liquids being used (a discussion of the problem is made in reference 1). Cold flow tests typically use kerosene or propane diol as liquid but these have severe temperature limitations. Following the advice of Dr A Boutier of ONERA, Cranfield has used silicon oil as a liquid

for seeding at temperatures up to 250°C but this appears to be the limit for liquid seeding. Whilst sufficient for some studies in compressors and cold turbine tests, there is a severe limitation for turbine tests and solid seeding techniques have to be adopted. Solid seeding methods have received little attention and are considerably more difficult to use than the liquid variety. When dealing with sub-micron solid particles it is essential to avoid compaction and to avoid moisture since the substances often involved (e.g. titanium dioxide) are highly hygroscopic and quickly form into aggregate lumps.

The method employed to generate these particles at Cranfield (Appendix C) takes a dry air supply through a set of porous plates of a fluidised bed which contains both the seed powder and some bronze beads. Injection of the seeding powder into the fluidised bed is arranged using a continuous loop of polyurethane cable 'drive chain' which feeds powder from a storage chamber. The 'drive chain' then returns by a series of pulleys back to the powder chamber. The seeding rate is controlled by the speed of this 'chain'. The powder storage chamber (or hopper) is vibrated using an air driven vibrator to minimise compaction. The powder is 'stirred' (and broken up) in the fluidised bed by the motion of the bronze beads and air. The particles are then carried by the feed air supply to the seeding injection point. Using this method the pressure level and subsequently the air flow rate of the fluidised bed are independent of the powder feed rate which is dependent on the speed of the 'drive chain' (this is controlled by a motor). Work on the device during the project permitted development of the solid seeder to a situation where it worked well although it could be prone to controlability problems and the shedding of accumulated material which collects in delivery pipes if insufficient care is taken.

In the present study both solid and liquid seeding were used. For the liquid seeder silicon oil was used in a DISA 55L aerosol seeding generator which produces the particles around a mean diameter of 0.5μm. In both cases the seeding particles were injected into the inlet flow at a considerable distance upstream so as to cause as little disturbance to the flow as possible. Provisions were made to vary the position of the seeding tube at the turbine inlet in order to obtain maximum response from the desired flow area. It was found that the response was very sensitive to the position of the seeding tube indicating surprisingly little mixing in the inlet chamber.

7. LASER MEASUREMENTS AT TURBINE OUTLET

7.1 Optical Access

Fig 4 shows two selected locations downstream of the turbine where flow measurements were made. Position B is located just downstream (35.5mm) of the rotor trailing edge tip and Position A further downstream (192.5mm). Position B was pre-defined by an existing instrumentation port and Position A was selected to be just downstream of the turbine inlet casing.

Considerable effort was spent on the design of the windows to allow optical access to the flow. The windows had to give clear access and they needed to withstand pressure and temperature and had to be sealed properly. There was also the requirements that windows should be easily removable from their positions to permit easy cleaning between operations. In order to avoid any obstruction to the flow, window mounts have been designed to match the curvature of the casing. The design of the windows has undergone considerable development as they were critical to the success of the project.

7.2 Initial Testing

For initial studies it was decided to run the unit at 3.5 pressure ratio with U/V_o = .64. During these runs it was observed that the turbine outlet temperature dropped to ≈-16°C during rig start up which caused a layer of ice to form on the glass window and to provide unacceptable optical access. Through experience it was found that after a run of at least 30 minutes the temperature of the inlet duct rose (due to the heat of compression from the plant compressors) and the turbine inlet temperature approached 70°C raising the outlet temperature to a low sub-zero temperature. Even at this temperature the optical window became wet from airborne moisture with water droplets appearing on the window again providing unacceptable optical access. In an attempt to keep the window dry, a small proportion of the hot air from the turbine inlet was bled through a tube and was directed to the glass window. This technique worked but detailed laser measurements could still not be made.

To overcome this problem it was decided that the inlet air should be heated to above 200°C, thereby increasing the turbine outlet temperature to avoid condensation. The experimental arrangement of the rig had a combustor

situated nearly two meters upstream of the turbine inlet but this was thought to be too uncontrollable and would dirty the optical windows with soot. Installation of electrical heaters was therefore undertaken. Eighteen heating elements (2.25KW per element) were installed far enough from the turbine inlet to cause negligible disturbance to the flow. A considerable amount of time was consumed in selecting the heating elements, preparing the air ducts and installation of the heating elements. Arrangements were made to avoid over-heating in cases of lower mass flow. Heating elements were arranged into three groups consisting of 9, 6 and 3KW elements each, thereby achieving some control over the air temperature. With the help of these arrangements it was possible to keep the turbine inlet temperature sufficiently high ($\approx 100^{\circ}$ C) to avoid any condensation on the optical windows. At this stage it became possible to take laser measurements at both the required downstream positions previously discussed and marked as window A and B in fig 4.

7.3 Laser Measurements at Window A

Fifteen radial positions were selected to perform laser measurements at window A. The separation between each radial station was 3.2mm (0.125in). Laser measurements provided the velocity, flow angle and turbulent intensities at all measuring positions. It was found to be difficult to make laser measurements at the centre of the duct.

Fig 5 shows laser results for window A taken at PR = 3.0 for selective values of U/V (i.e. .64, .68, .70, .72). It must be noted from the figure that no laser results could be obtained for the central annulus region of the graph (i.e. radius = 20 - 30mm) as only a small amount of seeding was passing through this region. There were also swirl angle changes from positive to negative values for this region as shown in fig 6 (+ve flow angle is one where the rotation is in the same direction as the rotor and flow moving away from the turbine, fig 7). Near the central region of the pipe, a swirl flow with -ve flow angles will be observed indicating a region of counter rotating (or overturned) flow.

Fig 8 shows velocity variation with the radius at window A for PR = 3.5 with different values of U/V (i.e. .64, .68, .70). The swirl angle variation for these conditions have been given in fig 9.

Discussion of all results is given in Section 7.8.

7.4 Laser Measurements at Window B

Ten radial positions. with a separation of 3.2mm. were chosen for carrying out laser anemometry work at window B (fig 4). As window B lies near the turbine wheel. it was very difficult to achieve a clean laser signal due to high turbulence in this region. Figs 10 and 11 give the velocity and flow direction obtained at different radial positions and for the various flow conditions. The variation in flow conditions across the annulus of this station was found to be smaller than observed for window A. There is further discussion in Section 7.8.

Figs 12 and 13 show the velocity and flow angle measurements for the same window for PR = 3.5 for the flow conditions of interest.

Strobe Results (Blade Passing Effects)

To investigate the blade passing effect on the flow at window B (which lies just downstream of the turbine rotor) a strobing unit was used so that measurements relative to fixed rotor positions could be established. To achieve this the blade to blade passing period for the turbine was divided into ten equal time files and laser anemometry results were taken at alternate files for the following running conditions:

i) PR = 3.5; U/V = .68

Four radial positions (r = 12.45 mm; 15.65mm, 21.95mm; 28.35mm) were selected for this purpose. Figs 14 to 17 show the strobe results for velocity and flow angles.

ii) PR = 3.5; U/V = .70

Results for three radial positions (r = 15.65mm; 21.95mm; 28.35mm) were obtained. Figs 18 to 20 give the variation in velocity and flow angles.

7.5 Cobra Probe Measurements

In order to compare the laser results with some conventional measurements, a cobra yawmeter probe was used. It was necessary to calibrate the probe

before its use in the actual flow situation. This was done by using a calibration tunnel facility available within the Department. The probe was rotated from -40° to +40°. One total pressure and two static readings were used to calculate the static pressure coefficient (C_s), the total pressure coefficient (C_T), and yaw angle coefficient (C_w). Data was obtained at various flow settings and the total pressure coefficient is presented in fig 21. An offset of -2.8° was calculated from this exercise and this angle was added to all the flow angles measured by the probe in the test arrangement.

7.6 Cobra Probe Measurements at Window A

The fifteen positions previously defined for laser work were selected for cobra probe measurements. Variation of velocity and air swirl angle with radius were plotted for each running condition along with their corresponding laser measurements so that a direct comparison of results could be made.

Figs 22 - 23 give the cobra probe velocity results at window A for PR = 3.0; 3.5 and for various values of U/V at different radial positions.

Figs 24 - 25 compares the cobra probe results with the laser anemometry results taken at the same positions and the running conditions. Results from both instruments follow the same trend except that the cobra results for velocity are a little lower. In general, the difference becomes smaller as the radius increases. Swirl angle variations with radius in both cases are similar. Results indicate a core of counter-rotating (overturned) flow eminating from the turbine hub. The difference in velocity for the cobra and laser measurements is possibly due to the interaction of the cobra sensor with the complex flow. Laser anemometry is a non-intrusive technique and it is felt to be more reliable in this confined region. It must be noted that the laser results were found to be very repeatable and in order to maintain accuracy, two or sometimes three readings were taken for a single position and were averaged to produce a more accurate result at particularly difficult points.

Figs 26 - 27 present similar results for the PR = 3.5 operating conditions for both instruments.

7.7 Cobra Probe Measurements at Window B

Ten radial stations were selected for these measurements and again the cobra probe results were plotted with the corresponding laser results in order to have direct comparisons. In the central region near the hub, the cobra probe produced very unstable results and as already noted it proved difficult to take laser measurements in that region.

Fig 28 presents the cobra results and figs 29 and 30 are the results for both instruments at PR = 3.0 and U/V = .64, .68, .70, .72. Figs 31 - 33 give similar data and comparisons for PR = 3.5. Again in these graphs, the presence of a counter-rotating core will be noted.

7.8 Results and Discussion (Phase 1 - Downstream of Rotor)

Both laser anemometer and cobra yawmeter results show similar trends (typically figs 24 and 25). Flow direction measurements from both instruments agree quite well but velocity measurements show some quantitative difference. Measurement experience in the group concerned has indicated that the most probable error is the measurement of static pressure (with the cobra probe) which has often proven difficult in a distorted flow environment as exists downstream of the rotor (an error in static pressure provides an error in dynamic head and subsequently in velocity).

Measurements far downstream (Window A - 192.5mm from the rotor tip) of the rotor indicate a flow field in which there is significant swirl in the direction of rotation towards the outer wall and a region of overturning (rotation against the direction of rotation) in the core. The extent of this core increases in intensity and size with decreasing flow coefficient (U/V) and increasing expansion ratio, figs 25 and 27. The matching velocity profiles do not vary very significantly with flow coefficient or expansion ratio except that the absolute level of velocity reduces with increasing flow coefficient and expansion ratio (as would be expected).

Closer to the turbine rotor (Window B - 35.5mm from the rotor tip) similar profiles are in evidence for flow direction and velocity. The profiles at this station, however, are incomplete due to measurement difficulties in the outer wall and core region. They indicate, figs 30 and 33, a situation where the counter-rotating core flow is more confined than in the downstream plane (Window A).

Measurements made using a blade strobe system indicated that at the station closer to the turbine (Window B) there is no evidence of a blade wake (or blade-to-blade profile) suggesting that any mixing has completed upstream of this station.

The above discussion has not mentioned the slight diffusion taking place between the measurement stations (fig 4) as its effect is not at all clear although this could be a reason for the developing region of counter-rotating flow further from the rotor trailing edge.

8. LASER MEASUREMENTS AT TURBINE INLET

In Phase 2 of the study an investigation of the flow between the nozzle guide vanes and the turbine rotor was undertaken.

8.1 Optical Access

Fig 34 shows the area of study immediately after the nozzle vanes where laser measurements are required across the channel (to provide NGV spanwise data) and at various circumferential positions (to provide NGV pitchwise data). It proved extremely difficult to provide an optical access for these measurements and considerable time was spent in analysing various schemes.

At first it was hoped to approach through of the turbine backplate but due to the construction of the nozzle guide vane rings complications arose making that approach impossible. The most appropriate way forward was to prepare the optical access as shown in fig 34 (and 35). In this arrangement the incident laser beams have been completely isolated from the flow in the plenum chamber by a cone assembly which has a mirror mounted to deflect the laser beam by 90° into the region of interest. Plate B shows the cone assembly where the mirror was fitted.

The cone assembly was inserted into the machine as one unit and could be located such that the laser beams could "see" the flow through the small pinholes made in the turbine assembly without any truncation. It must be pointed out that the two-spot laser system being used for the study is a backscatter system, so that the cone assembly both transmits and collects the light scattered by the airborne seed particles which were introduced into the flow at a suitable distance upstream of the rotor inlet.

The size of the cone assembly was kept small to cause as little disturbance to the flow as possible. Once the cone assembly is in position, the guide vane exhaust flow is sealed from the plenum chamber using a high temperature 'O-ring' system.

In practice, it was not possible to machine five pinholes (each 2mm in diameter) across a single vane pitch and it was necessary to stagger the five measurement locations (W_1 - W_5) as shown in fig 36. The "effective" positions of these five pinholes between two consecutive trailing edges has been separately shown in this figure. Position 1 lies almost at the trailing edge of the vane and has been taken as a datum position whilst the other four positions have been marked relative to that datum.

A special tool was made to rotate the inner casing of the shroud to change the window position without dismounting the whole assembly. Five positions were marked on the assembly to align the different window positions with the cone assembly (the 'windows' were blanked when not in use).

As described previously, the laser anemometer was installed on a machine bed to achieve the movements in X, Y and Z required for the beam alignment through the pinholes. Experience showed that extreme care in aligning the system had to be taken in setting the position of the laser system.

8.2 Results and Discussions (Phase II - Upstream of Rotor)

Laser measurements were made at the five positions (W_1, W_2, W_3, W_4, W_5) described above. At these stations the channel depth is approximately 6mm and five positions (depth (d) = 1mm, 2, 3, 4, 5) across the passage were selected for measurement. (Distance d defined from the shroud surface towards the backplate is as shown in fig 35). For initial studies the mid channel position (d = 3mm) was chosen. It was necessary first to set a datum position for the laser which could be examined during the running of the machine as rig movement between static and test conditions was unavoidable. This datum was taken as the outside surface of the window and intially, the laser was focussed on this datum and subsequently all distances measured relative to that position.

Initial tests were performed at a low speed but no result could be obtained due to large amounts of flare from the backplate of the nozzle vane

assembly. The backplate was painted black and experiments were repeated and after careful re-arrangement. and a considerable amount of time spent in overcoming this problem. success was achieved.

Excellent and highly repeatable results were thus eventually obtained for all windows and for the five positions across the channel. Turbulent intensities were very moderate (up to 4-5%) for all windows except window W_1 which lies very near to the trailing edge of the vane where they were up to 7% - 8%.

Figs 37 - 71 show the velocity and flow angle variations across the channel. The flow angle is defined from the horizontal radial position as shown in fig 36.

The running conditions used for laser measurements for all windows are given below:-

PR = 3.0 ; U/V = .64. .68. .70. .72
PR = 3.5 ; U/V = .64. .68. .70

d = 1mm to 5mm.

The figures show very little velocity or flow angle change across the channel although for d = 5mm (at almost all running conditions in all windows) both flow angle and velocity reduce to lower values. This could result from near wall effect as this position is only 1mm away from the back wall.

In order to see the blade passing effect on the flow at these positions a strobing unit was used. The blade to blade distance in the turbine was divided into ten time files and five laser measurements were taken at alternate time files. The following running conditions were selected for this study.

PR = 3.5 ; U/V = .68; d = 1,3,5

Figs 72 - 86 show the velocity and flow angle variations along with the time files and it clearly gives no indication that the passing blade has any effect on the flow conditions at the positions under investigation.

Results shown in figs 37 - 71 have been re-expressed by averaging the NGV pitchwise variation and displaying the spanwise flow. fig 87 - 93. These indicate almost uniform spanwise conditions with a small reduction in flow angle towards the shroud surface. The same angular data is presented in figs 94 and 95 which indicate that the flow is very well guided by the NGV's and independent of both operating conditions and spanwise position providing almost uniform conditions for the rotor.

9. CONCLUSIONS

Experimental work has been carried out on a small radial inflow turbine which included laser anemometry traverses at two positions downstream of the turbine rotor. Initial testing of the machine showed a temperature drop at the outlet of the turbine thereby producing an ice layer on the glass window and prohibiting any laser measurements at these positions. The problem was solved partially by changing the design of the optical window and by heating the air up to 200°C at the inlet of the turbine. Electrical heaters were installed for this purpose at an appropriate distance from the turbine inlet.

Laser anemometry measurements were then possible which indicated a swirling flow with a region of counter-rotating flow in the centre. A cobra probe was used to compare with the laser anemometry results. Both measuring techniques show similar trends of flow velocity and flow angle at various running conditions. The extent of the region of counter-rotating flow increased with decreasing flow coefficient and was more confined closer to the turbine rotor trailing edge.

A strobing unit was used to examine the extent of blade passing effect on the flow at the window located closest to the rotor trailing edge. No noticeable effect could be observed indicating mixing was complete at this station.

Laser anemometry work was also carried out at the inlet of the turbine rotor (just downstream the nozzle guide vanes). It was found very difficult to provide adequate optical access for the laser work but after careful development five windows at different circumferential positions were provided and a special arrangement made to align the laser system.

The laser work showed a largely two-dimensional flow in the area between the nozzle guide vanes and rotor. Strobing was undertaken to observe the blade passing effect on the flow conditions at the windows. Results show that there is hardly any unsteadiness in the flow caused by the passing blades at these positions. Interestingly, this contrasts with similar measurements made on another turbine studied.

The results of this study are velocity measurements obtained from the small internal passages of a high speed turbine. Some conclusions such as those reported are immediately possible but further consideration should be undertaken by comparing results with computations which were outside the scope of this project.

REFERENCE

1. Application of Doppler and Transit Laser Anemometry in Small Turbomachines.
   R L Elder, C P Forster, M E Gill
   AGARD Propulsion and Energetics Panel 67th Symposium, Philadelphia, May 1986, AGARD-CPP-399, paper 10.

R7-8.43/IH

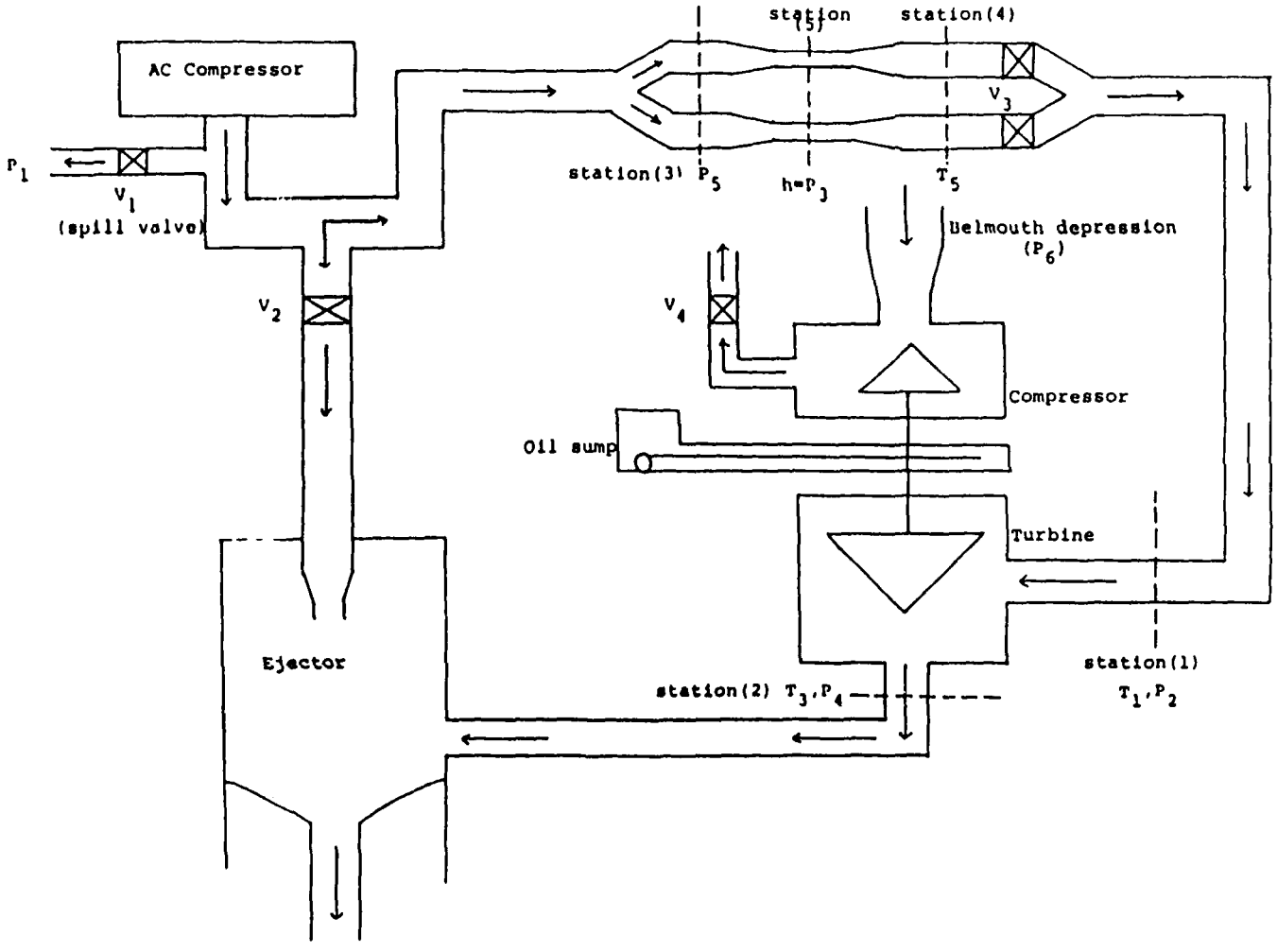

Fig. 1 - Schematic diagram for rig installation

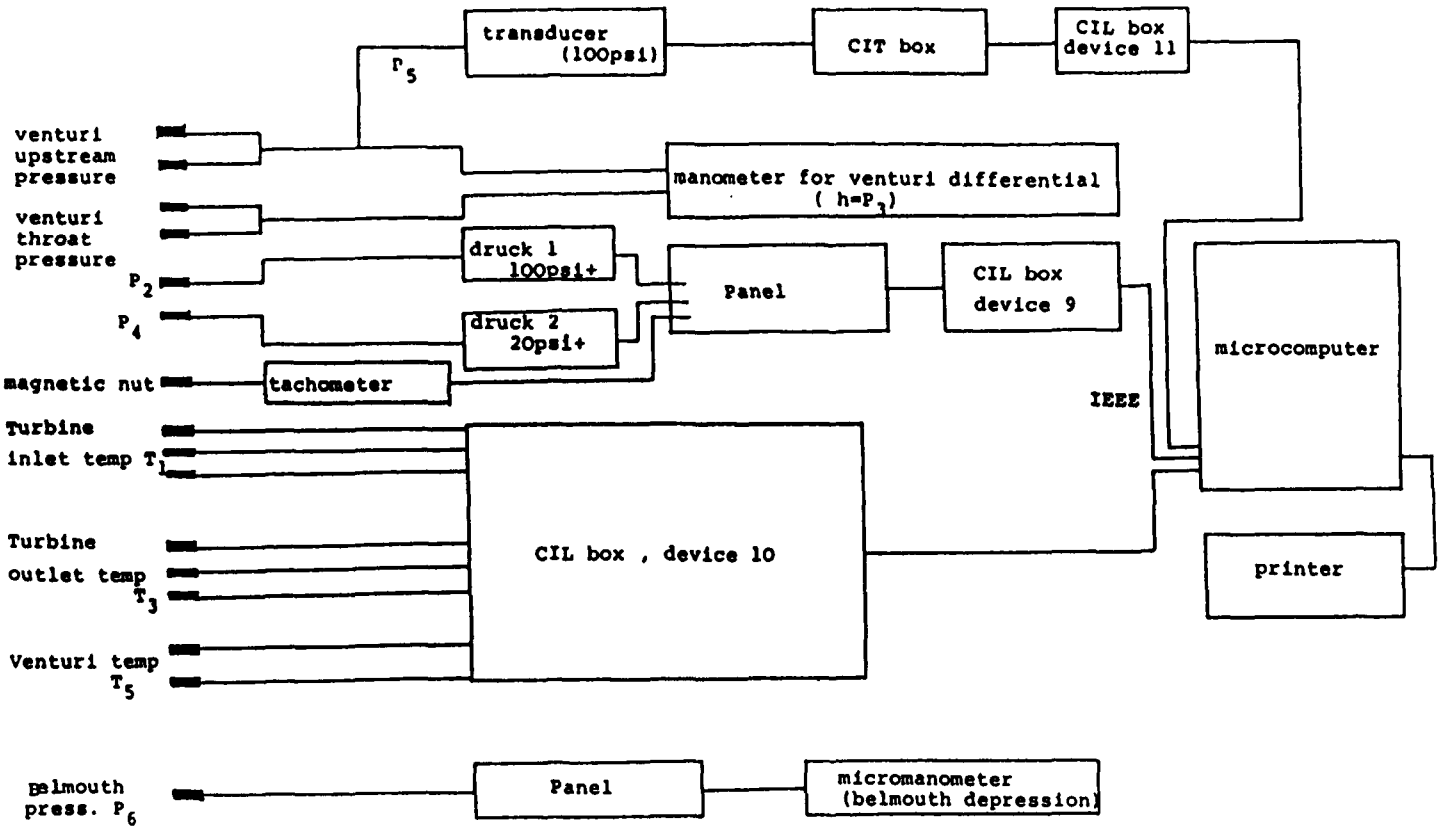

Fig 2 - Data collection scheme for TURBOMACH turbine performance mapping

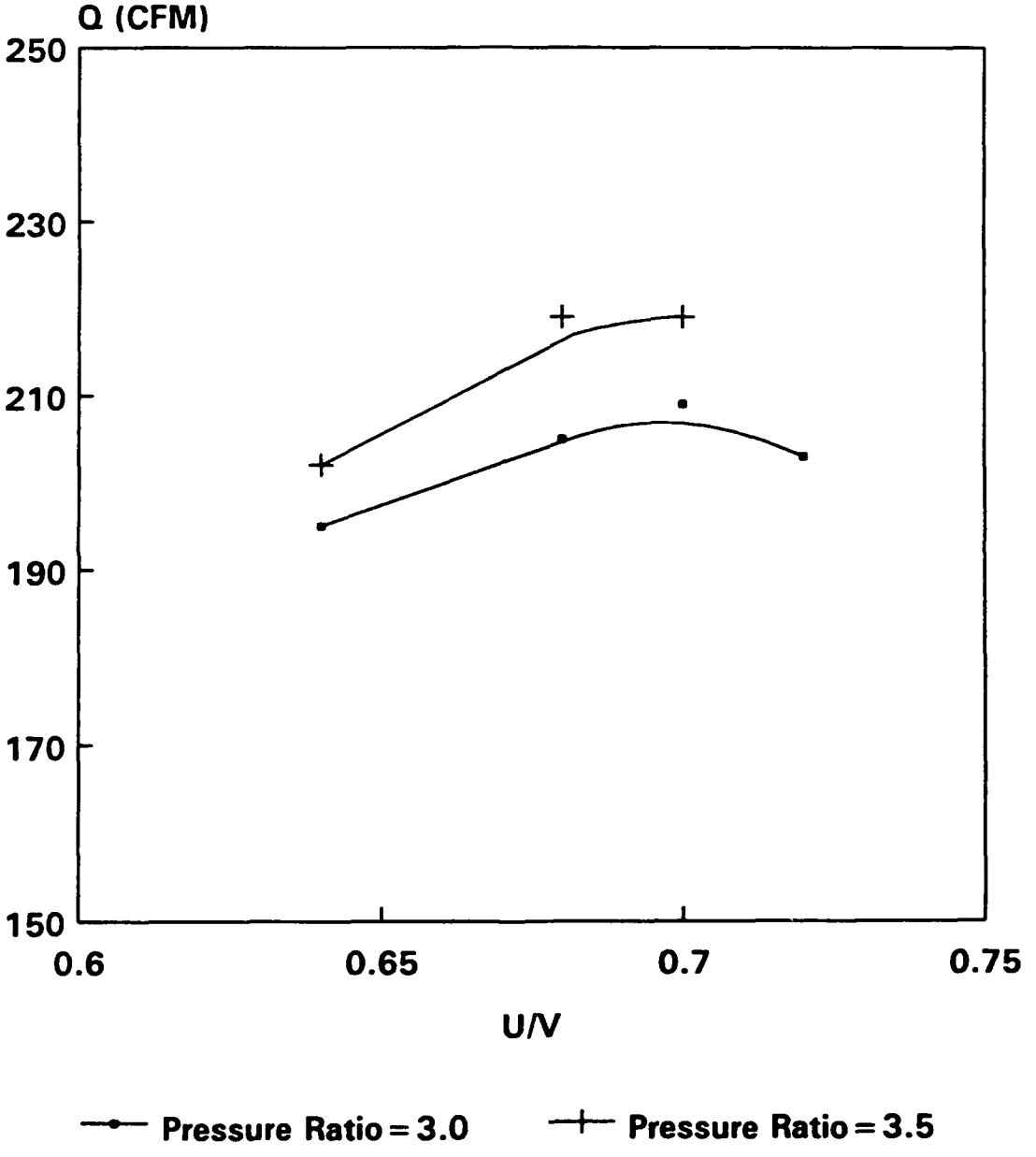

Turbine Performence

Figure 3 - Turbine Overall Performance

NOT TO SCALE

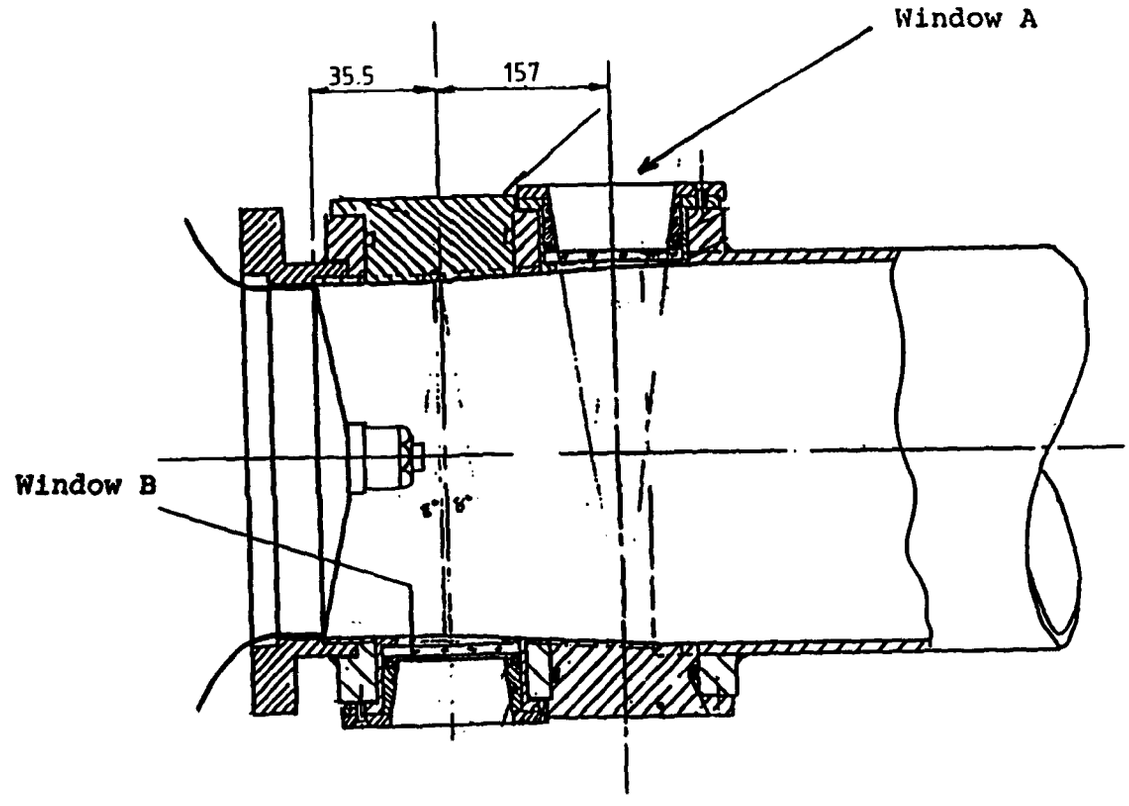

Note ; In practice both windows are on the same side.

Fig 4 - WINDOWS FOR OPTICAL ACCESS

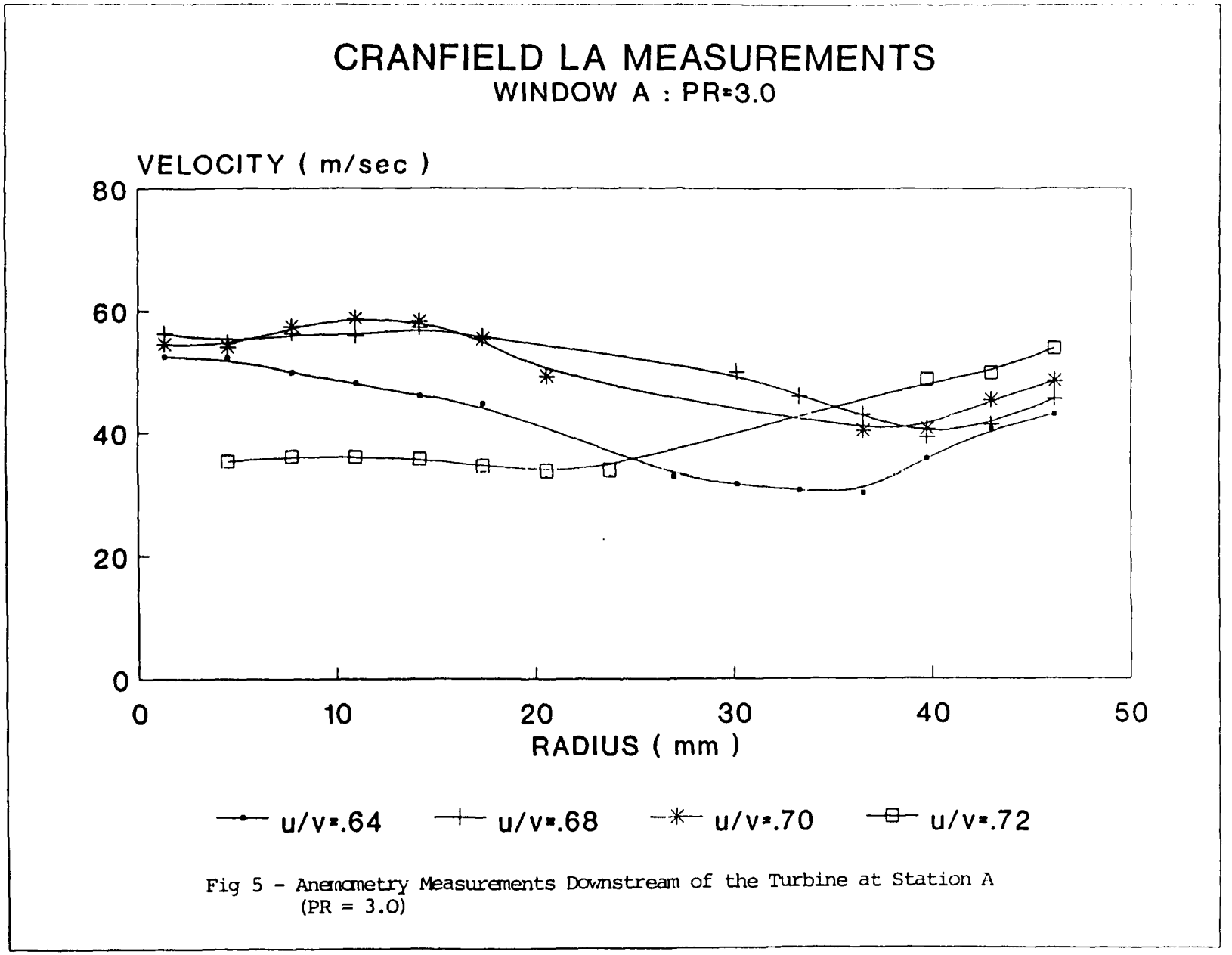

Fig 5 - Anemometry Measurements Downstream of the Turbine at Station A (PR = 3.0)

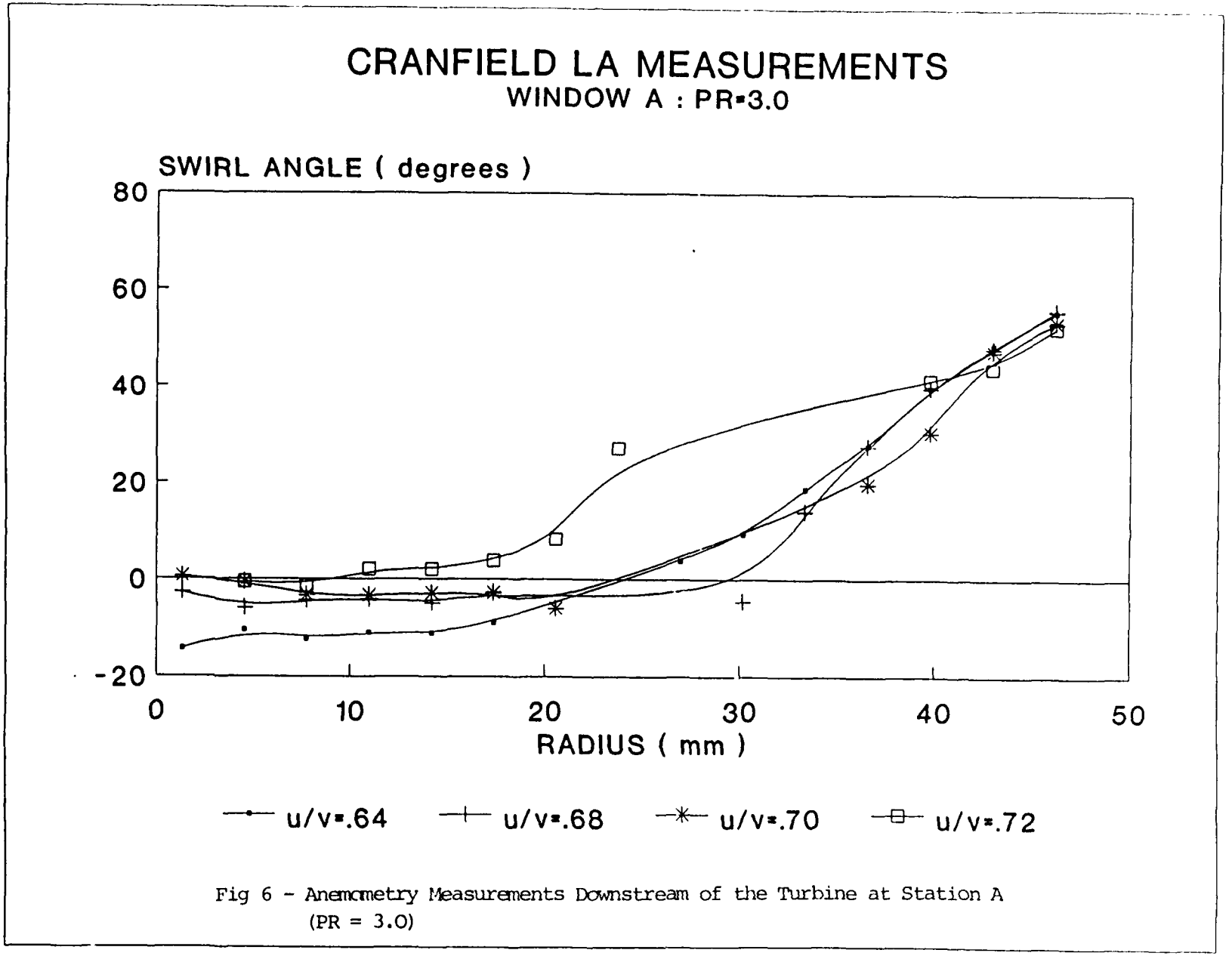

Fig 6 - Anemometry Measurements Downstream of the Turbine at Station A (PR = 3.0)

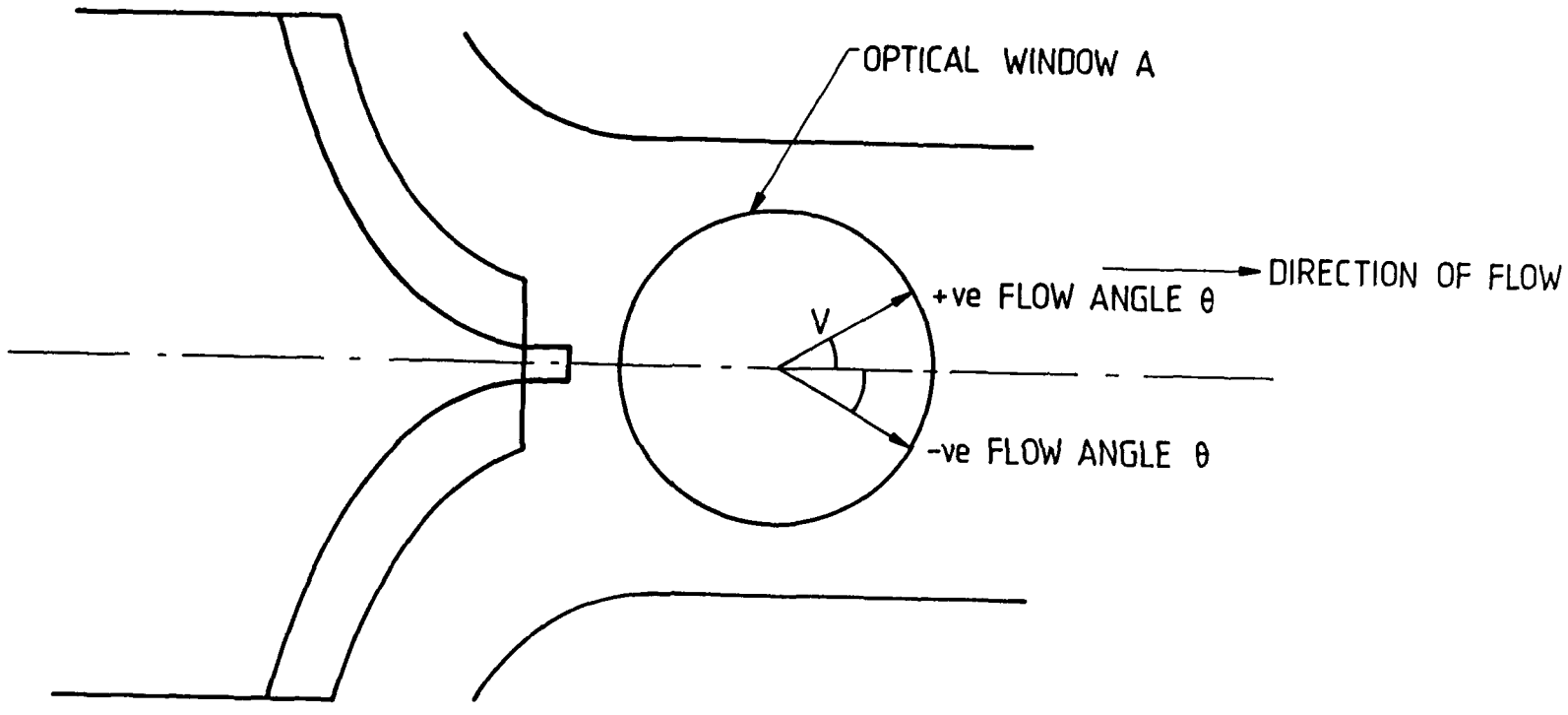

Fig 7 - Definitions of +ve and -ve flow angles

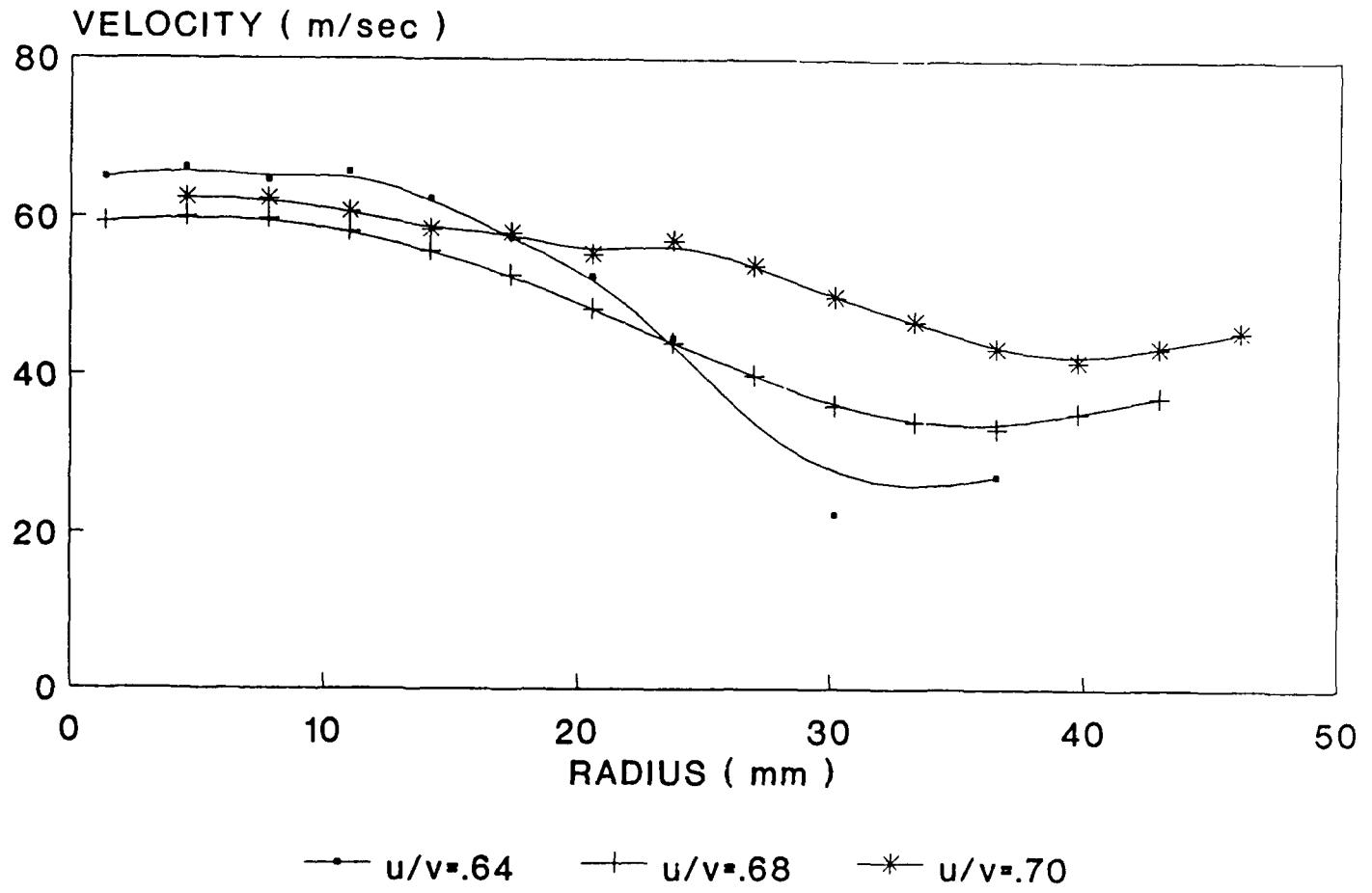

Fig 8 - Anemometry Measurements Downstream of the Turbine at Station A (PR = 3.5)

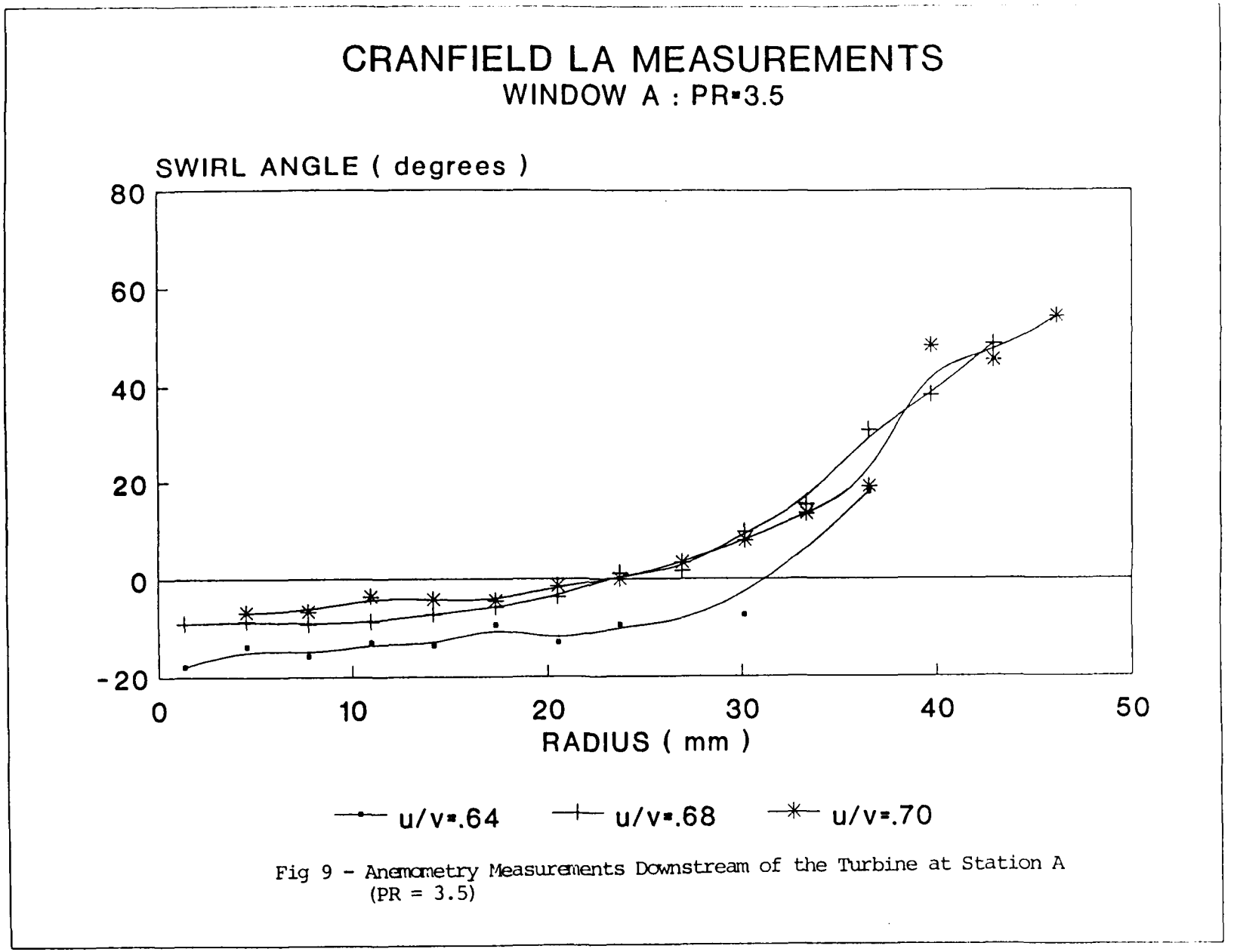

Fig 9 - Anemometry Measurements Downstream of the Turbine at Station A (PR = 3.5)

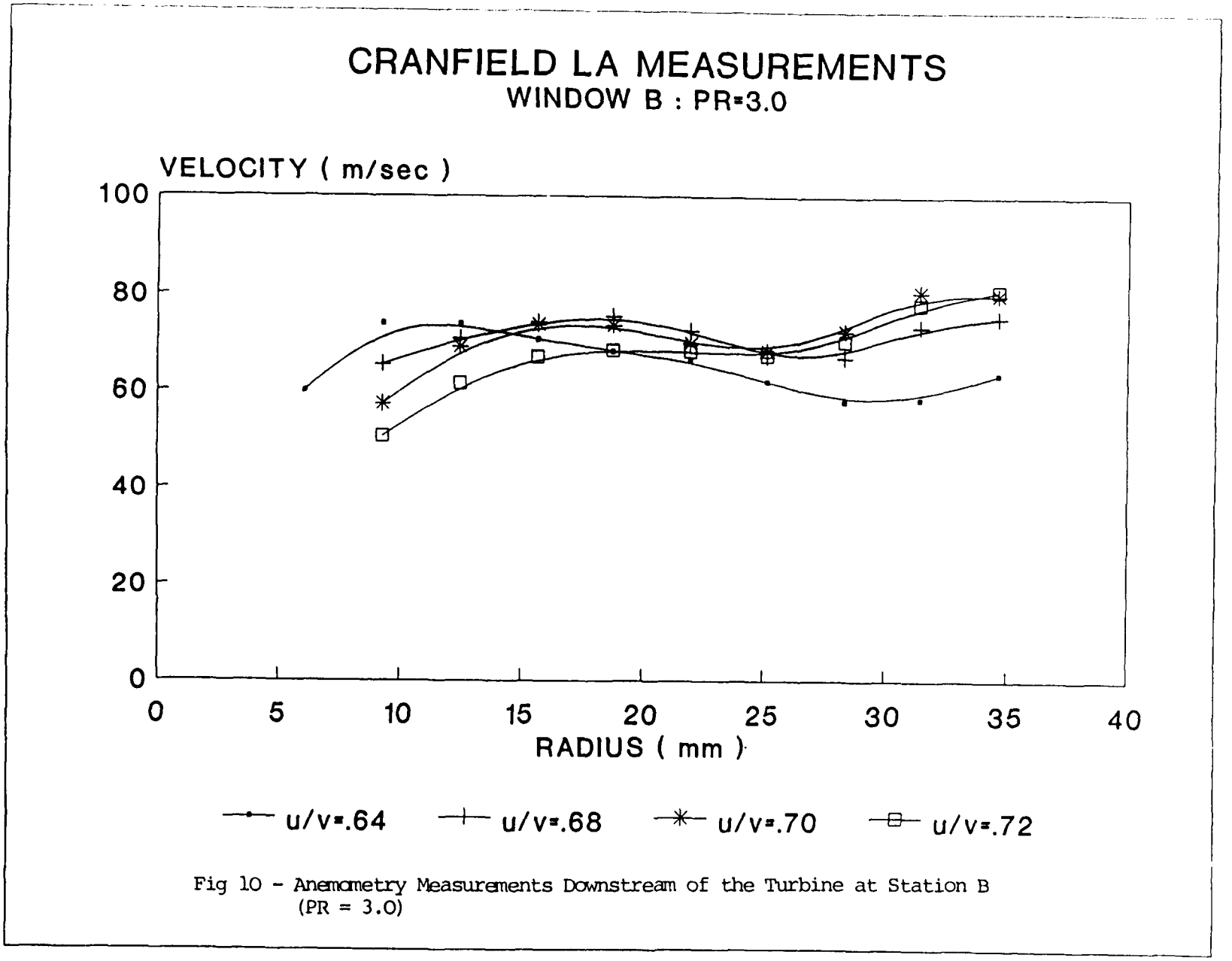

Fig 10 - Anemometry Measurements Downstream of the Turbine at Station B (PR = 3.0)

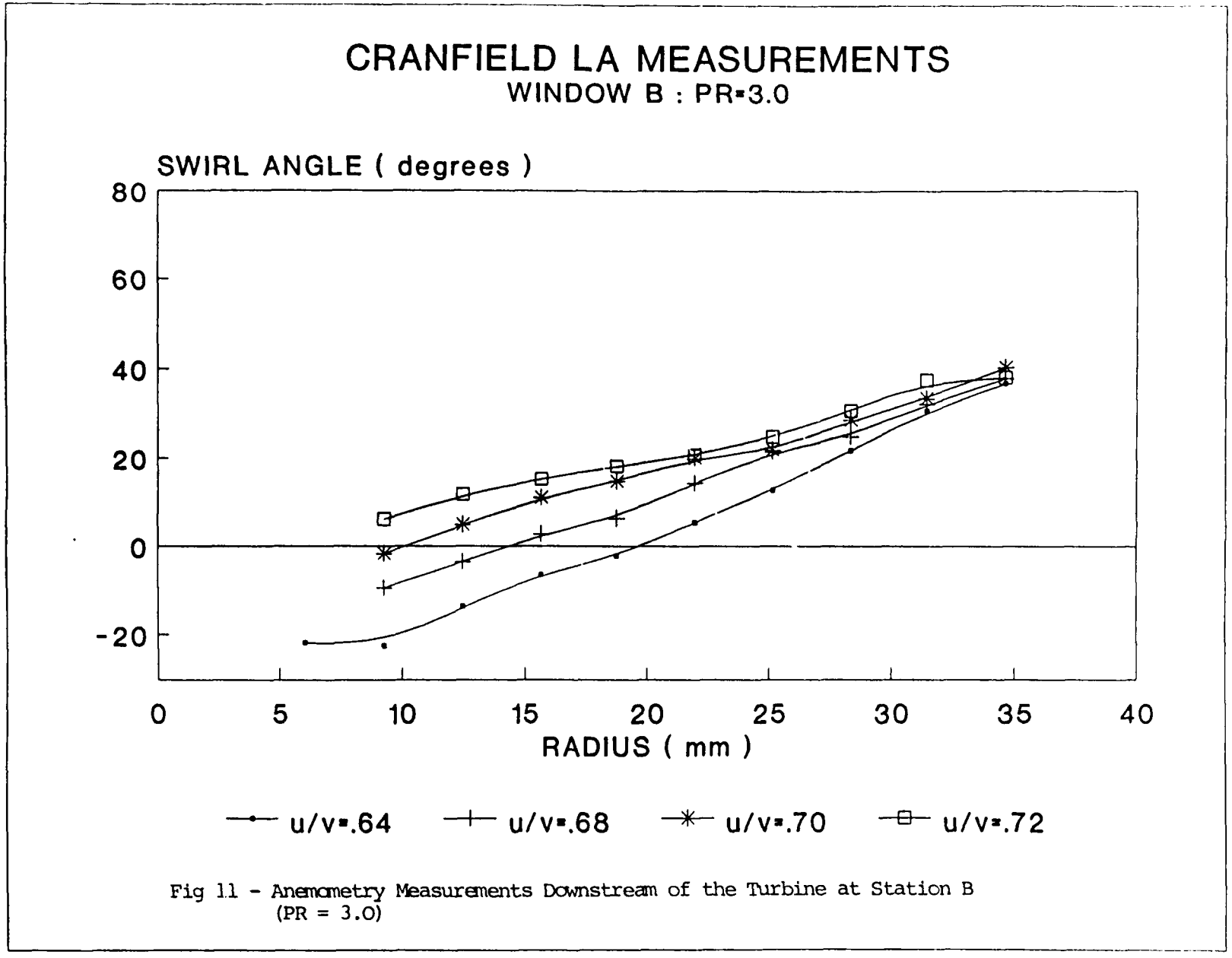

Fig 11 - Anemometry Measurements Downstream of the Turbine at Station B (PR = 3.0)

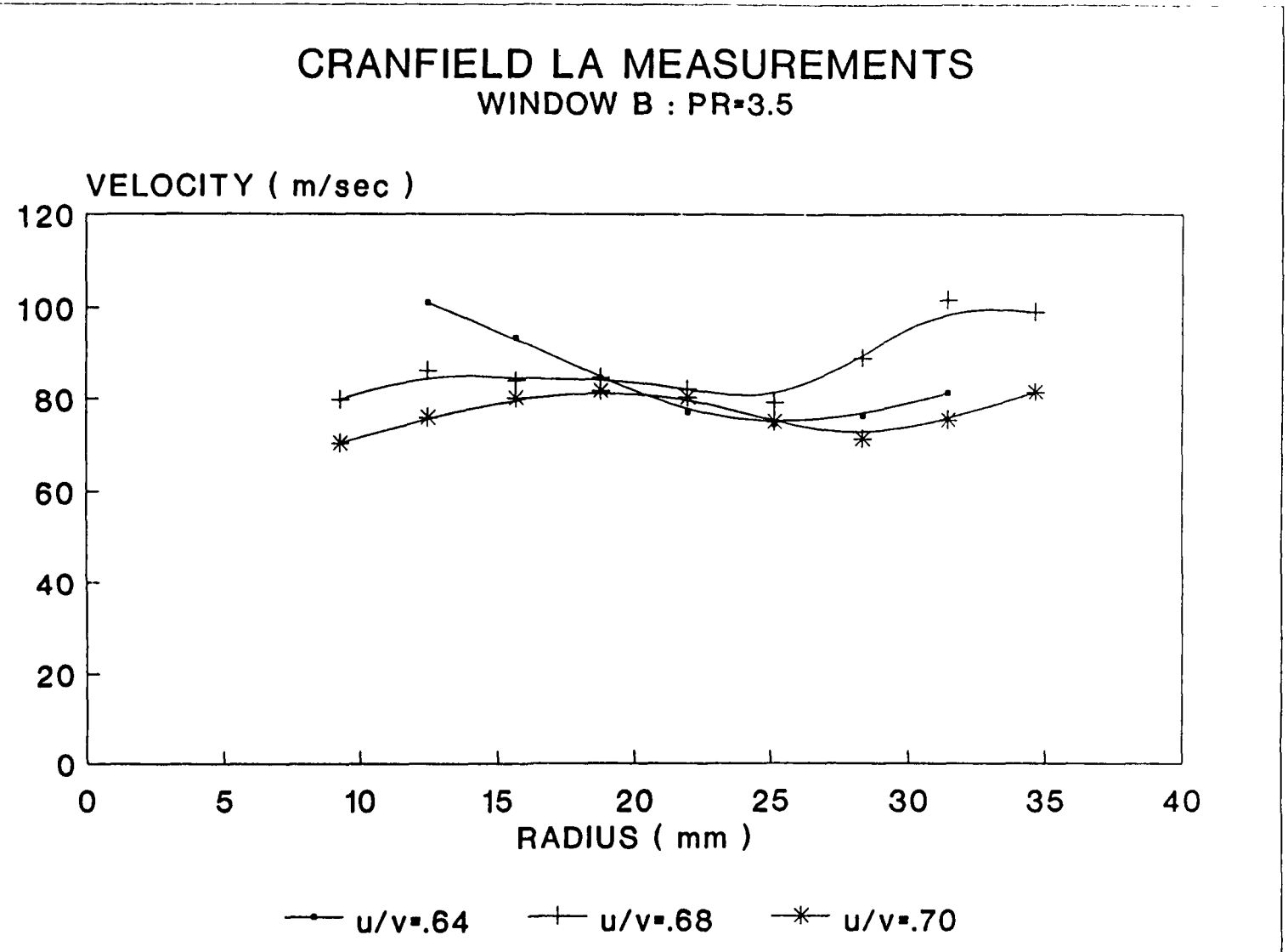

Fig 12 - Anemometry Measurements Downstream of the Turbine at Station B (PR = 3.5)

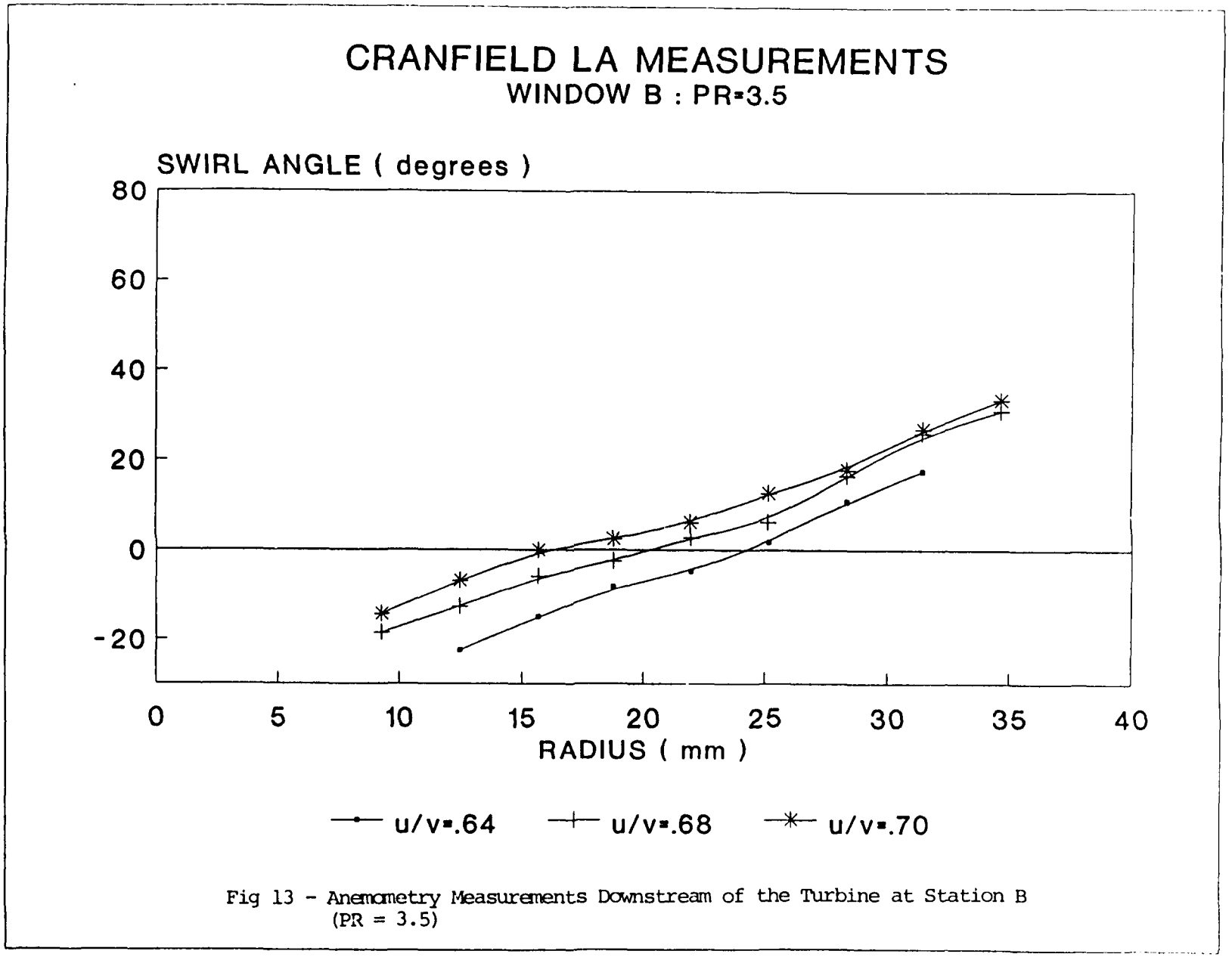

Fig 13 - Anemometry Measurements Downstream of the Turbine at Station B (PR = 3.5)

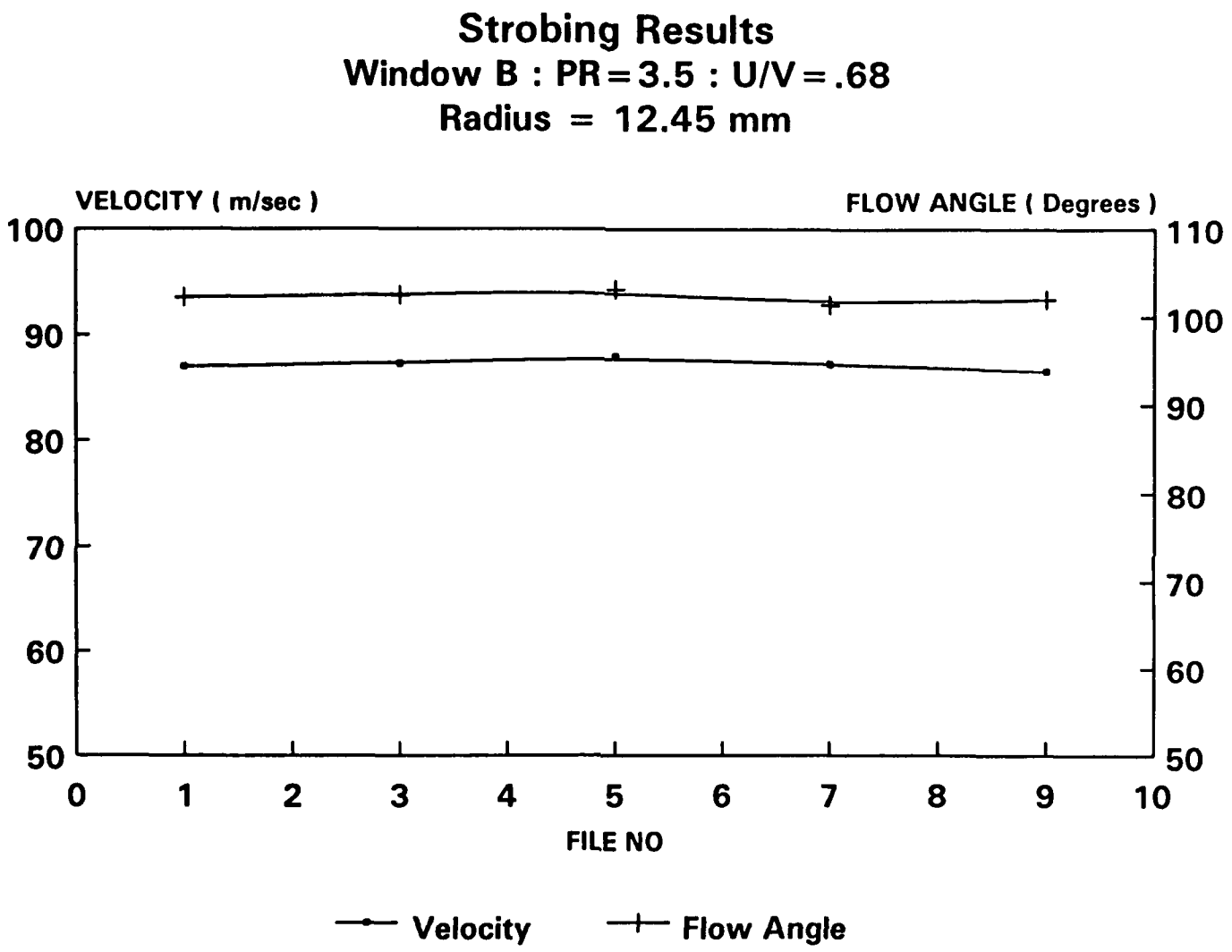

Fig 14 - Blade Strobed Results Downstream of Turbine at Station B
(PR = 3.5, U/V = 0.68 at Radius 12.45mm)

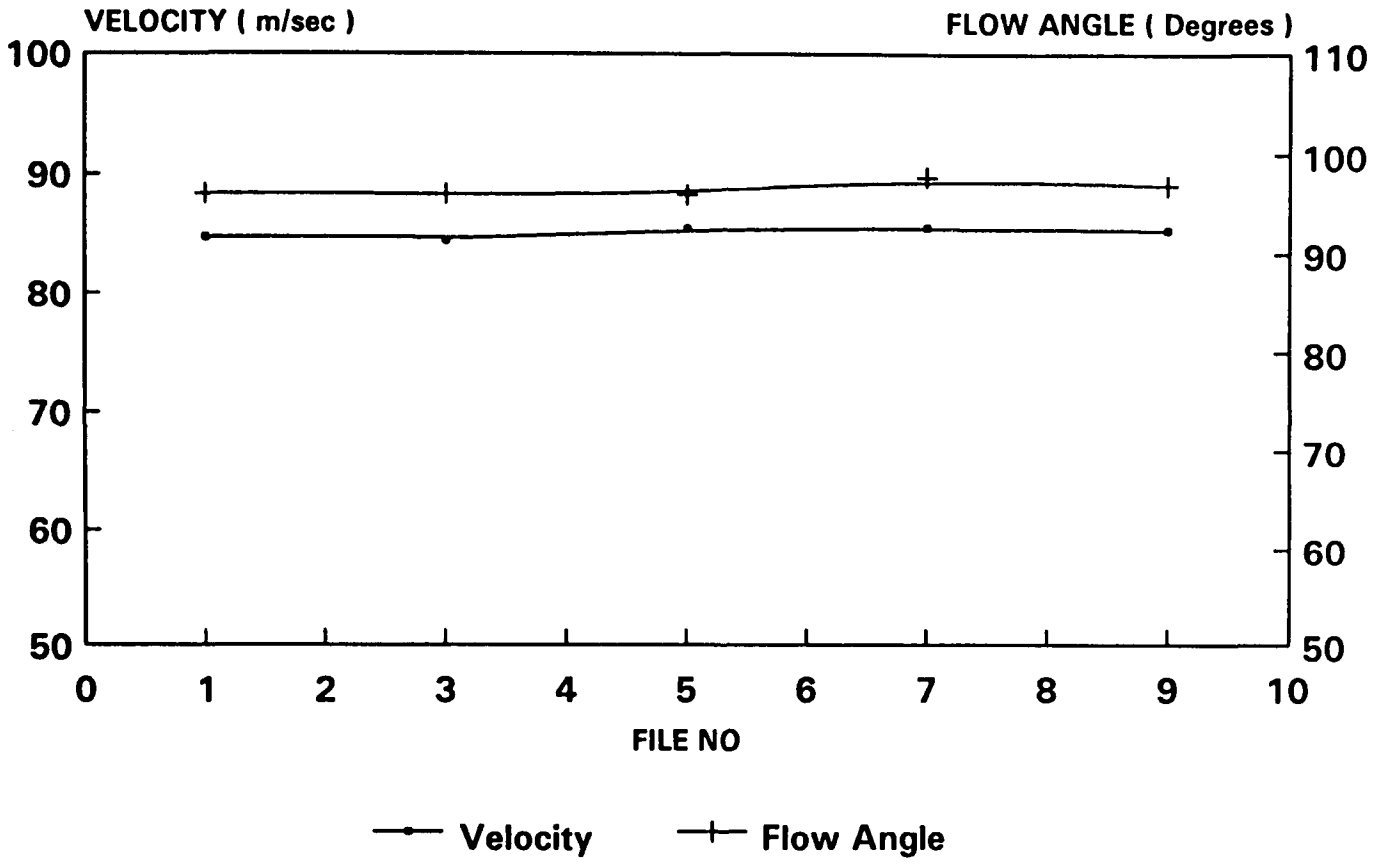

Fig 15 - Blade Strobed Results Downstream of Turbine at Station B
(PR = 3.5, U/V = 0.68 at Radius 15.65mm)

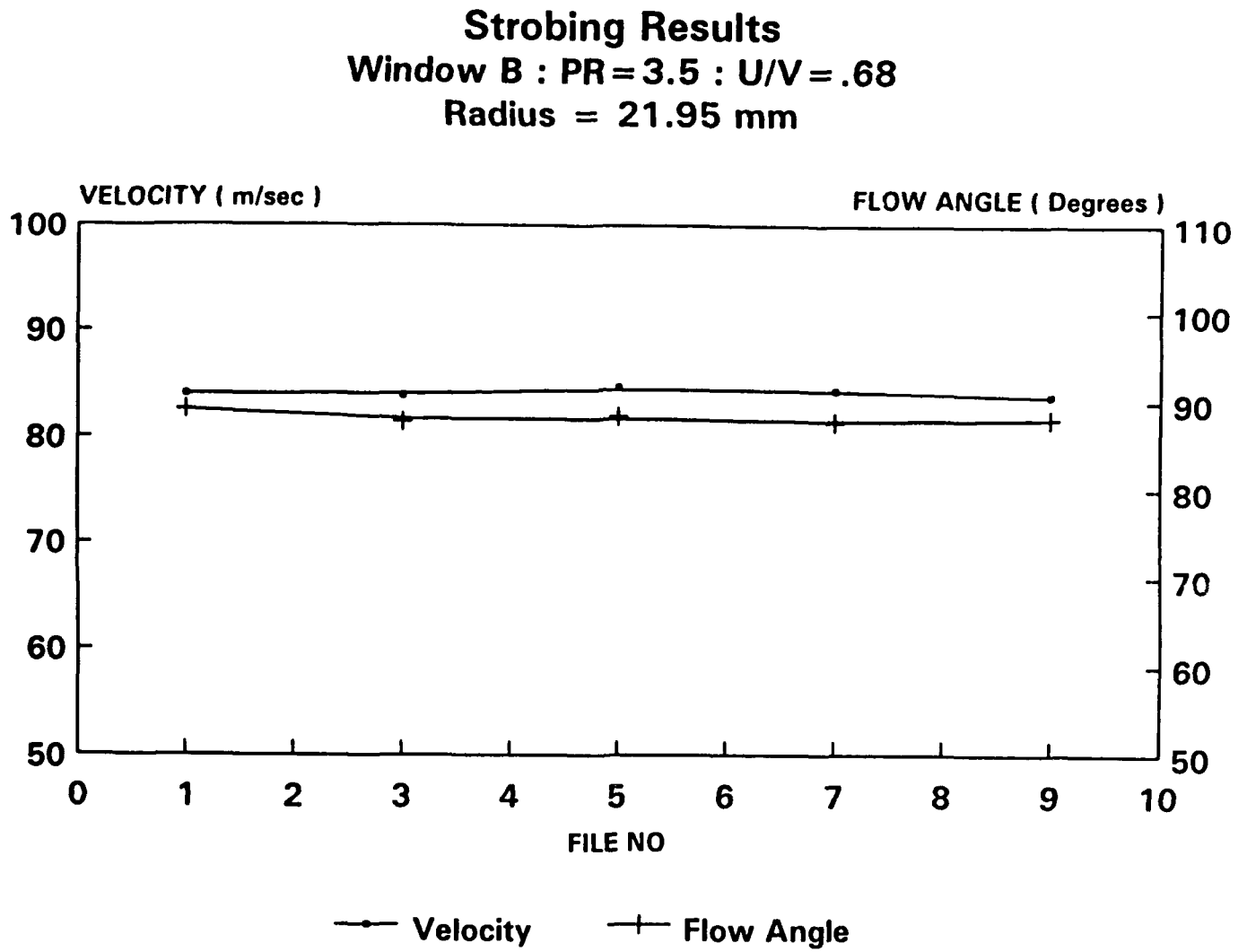

Fig 16 - Blade Strobed Results Downstream of Turbine at Station B
(PR = 3.5, U/V = 0.68 at Radius 21.95mm)

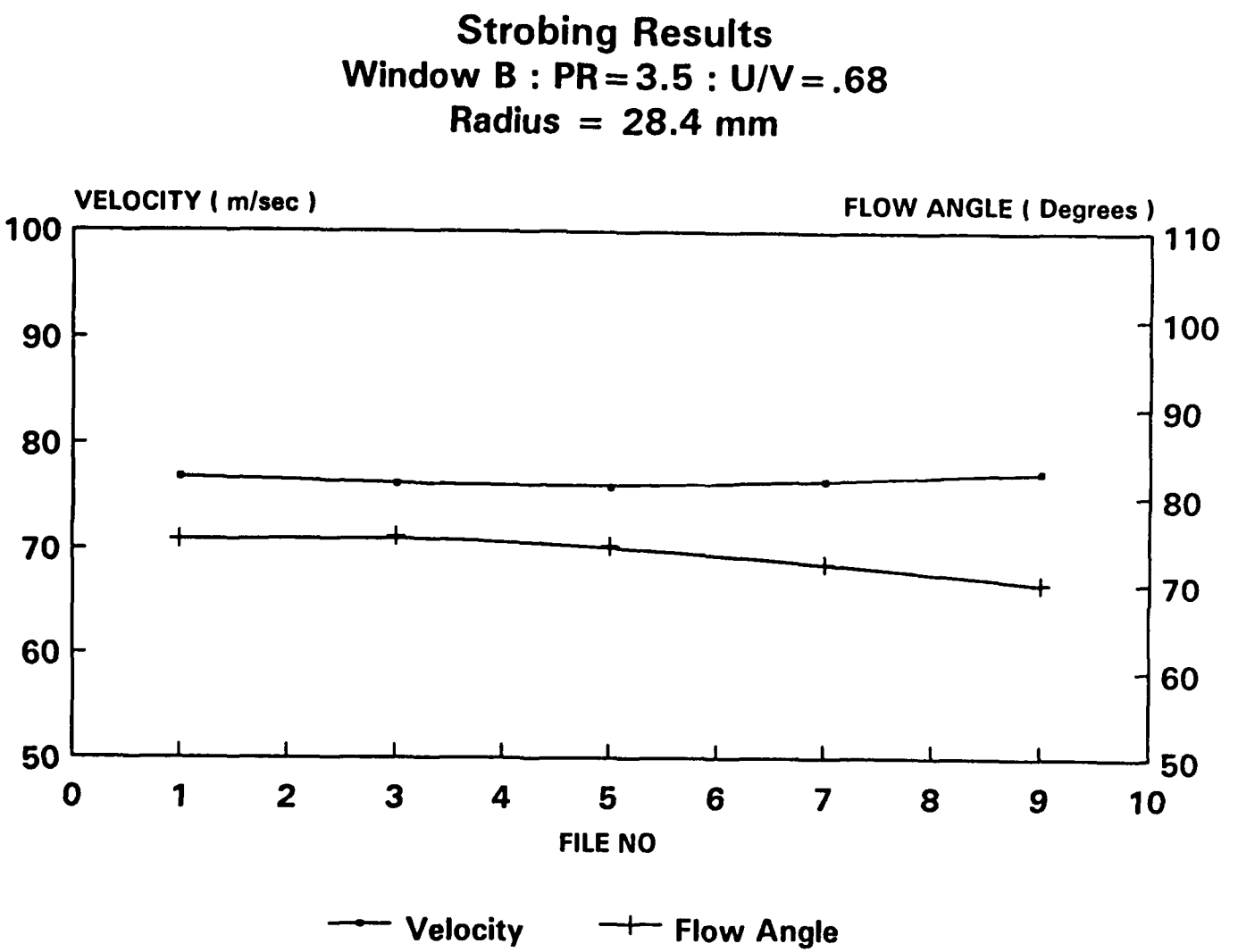

Fig 17 - Blade Strobed Results Downstream of Turbine at Station B
(PR = 3.5, U/V = 0.68 at Radius 28.45mm)

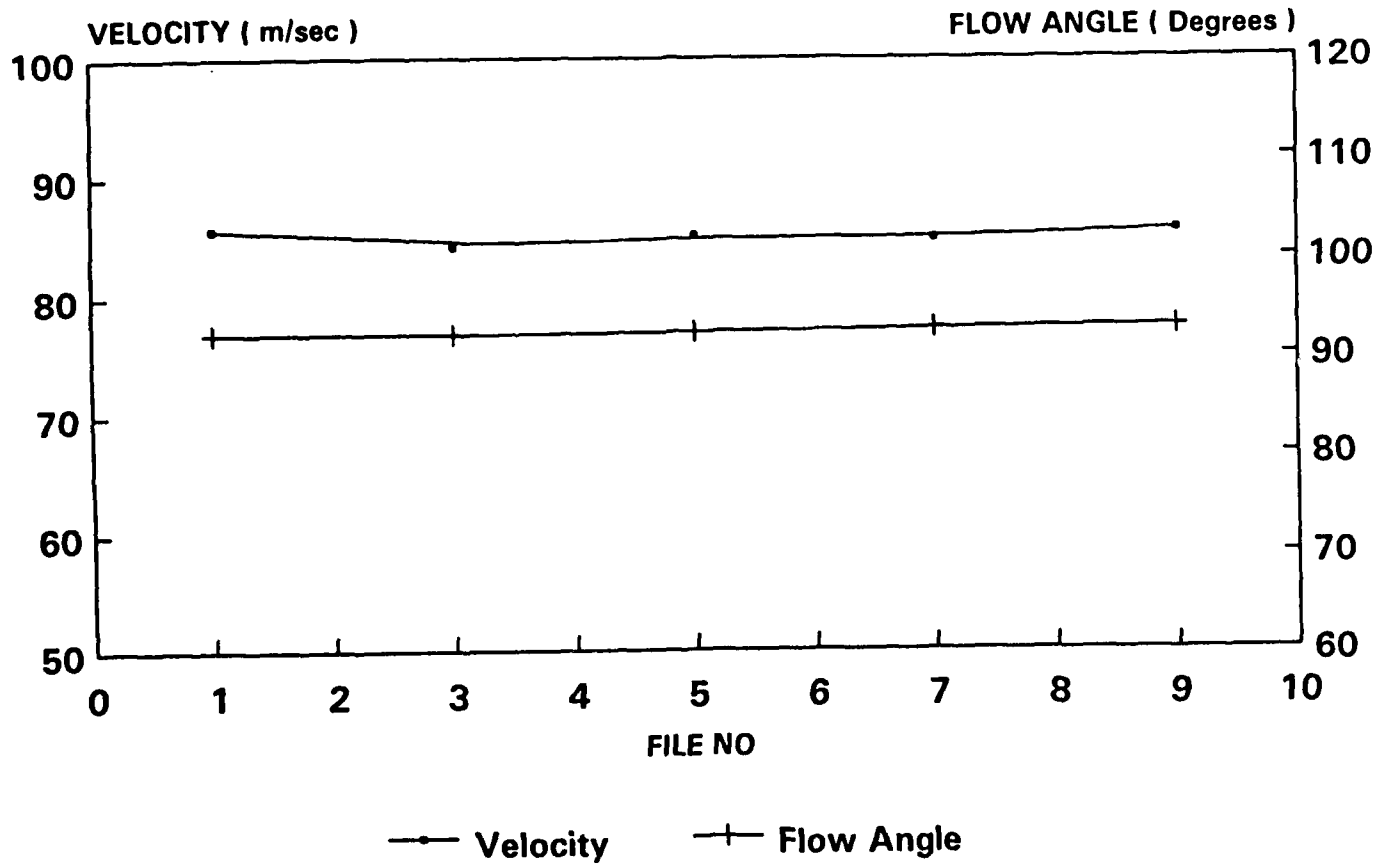

Fig 18 - Blade Strobed Results Downstream of Turbine at Station B
(PR = 3.5, U/V = 0.70 at Radius 15.65)

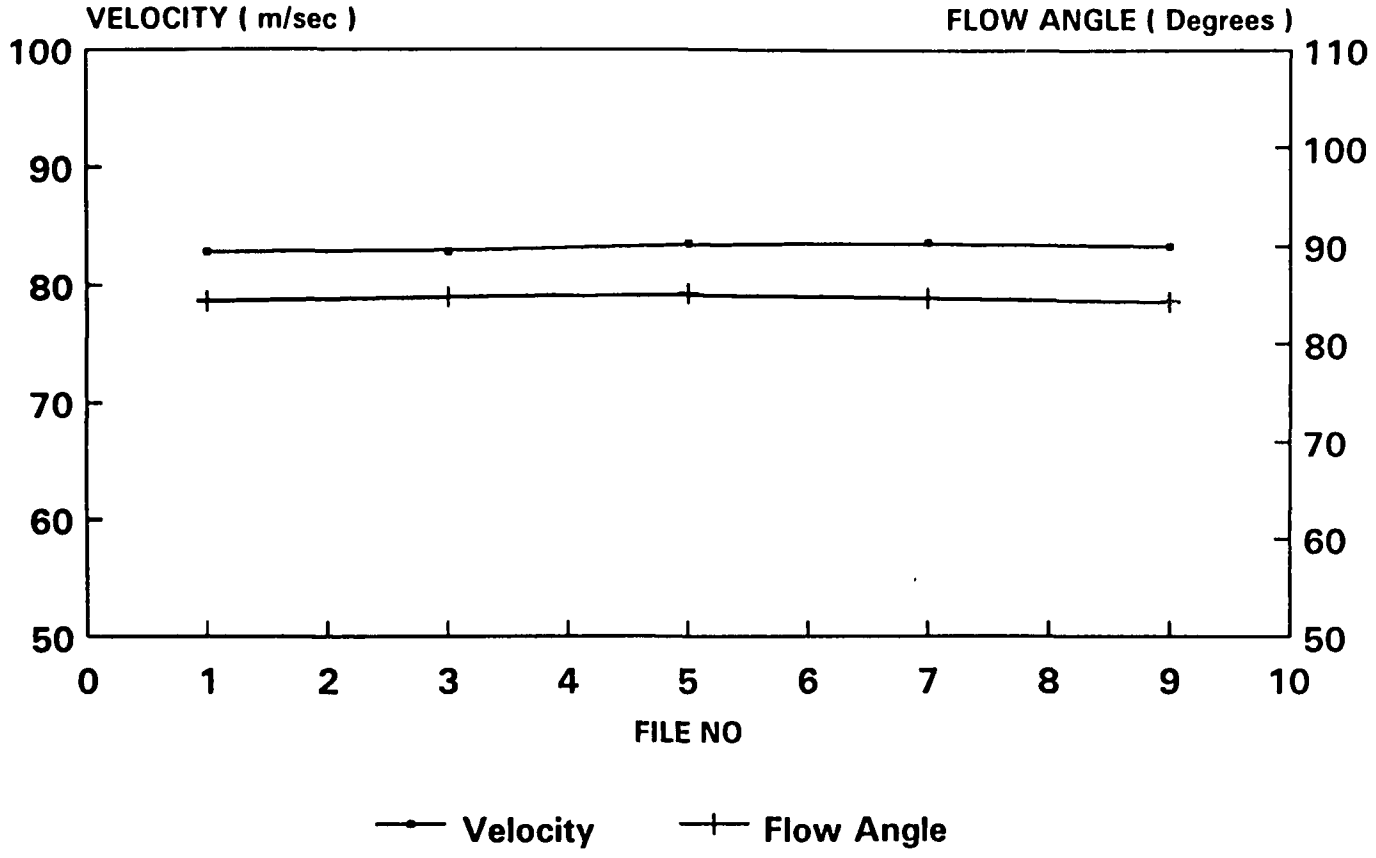

Fig 19 - Blade Strobed Results Downstream of Turbine at Station B
(PR = 3.5, U/V = 0.70 at Radius 21.95)

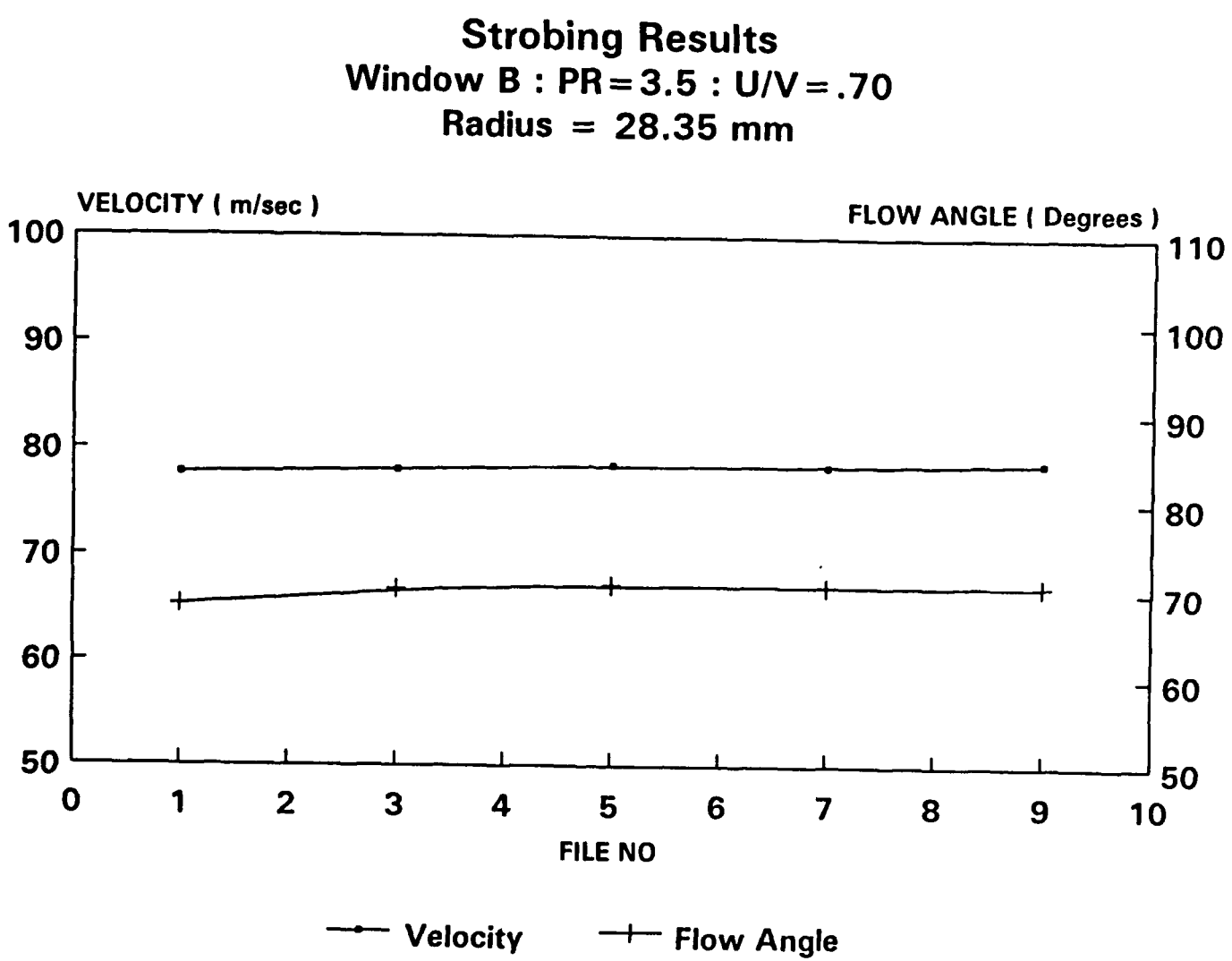

Fig 20 - Blade Strobed Results Downstream of Turbine at Station B
(PR = 3.5, U/V = 0.70 at Radius 28.35)

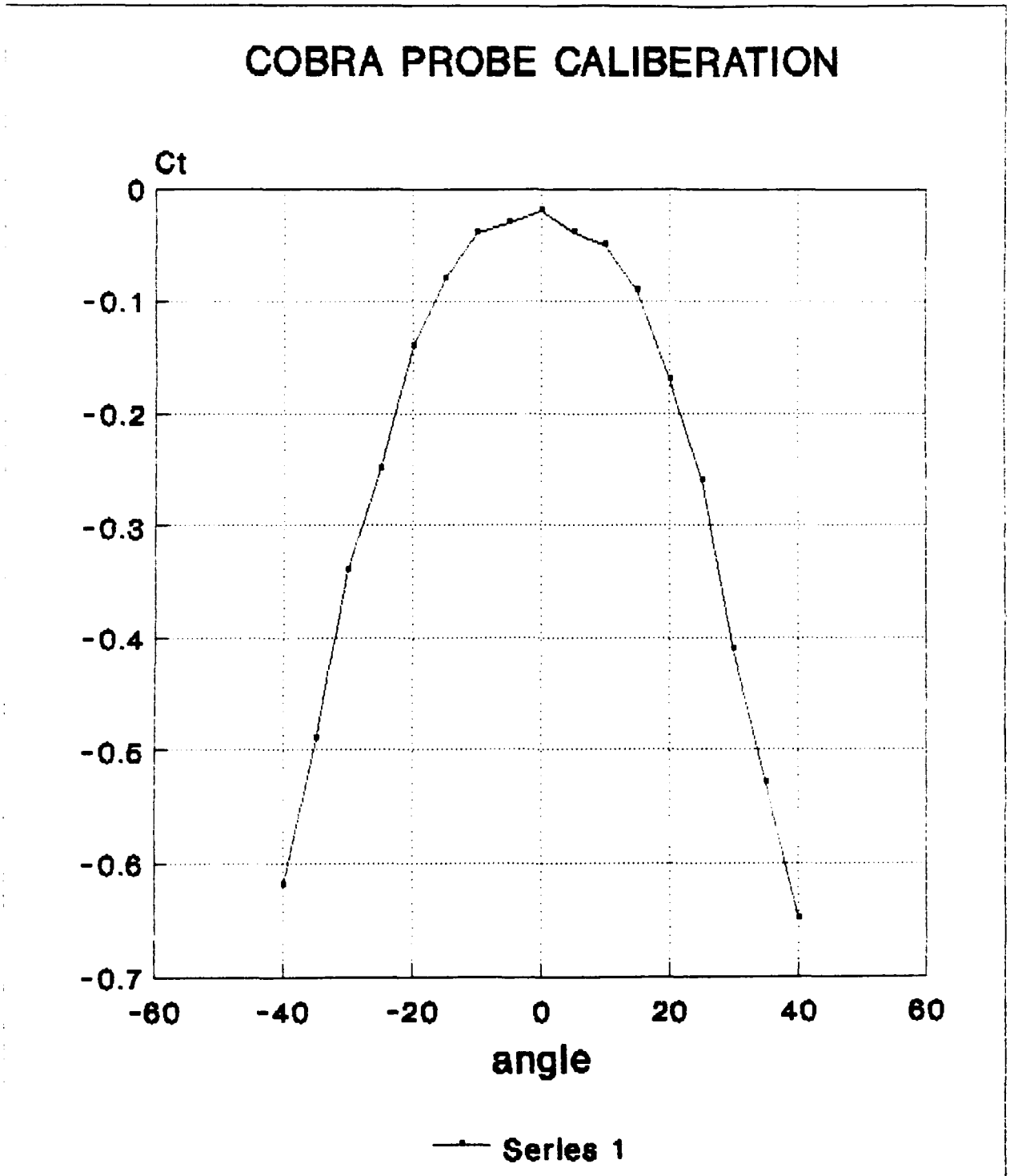

Fig 21 : Cobra probe calibration

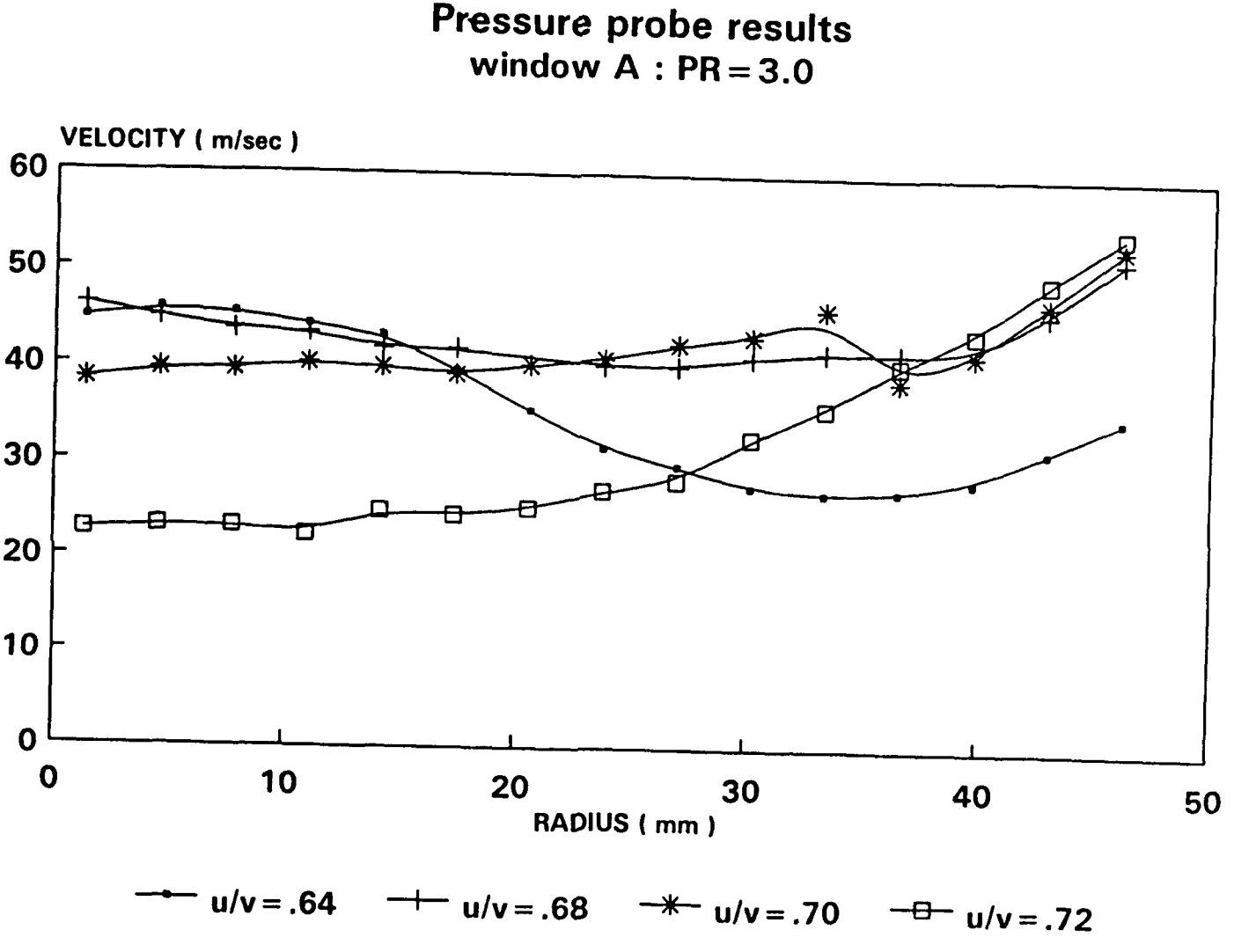

Fig 22 - Cobra Probe Results from Downstream of the Turbine at Station A (PR = 3.0)

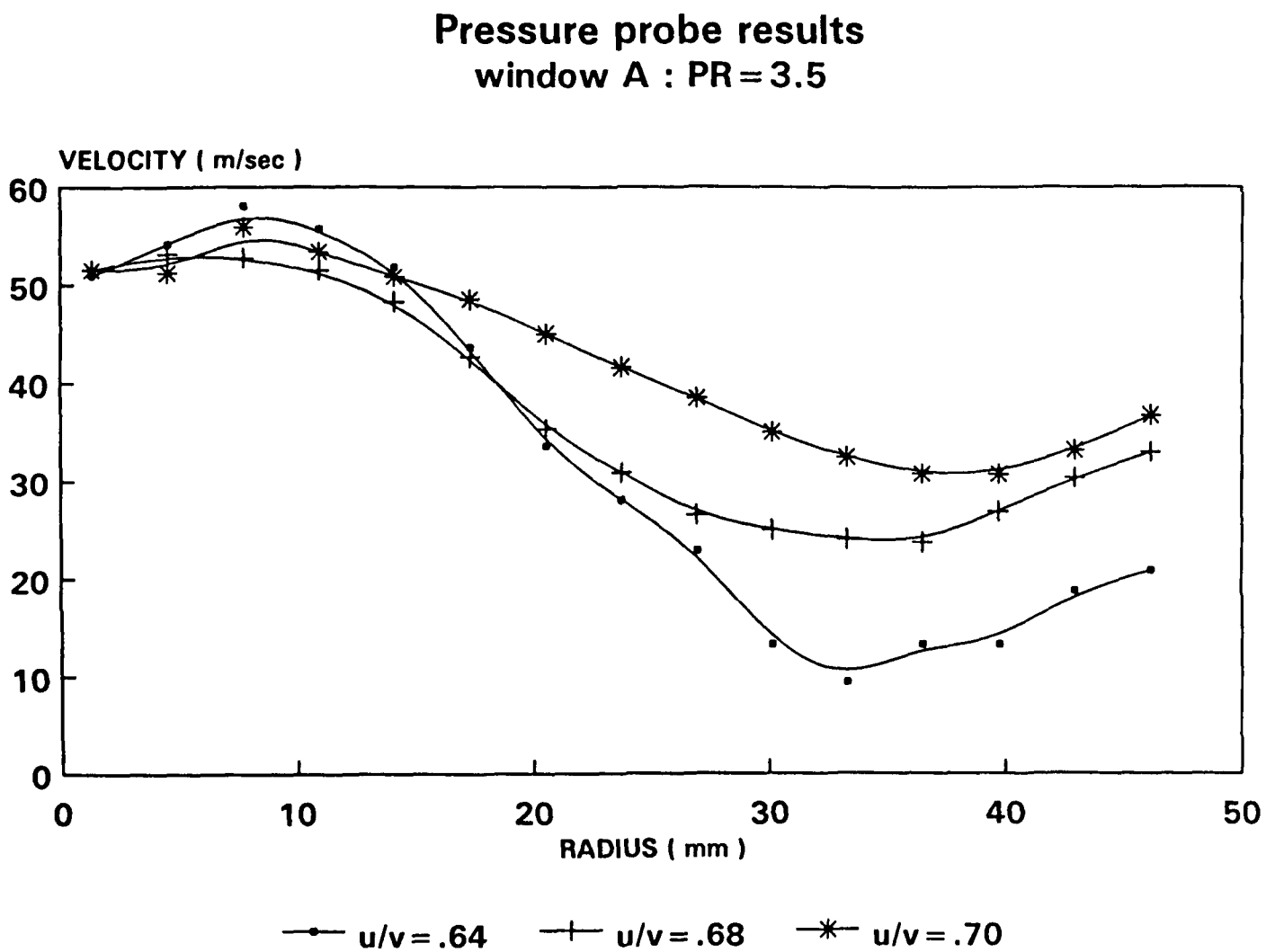

Fig 23 - Cobra Probe Results from Downstream of the Turbine at Station A (PR = 3.5)

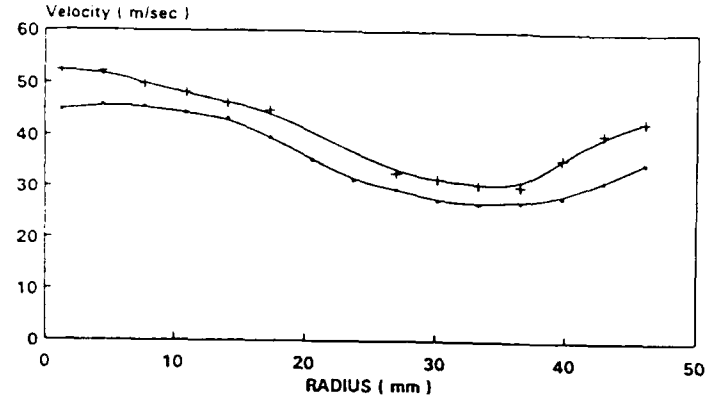

PR = 3.0 U/V = .64

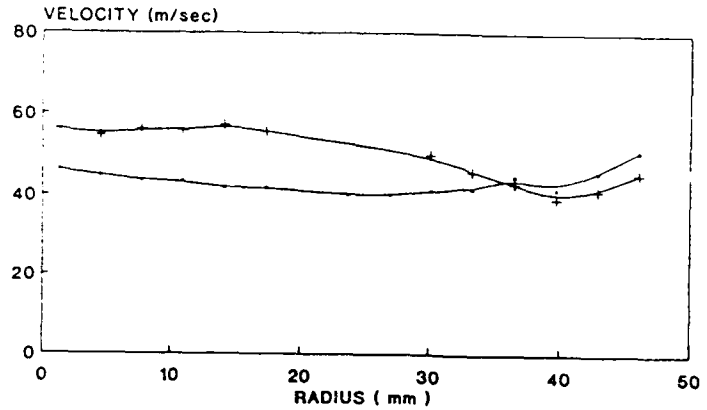

PR = 3.0 U/V = .68

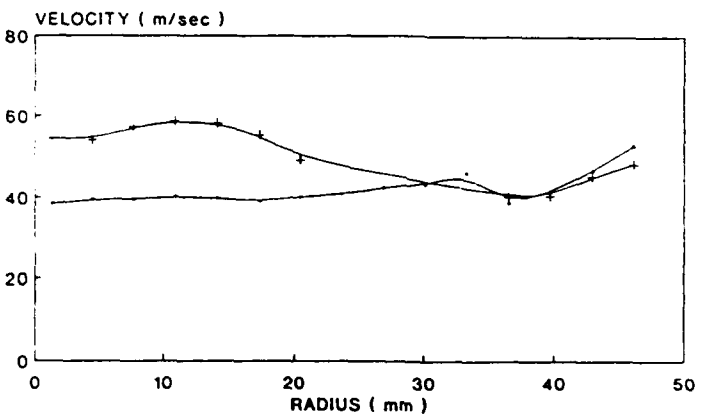

PR = 3.0 U/V = .70

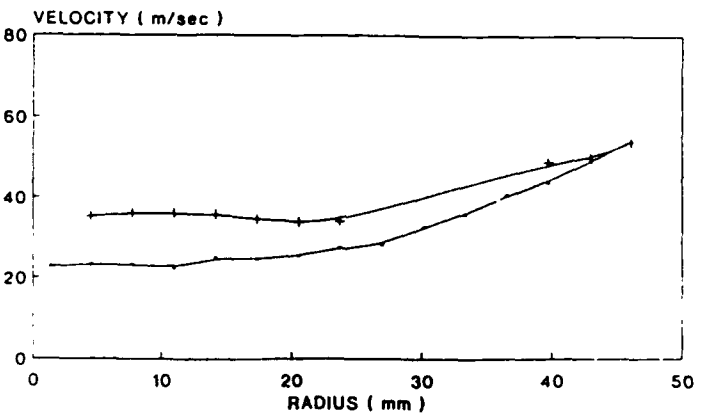

. Cobra
+ Laser

PR = 3.0 U/V = .72

Fig 24 - Laser Anemometry Results and Cobra Probe Results at Window A
(Velocity, PR=3.0)

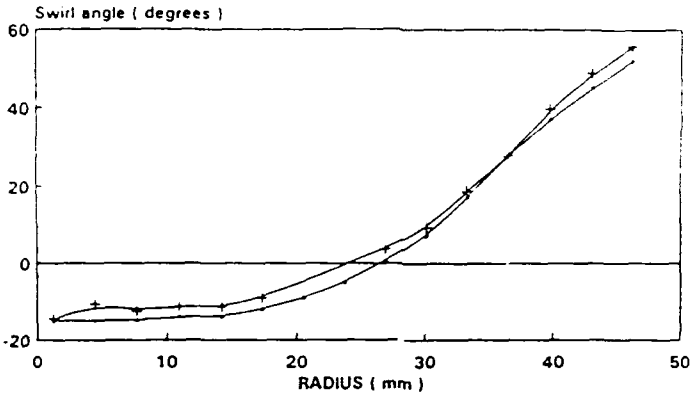

PR = 3.0 U/V = .64

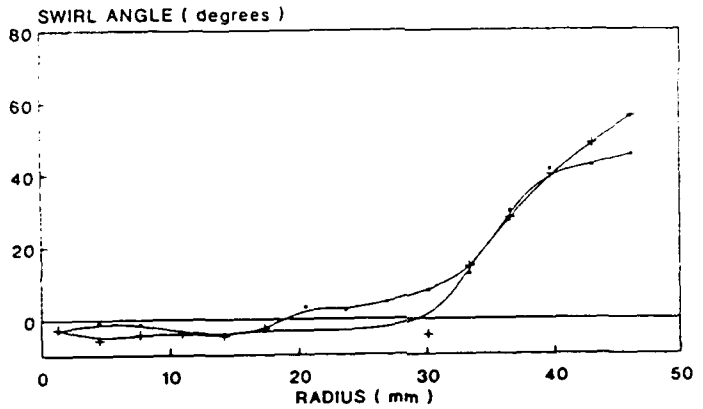

PR = 3.0 U/V = .68

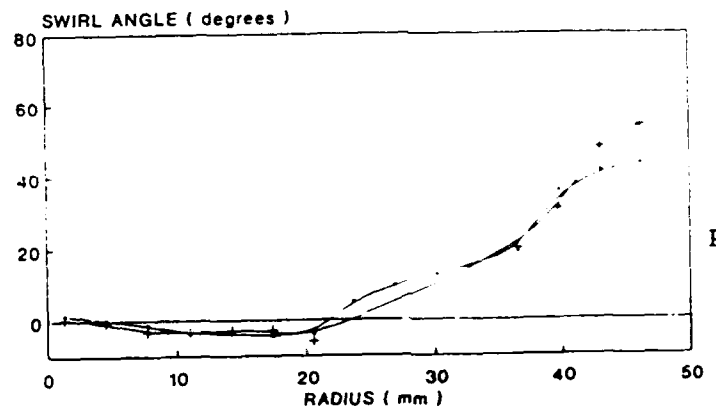

PR = 3.0 U/V = .70

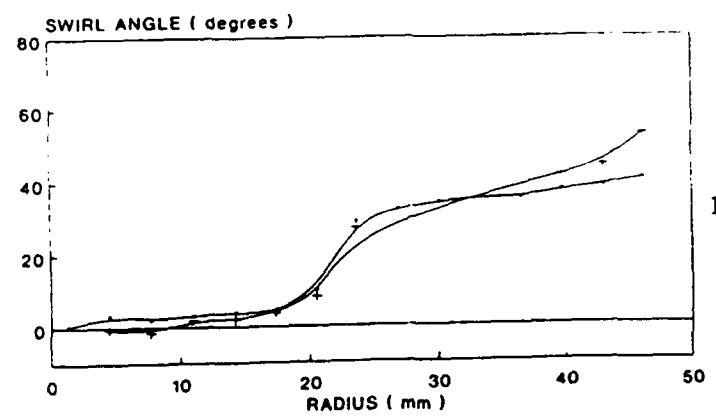

PR = 3.0 U/V = .72

. Cobra
+ Laser

Fig. 25 - Laser Anemometry Results and Cobra Probe Results at Window A

(Flow angle, PR= 3.0)

Window A : PR = 3.5 : U/V = .64

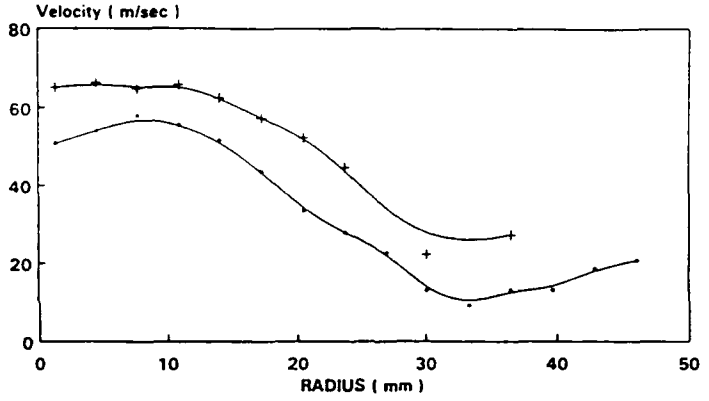

Window A : PR = 3.5 : U/V = .68

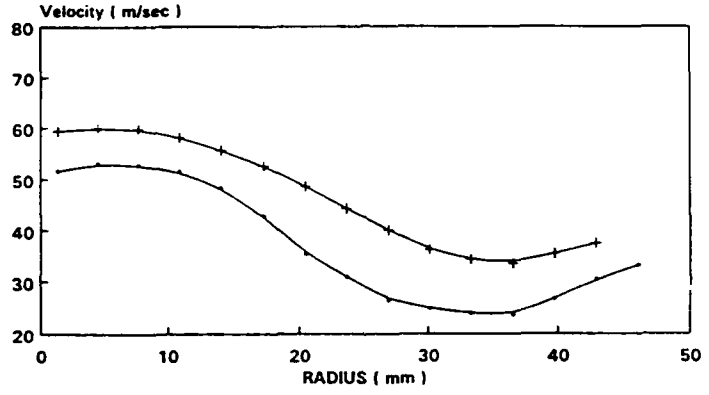

Window A : PR = 3.5 : U/V = .70

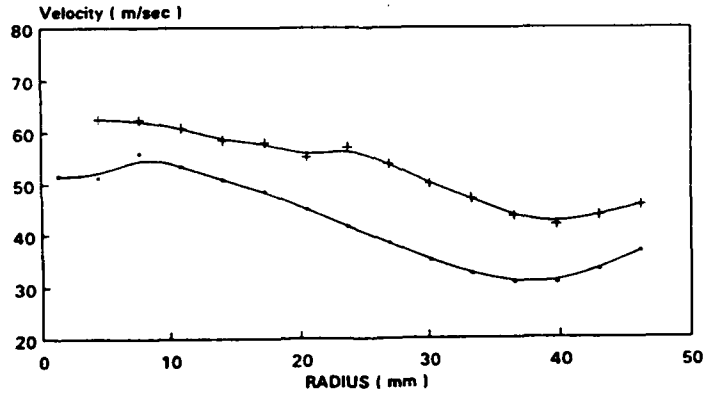

. Cobra
+ Laser

Fig 26 - Laser Anemometry Results and Cobra Probe Results at Window A
(Velocity, PR= 3.5)

Window A : PR = 3.5 : U/V = .64

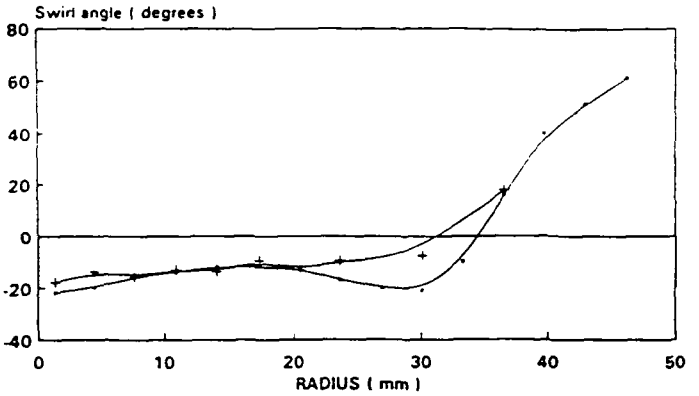

Window A : PR = 3.5 : U/V = .68

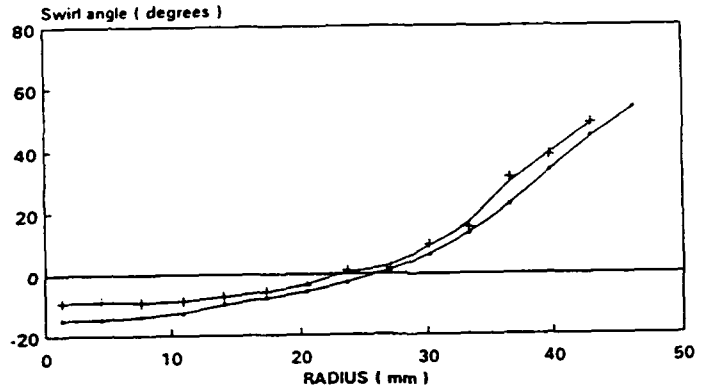

Window A : PR = 3.5 : U/V = .70

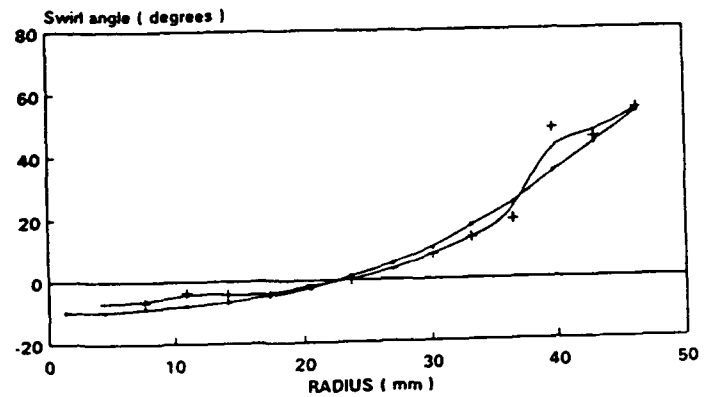

. Cobra
+ Laser

Fig 27 - Laser Anemometry Results and Cobra Probe Results at Window A
(Flow angle, PR= 3.5)

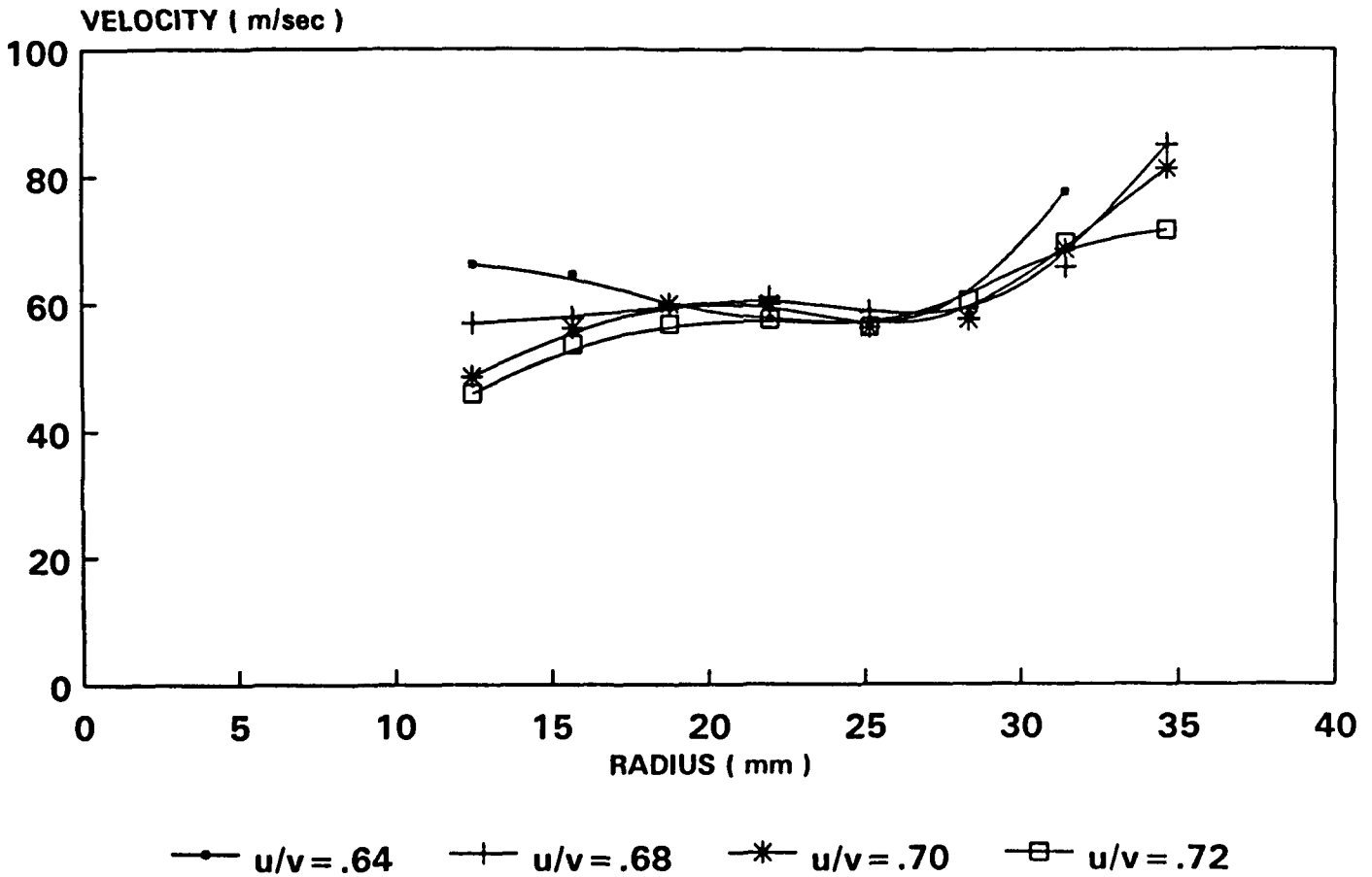

Fig 28 - Cobra Probe Results Downstream of the Turbine at Station B
(PR = 3.0)

WINDOW B

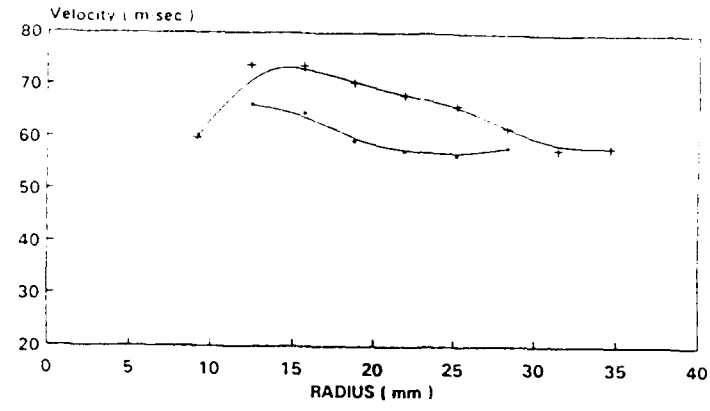

PR = 3.0 U/V = .64

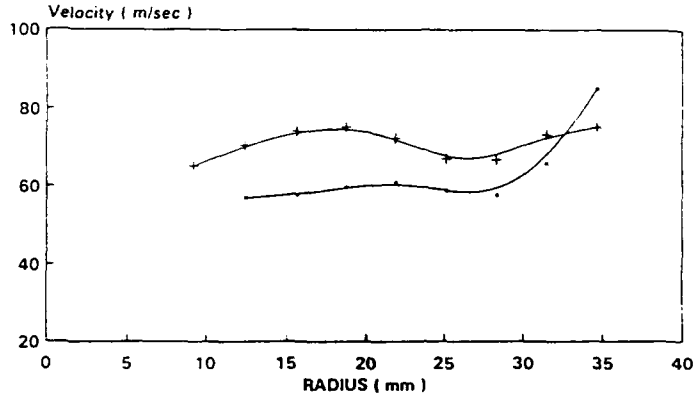

PR = 3.0 U/V = .68

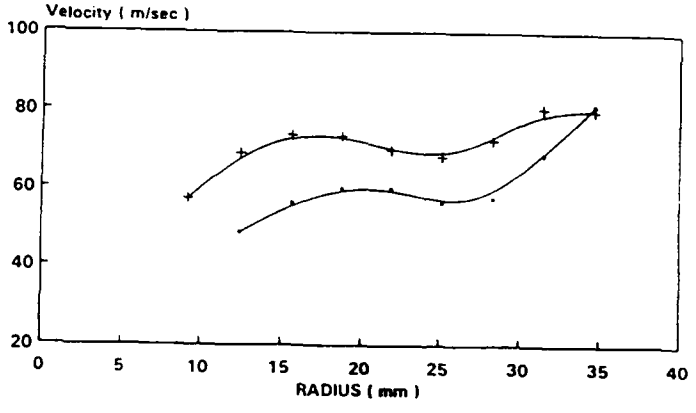

PR = 3.0 U/V = .70

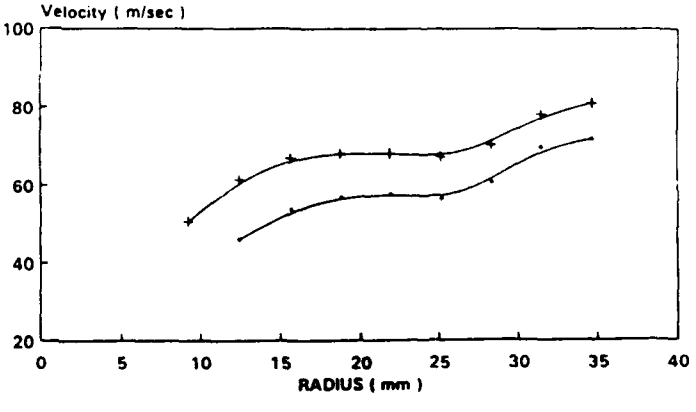

PR = 3.0 U/V = .72

. Cobra
+ Laser

Fig 29 - Laser Anemometry Results and Cobra Probe Results at Window B

(Velocity, PR= 3.0)

WINDOW B

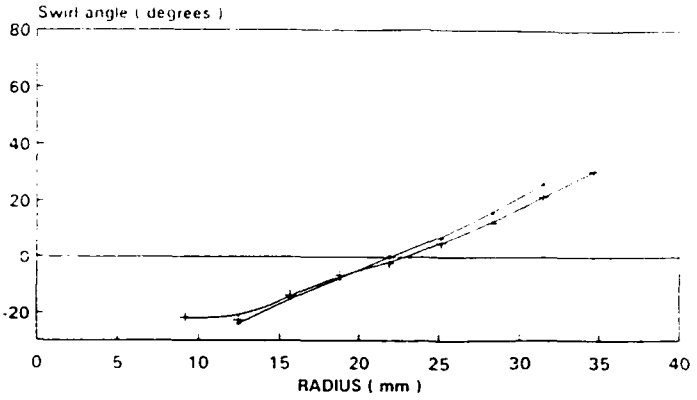

PR = 3.0 U/V = .64

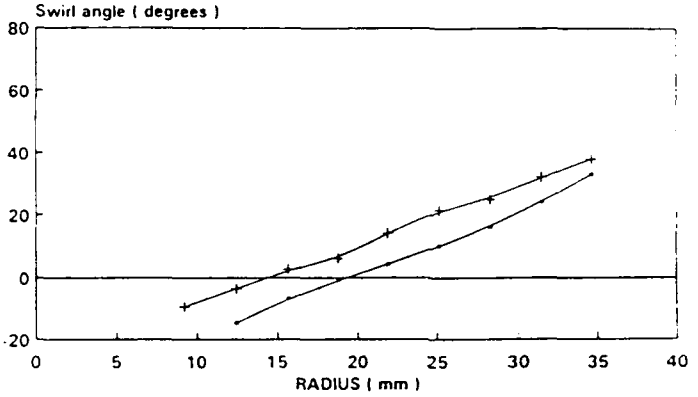

PR = 3.0 U/V = .68

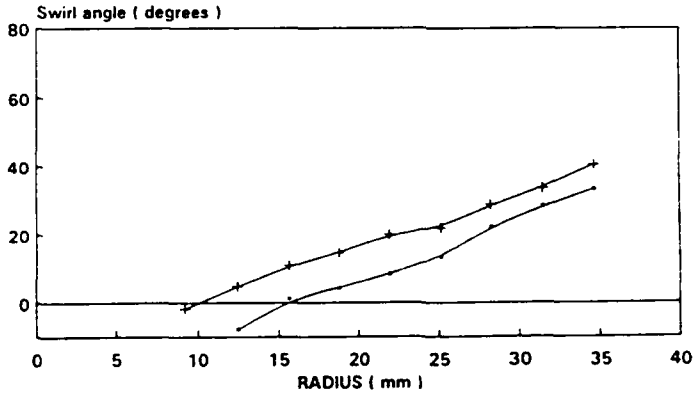

PR = 3.0 U/V = .70

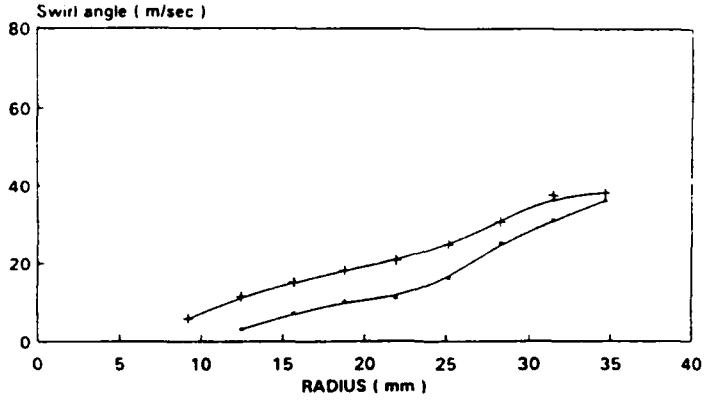

PR = 3.0 U/V = .72

. Cobra
+ Laser

Fig 30 - Laser Anemometry Results and Cobra Probe Results at Window B

(Flow angle, PR= 3.0)

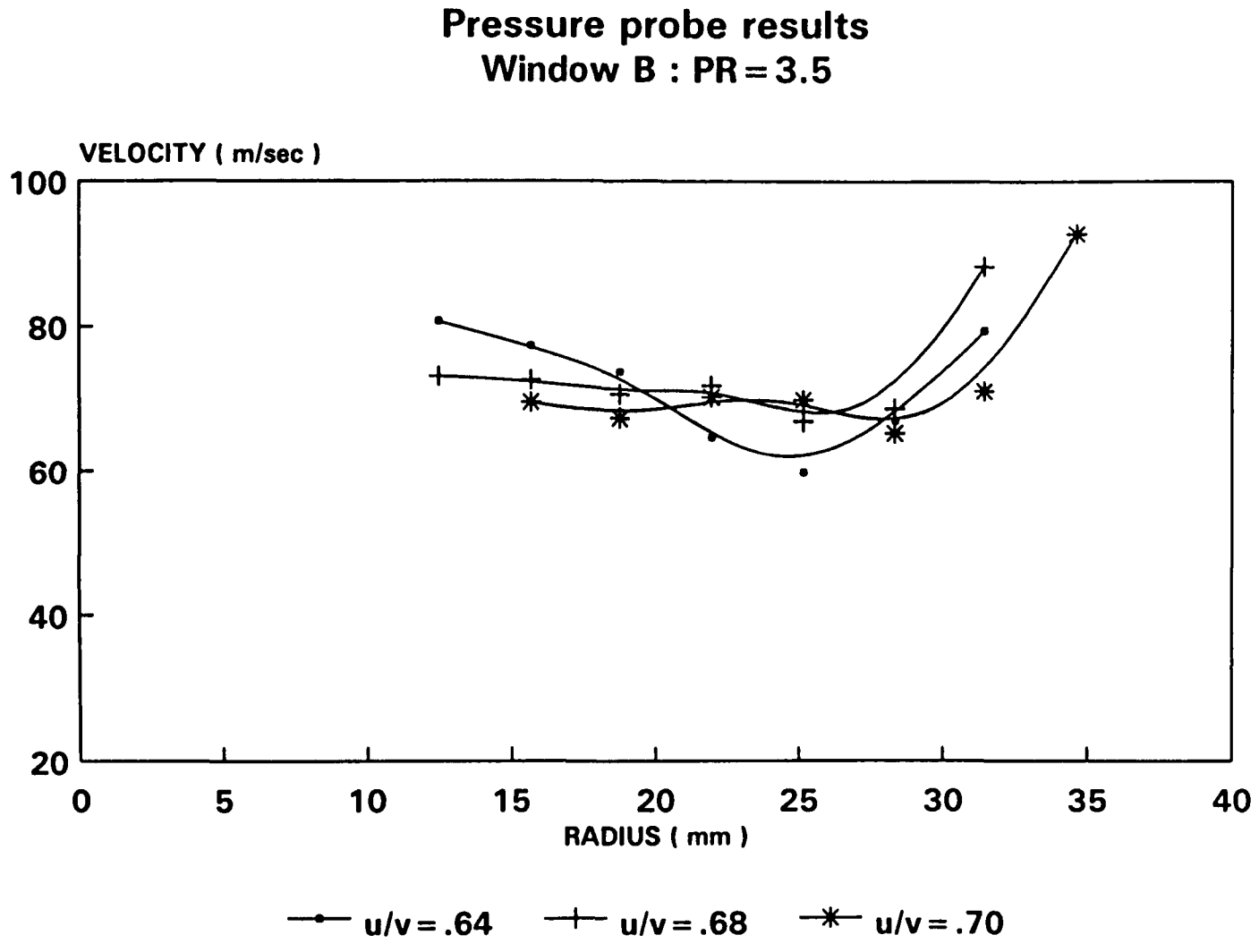

Fig 31 - Cobra Probe Results Downstream of the Turbine at Station B
(PR = 3.5)

Window B : PR = 3.5 : U/V = .64

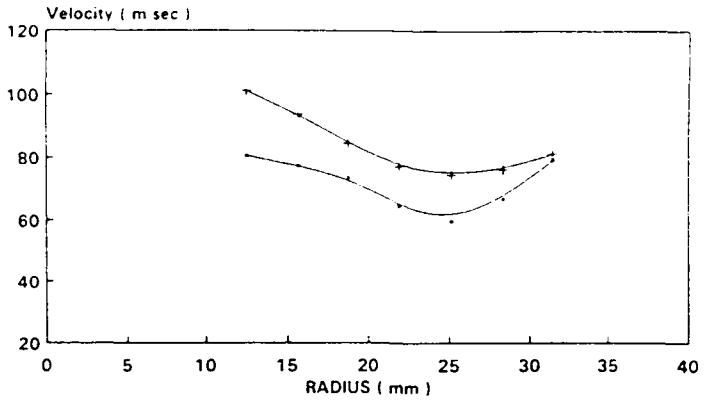

Window B : PR = 3.5 : U/V = .68

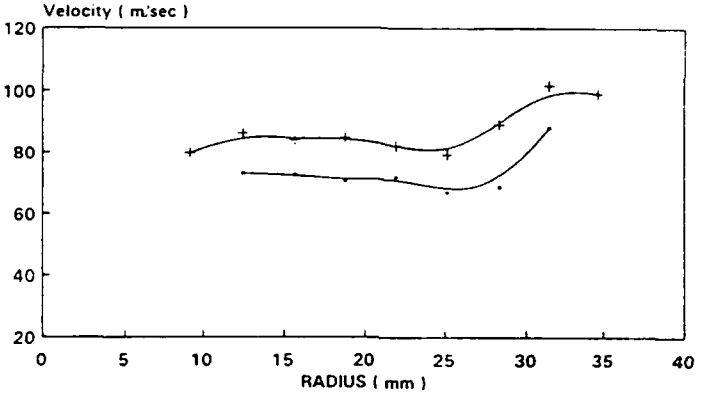

Window B : PR = 3.5 : U/V = .70

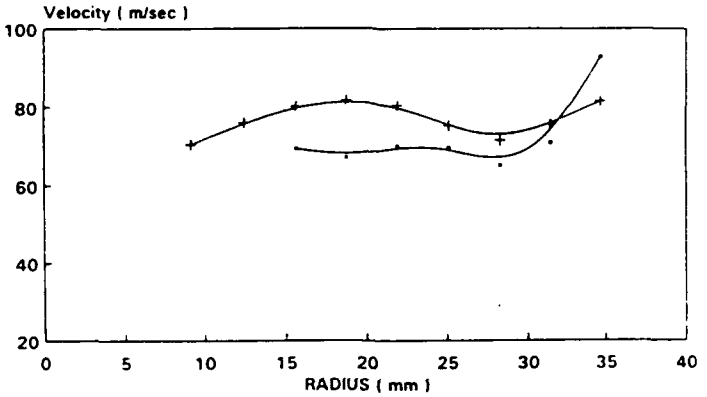

. Cobra
+ Laser

Fig 32 - Laser Anemometry Results and Cobra Probe Results at Window B

(Velocity, PR= 3.5)

Window B : PR = 3.5 : U/V = .64

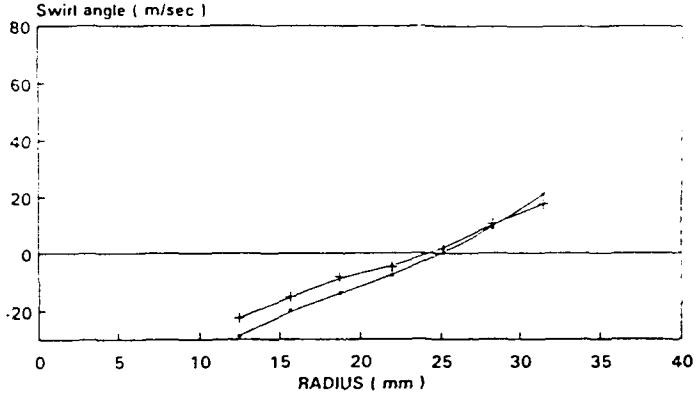

Window B : PR = 3.5 : U/V = .68

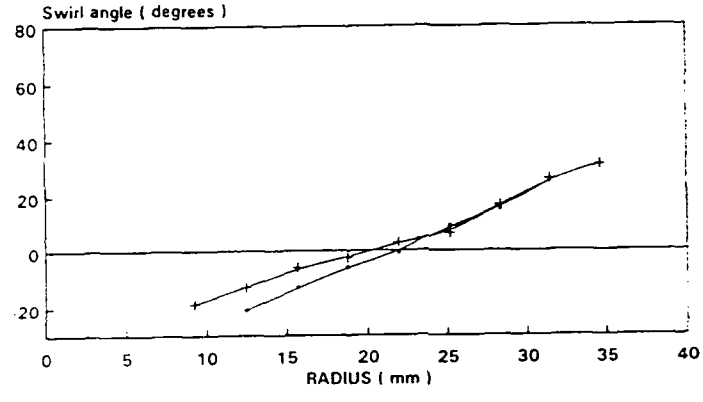

Window B : PR = 3.5 : U/V = .70

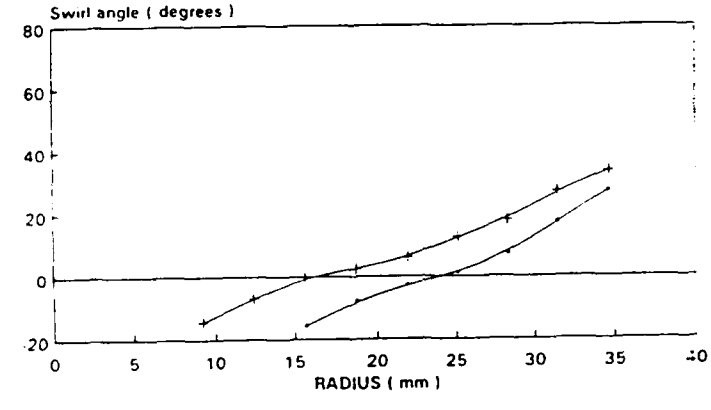

. Cobra
+ Laser

Fig 33 - Laser Anemometry Results and Cobra Probe Results at Window B
(Flow angle, PR= 3.5)

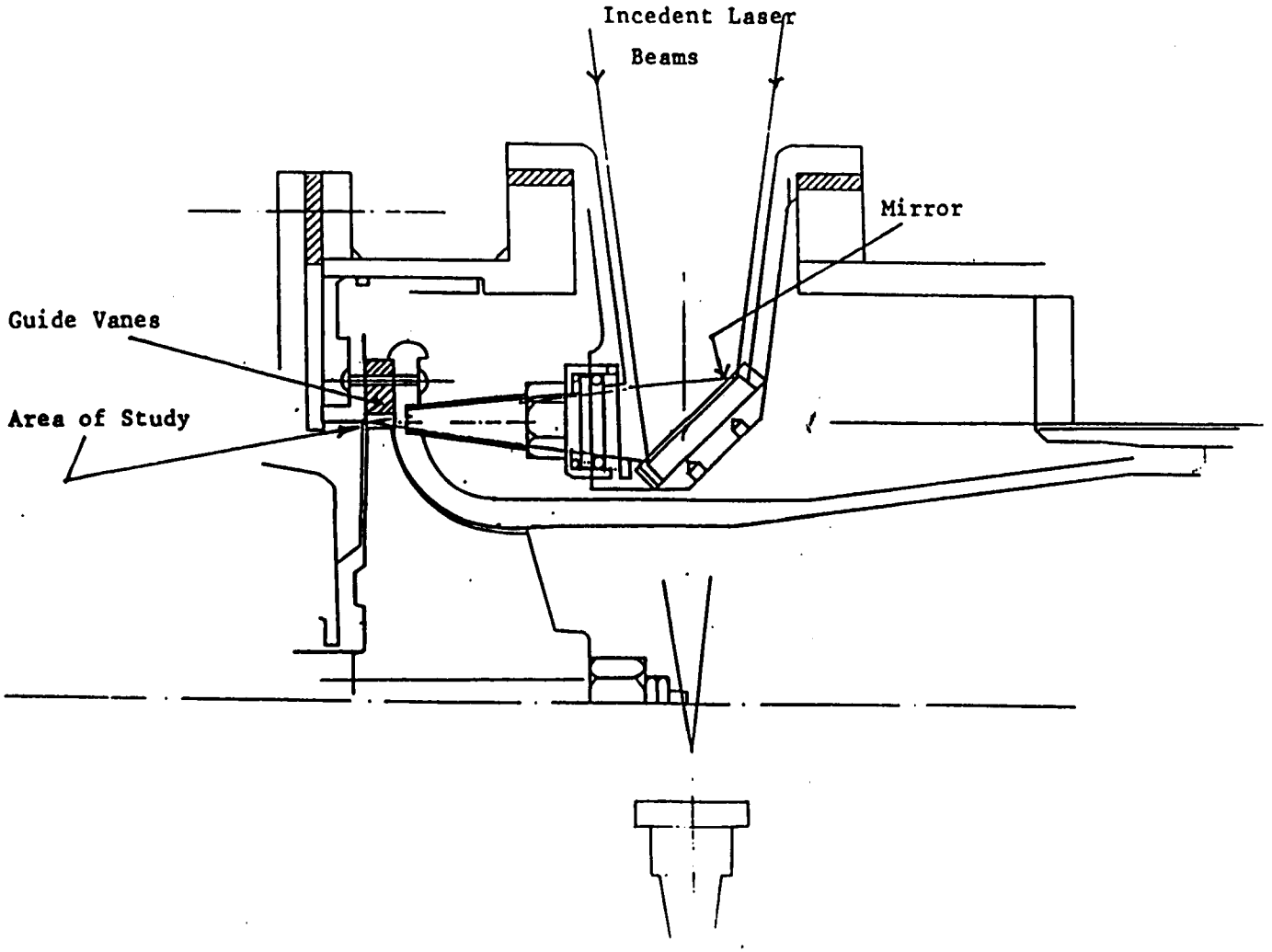

Fig 34 : Laser Anemometry setup to take measurements at the turbine rotor inlet.

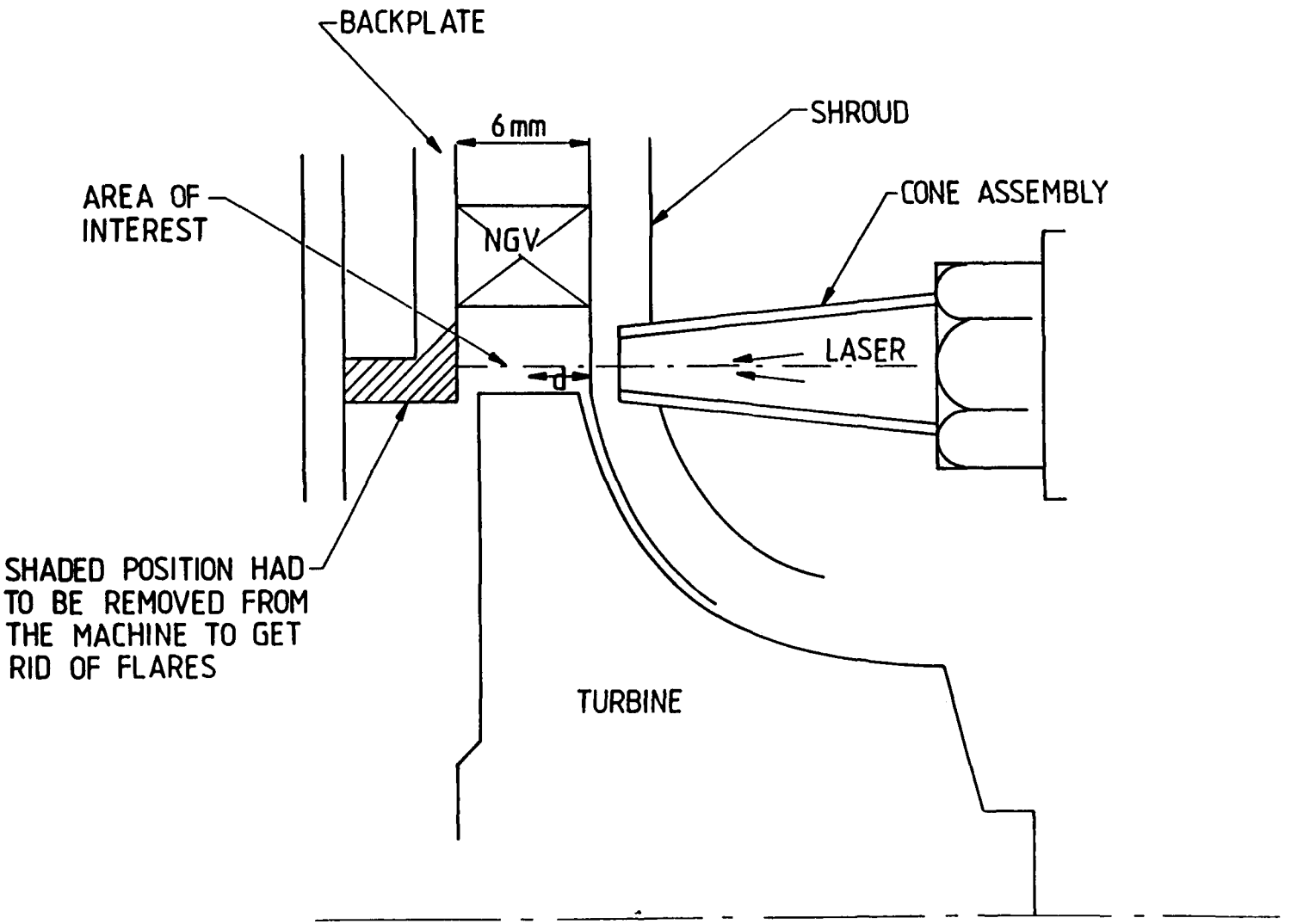

Fig 35 - Definition of d in the passage between nozzle vanes and turbine wheel

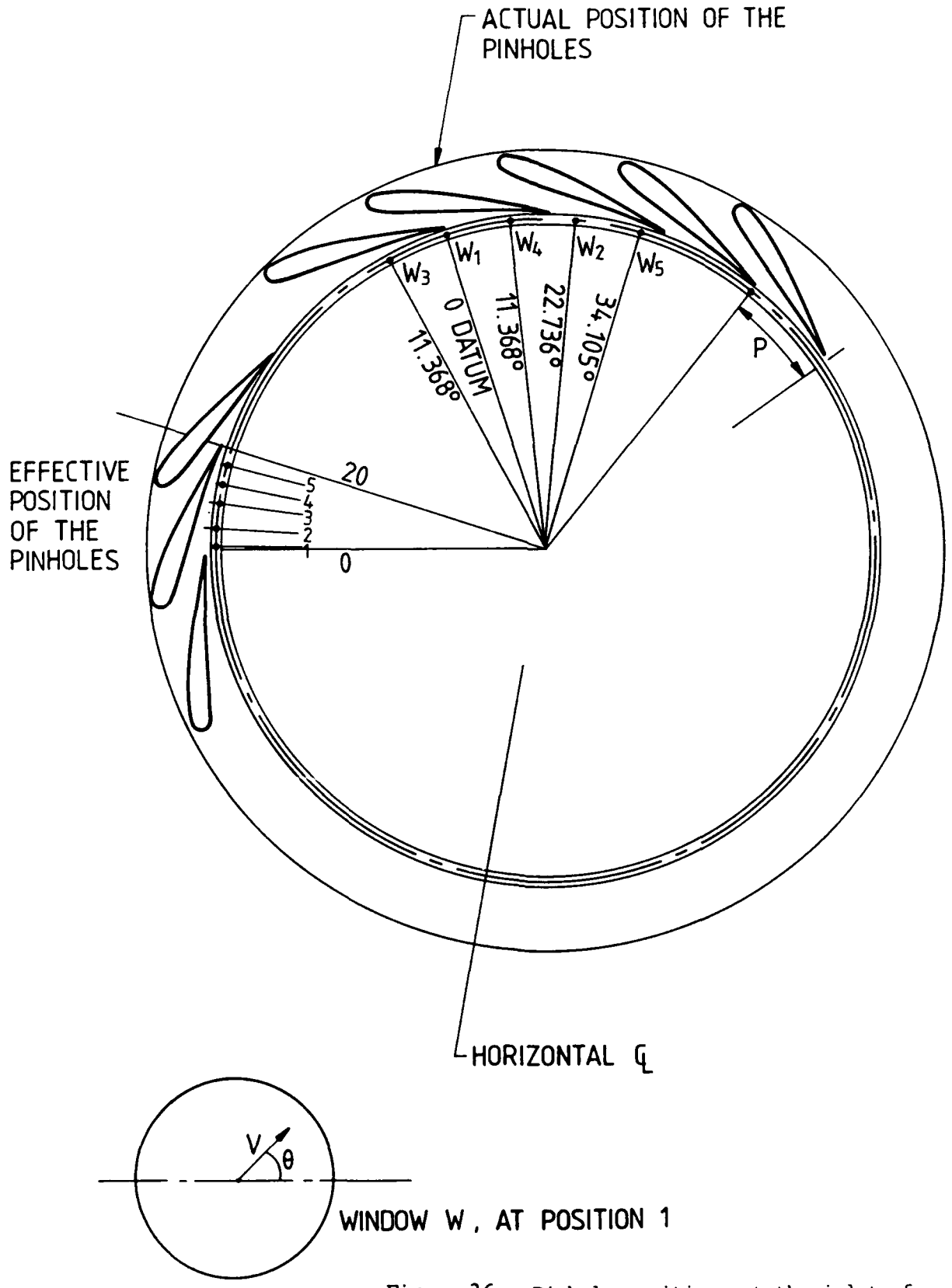

Figure 36 - Pinhole positions at the inlet of the turbine for Laser Anemometry measurements

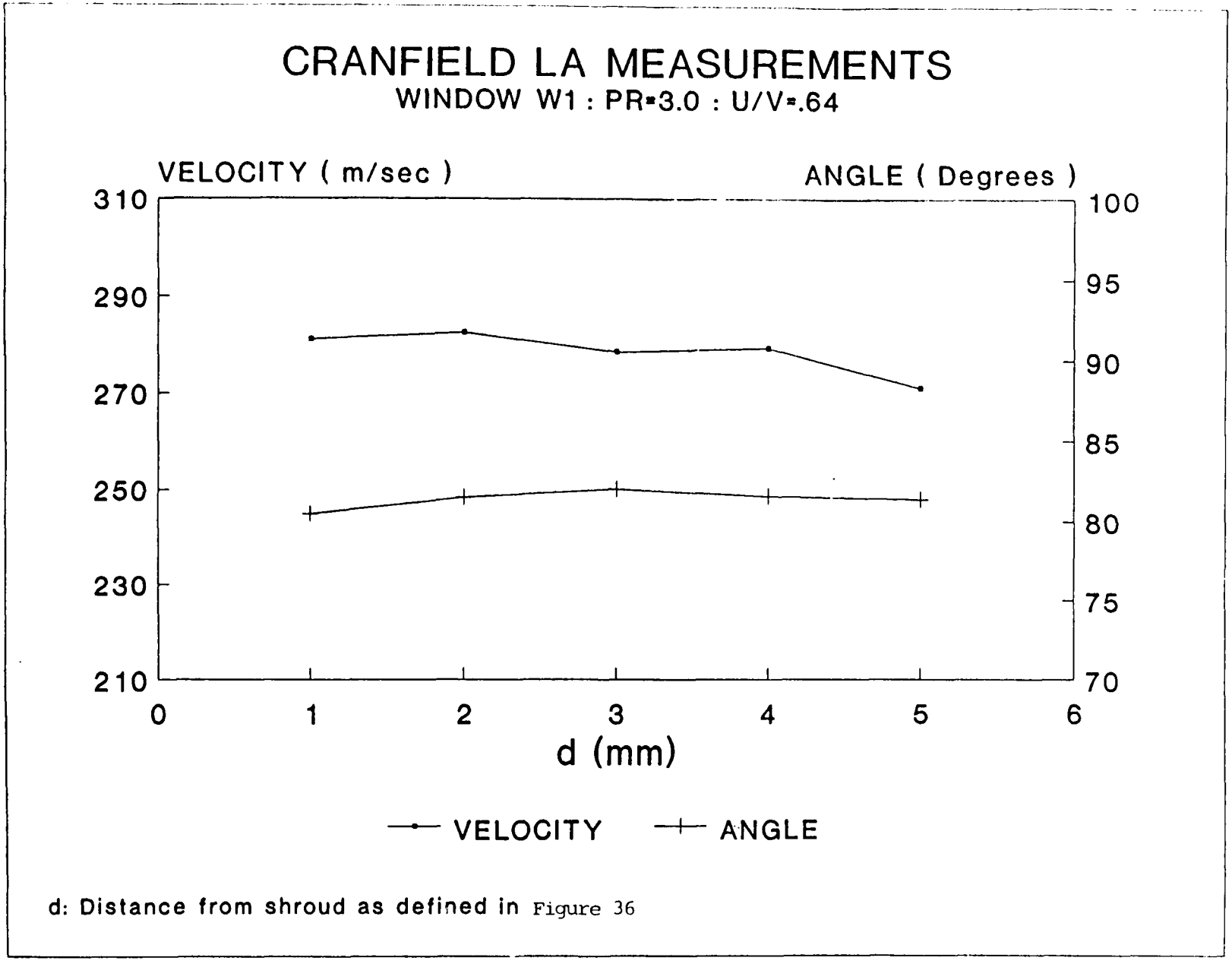

Fig 37 - Laser Anemometry Measurements between NGV and Rotor. (Window W1, PR = 3.0, U/V = .64)

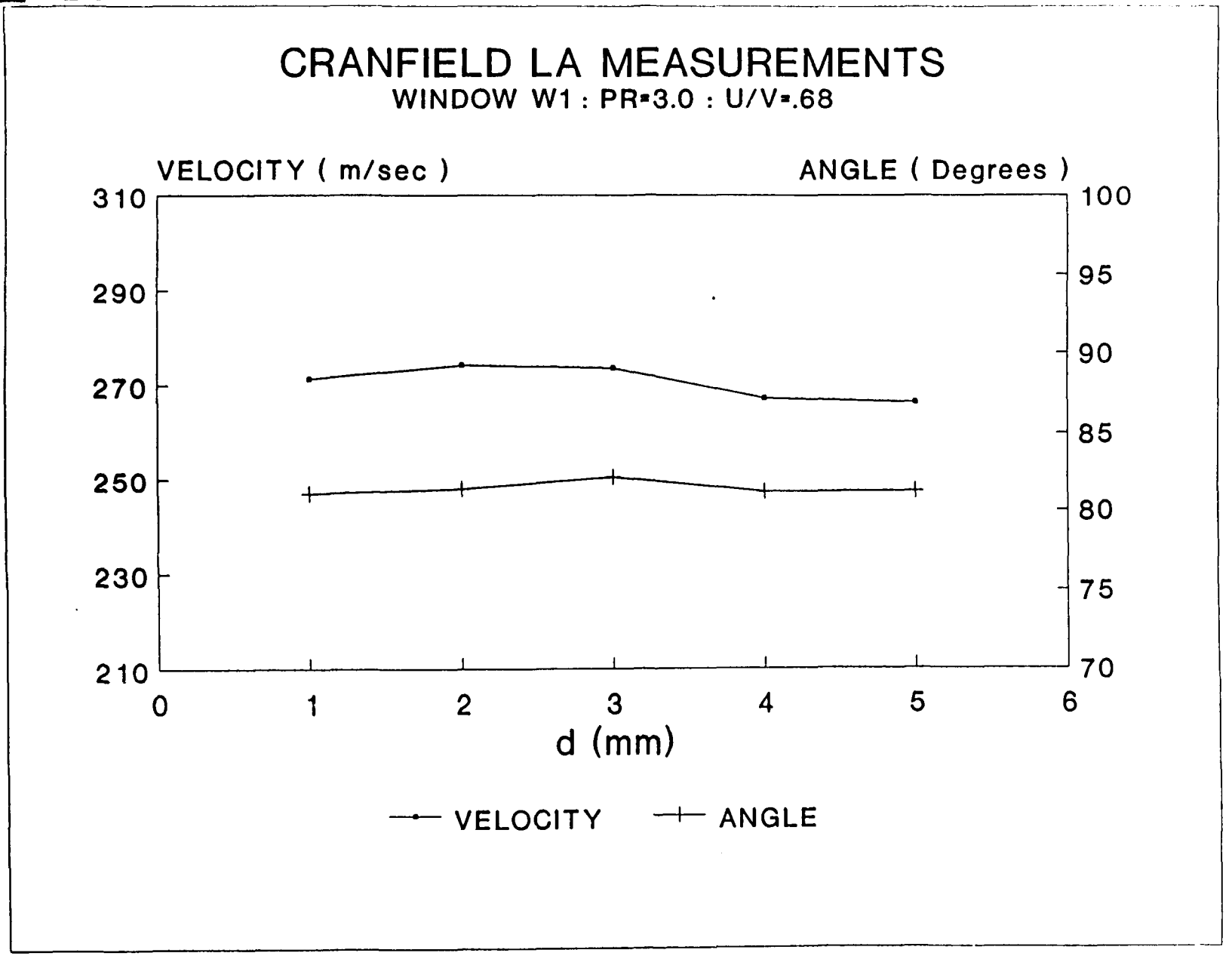

Fig 38 - Laser Anemometry Measurements between NGV and Rotor. (Window W1, PR = 3.0, U/V = .68)

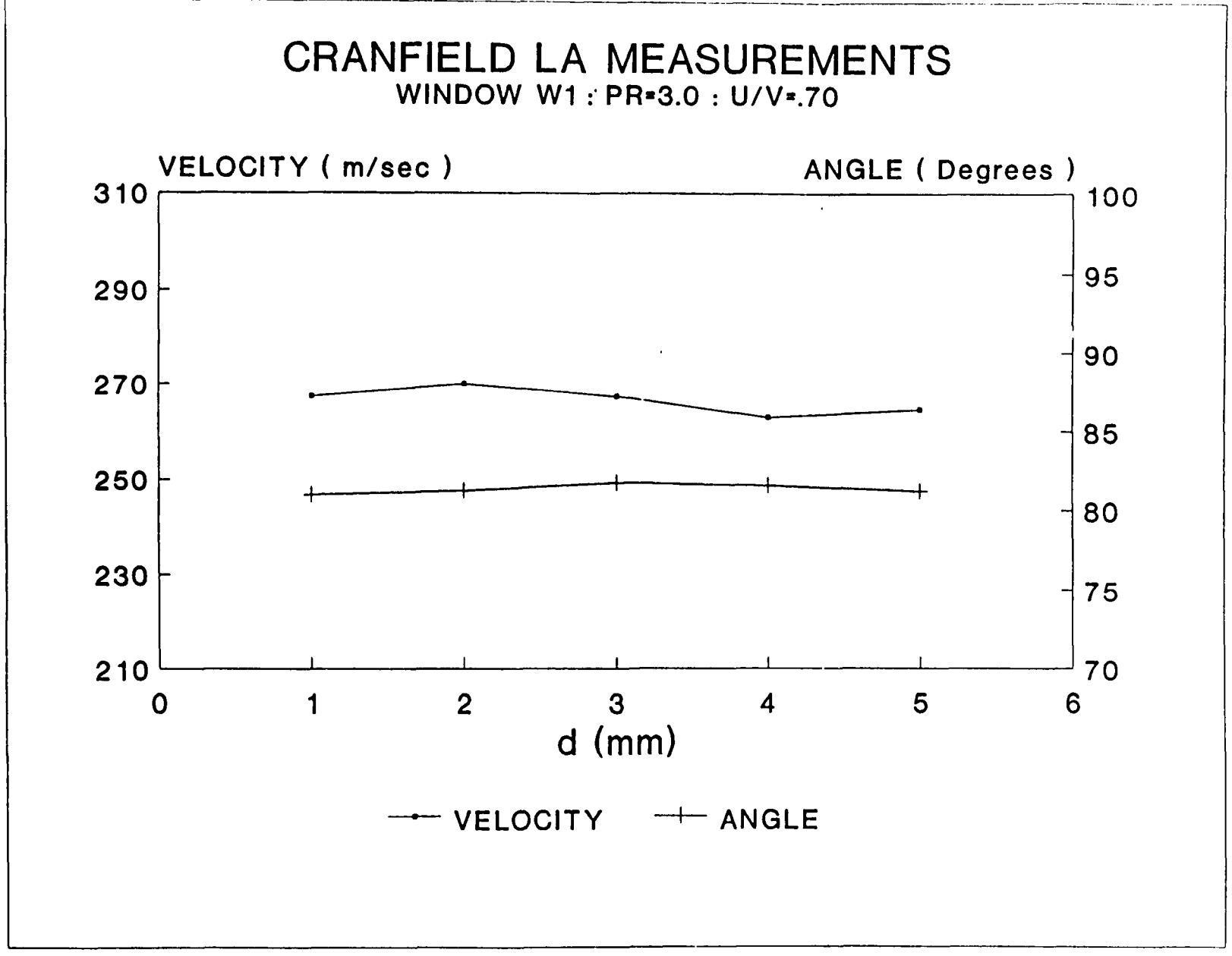

Fig 39 - Laser Anemometry Measurements between NGV and Rotor (Window W1, PR = 3.0, U/V = .70)

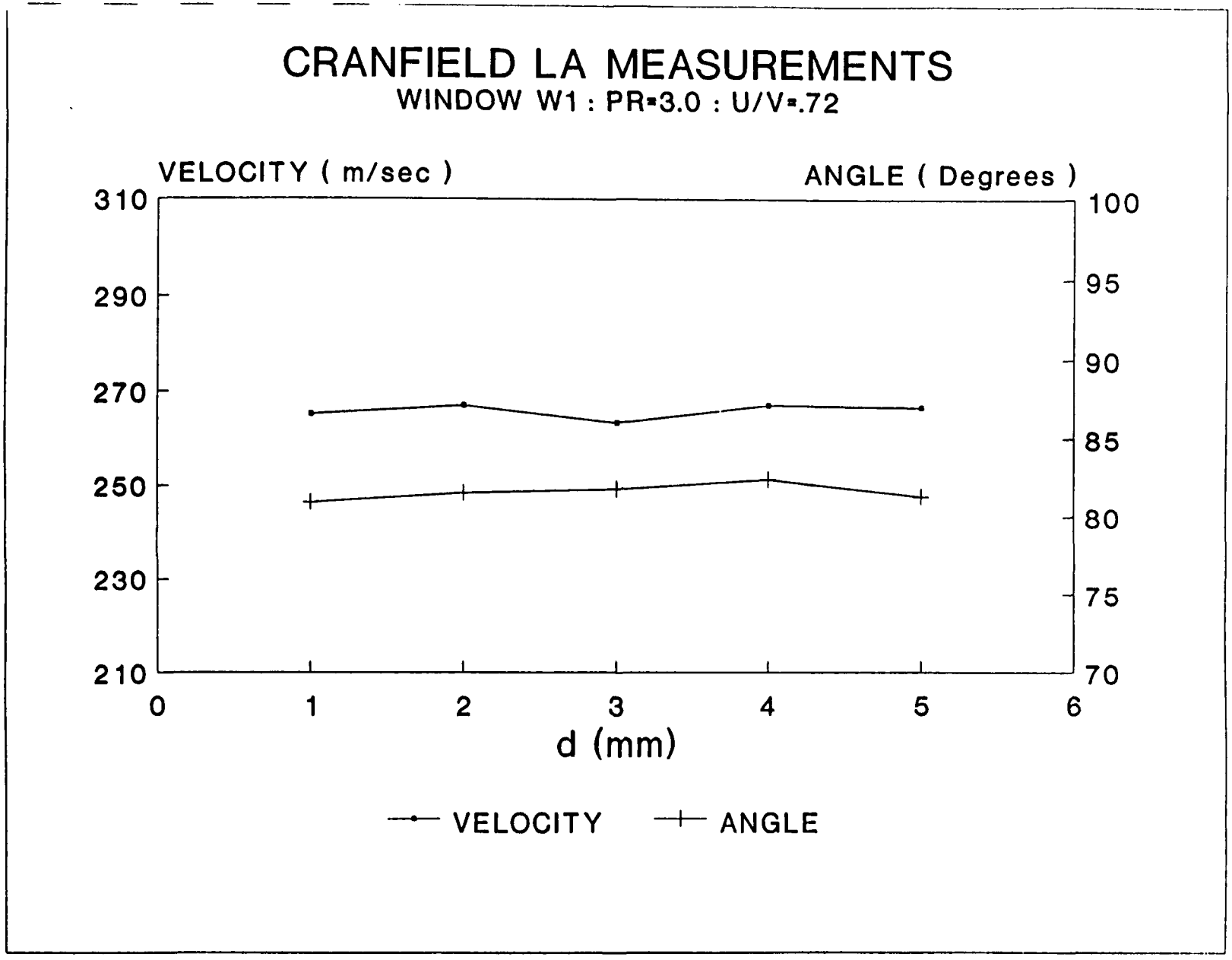

Fig 40 - Laser Anemometry Measurements between NGV and Rotor (Window W1, PR = 3.0, U/V = .72)

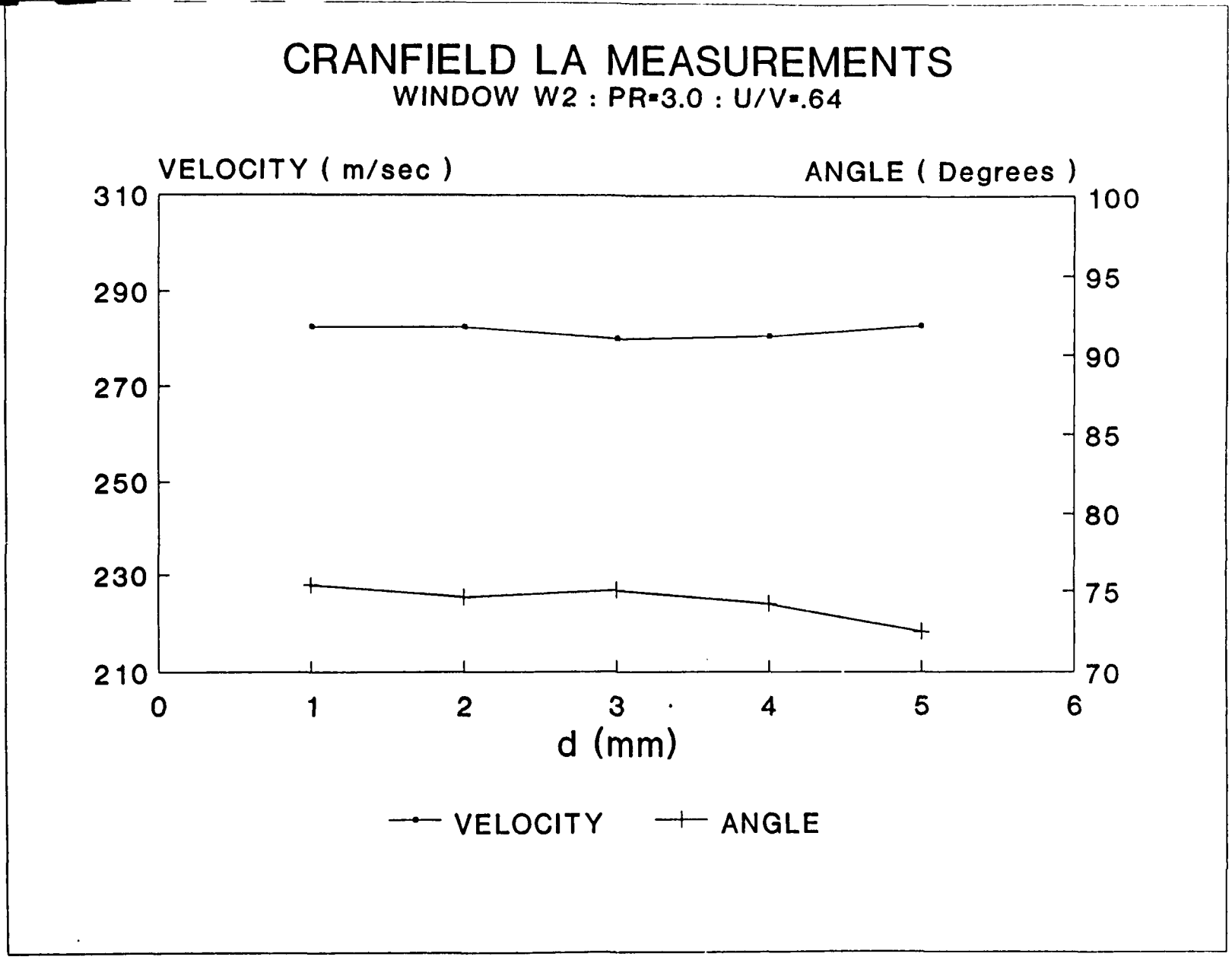

Fig 41 - Laser Anemometry Measurements between NGV and Rotor (Window W2, PR = 3.0, U/V = .64)

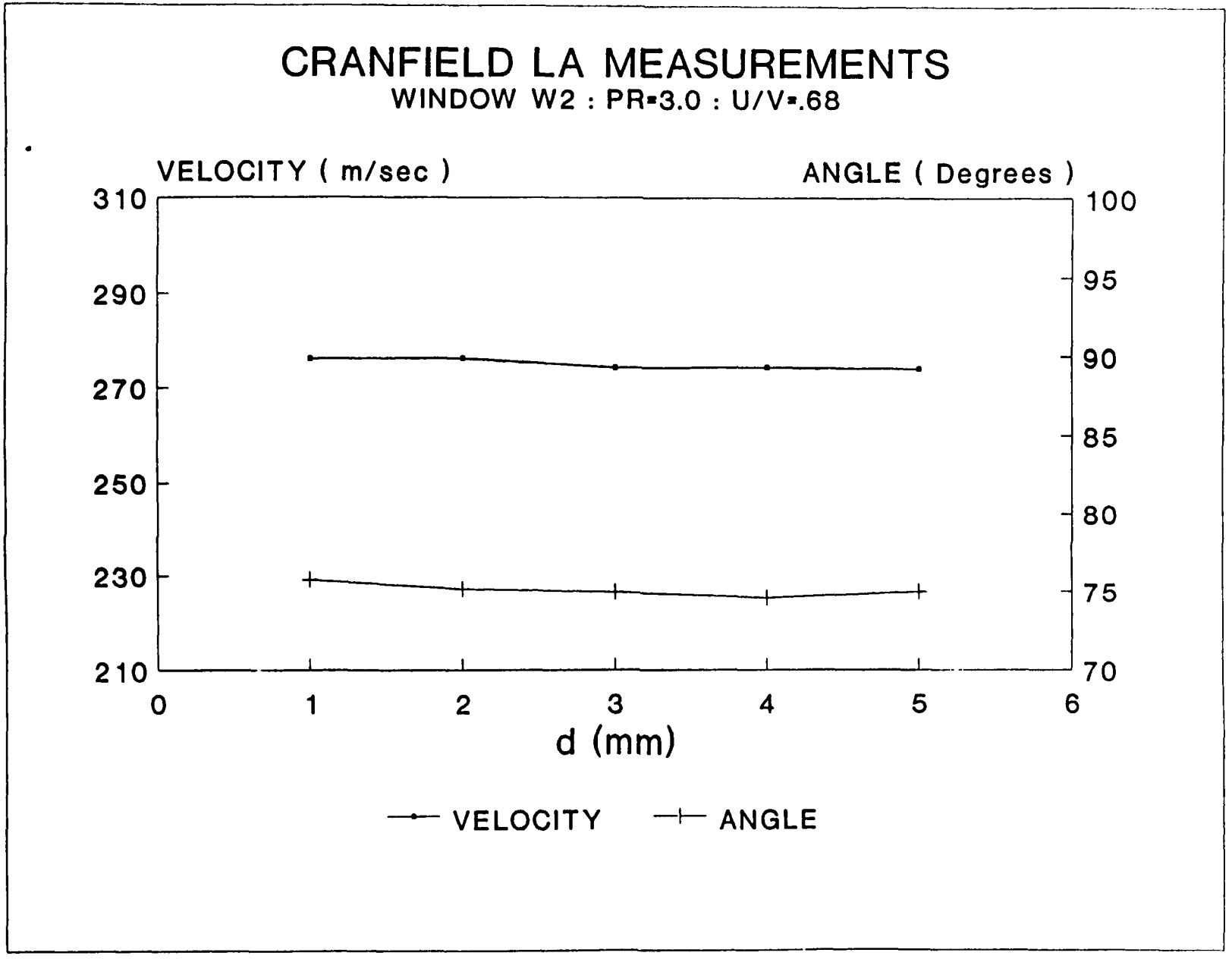

Fig 42 - Laser Anemometry Measurements between NGV and Rotor (Window W2, PR = 3.0, U/V = .68)

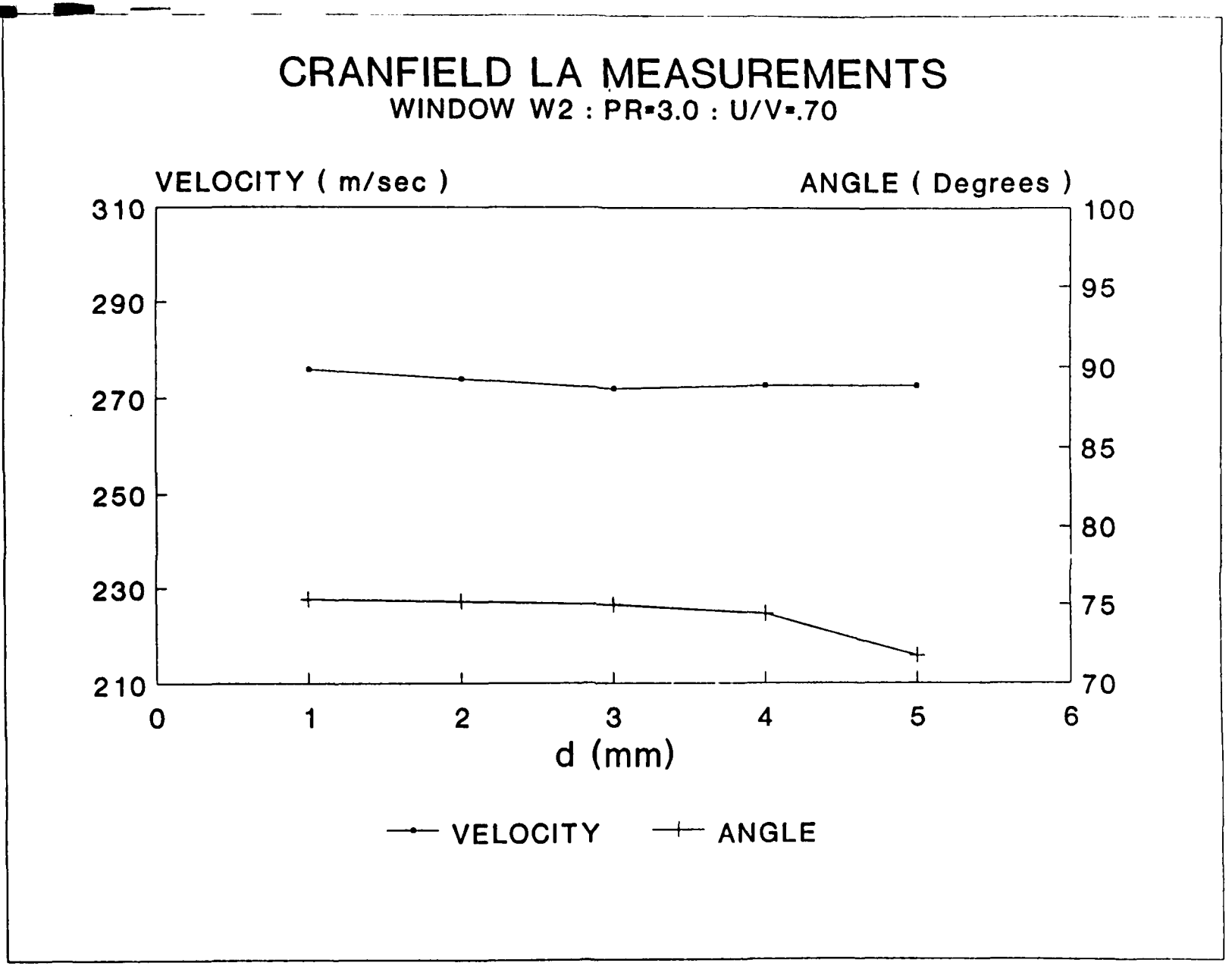

Fig 43 - Laser Anemometry Measurements between NGV and Rotor (Window W2, PR = 3.0, U/V = .70)

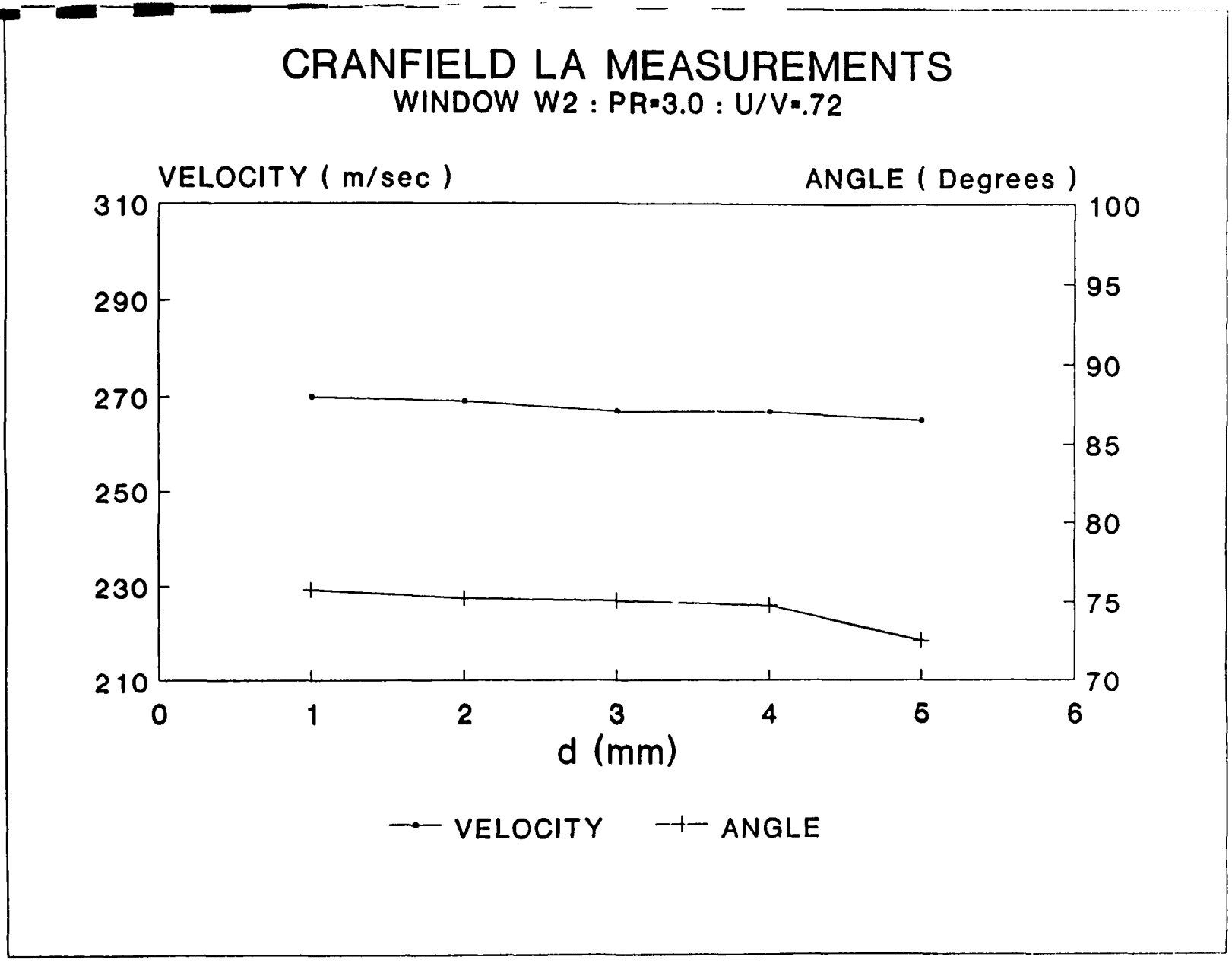

Fig 44 - Laser Anemometry Measurements between NGV and Rotor (Window W2, PR = 3.0, U/V = .72)

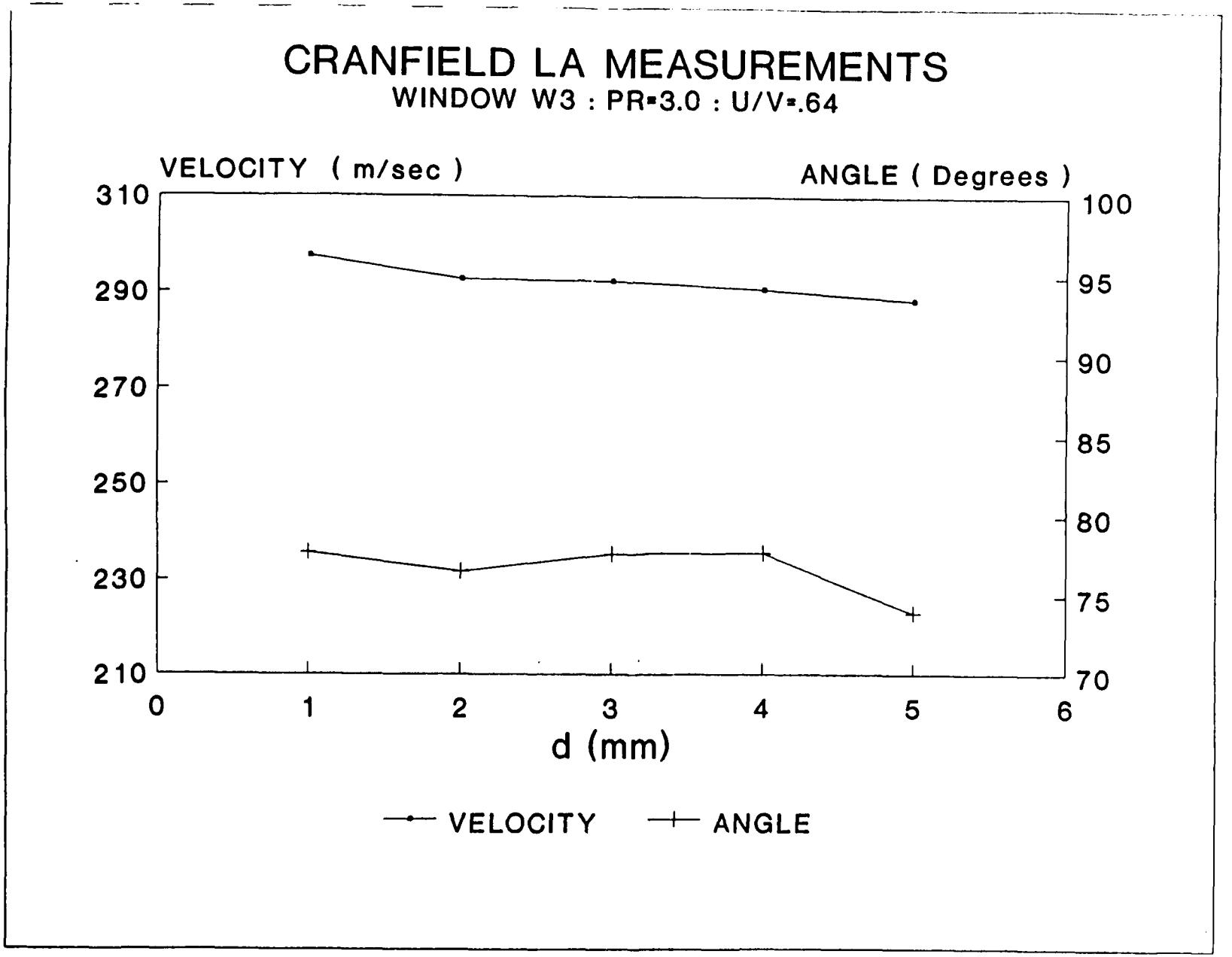

Fig 45 - Laser Anemometry Measurements between NGV and Rotor. (Window W3, PR=3.0, U/V=.68)

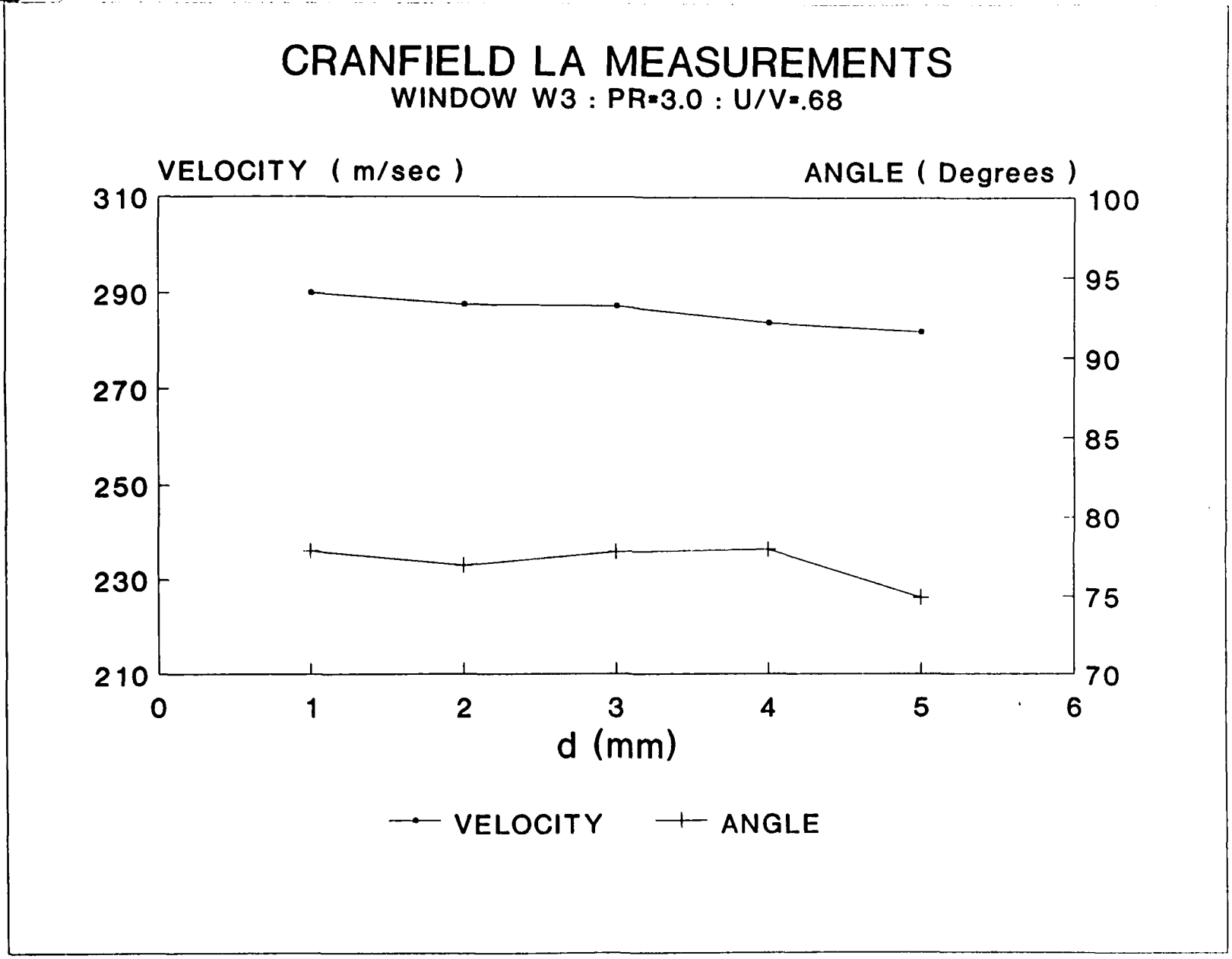

Fig 46 - Laser Anemometry Measurements between NGV and Rotor. (Window W3, PR=3.0, U/V=.68)

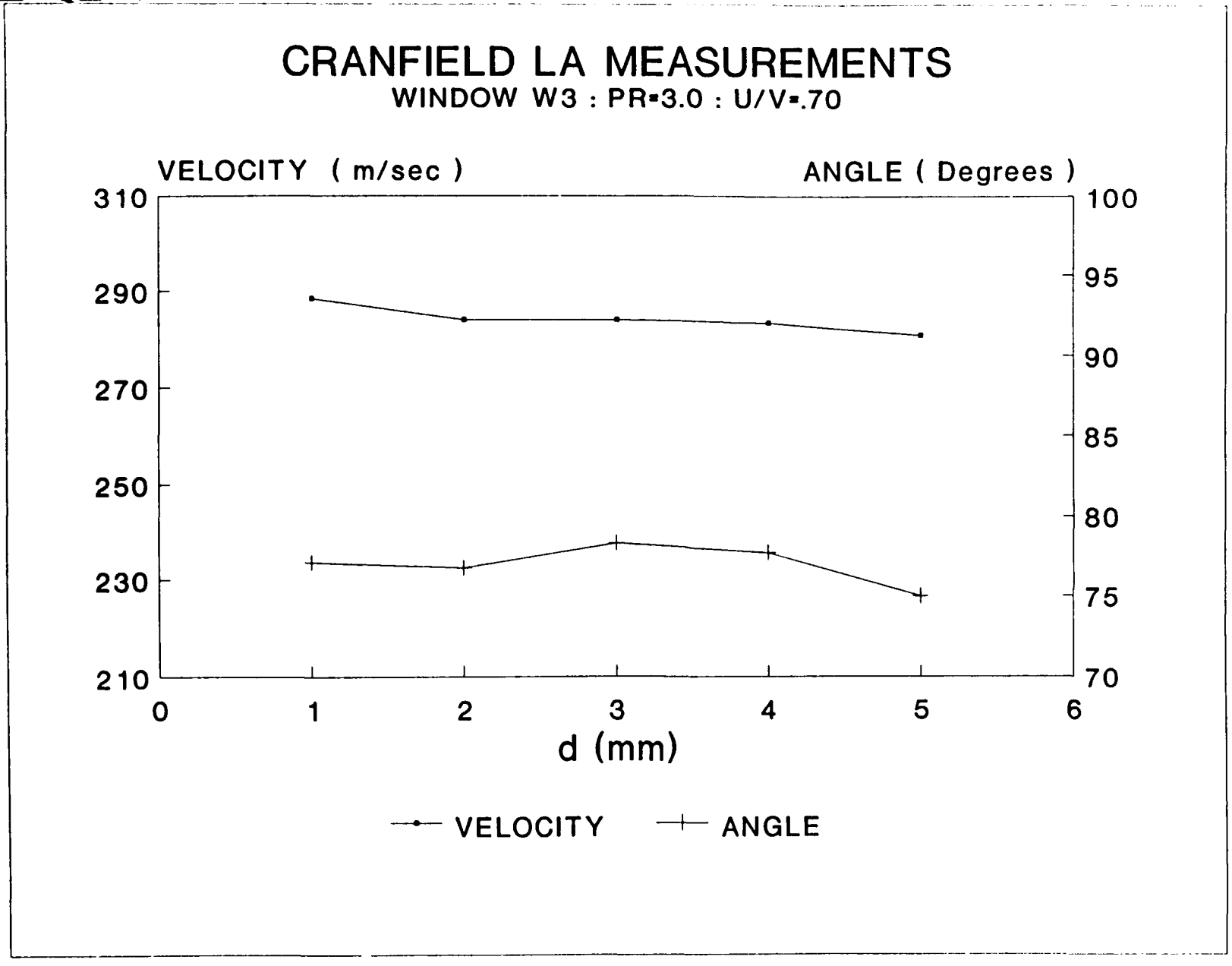

Fig 47 - Laser Anemometry Measurements between NGV and Rotor. (Window W3, PR=3.0, U/V=.70)

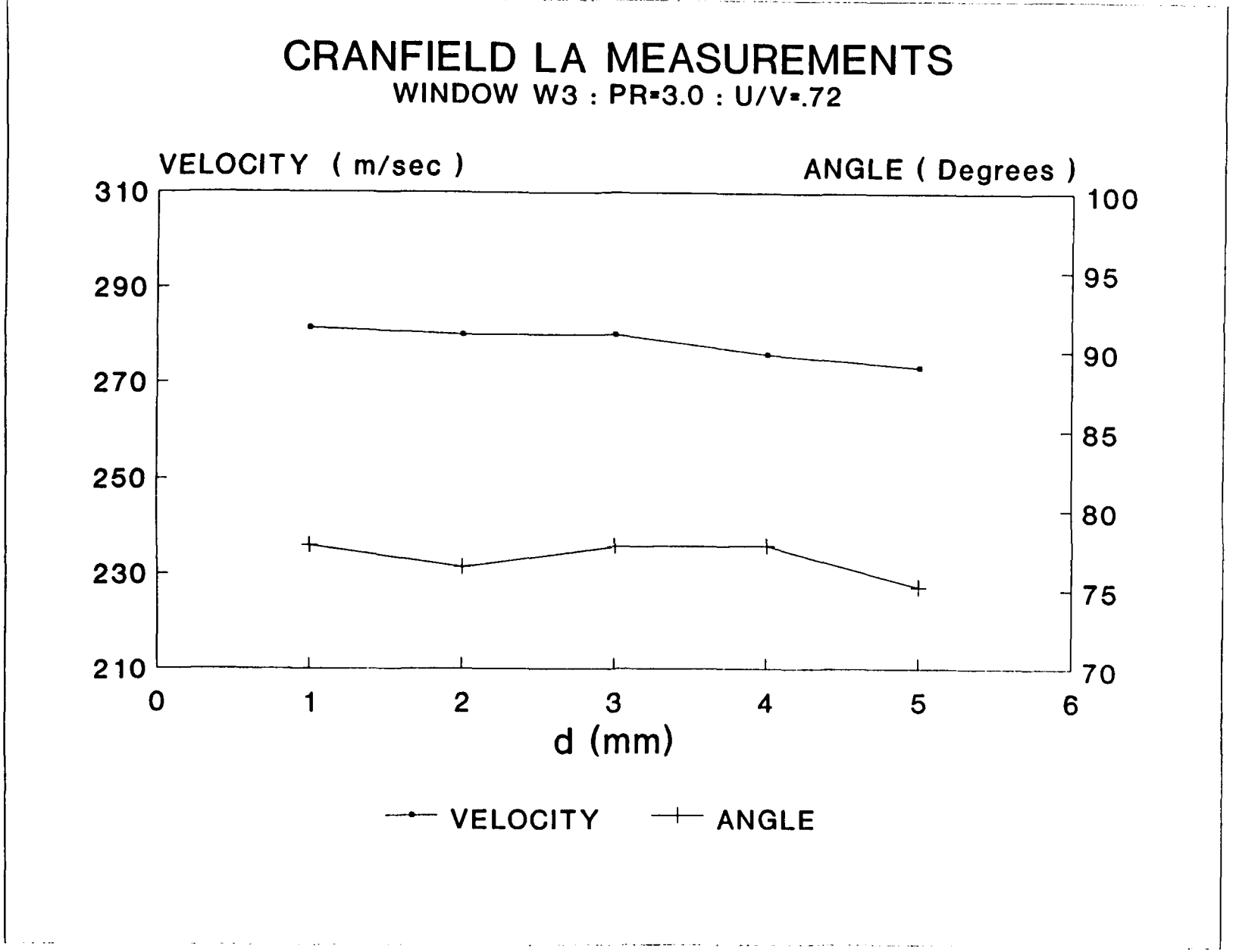

Fig 48 - Laser Anemometry Measurements between NGV and Rotor. (Window W3, PR=3.0, U/V=.72)

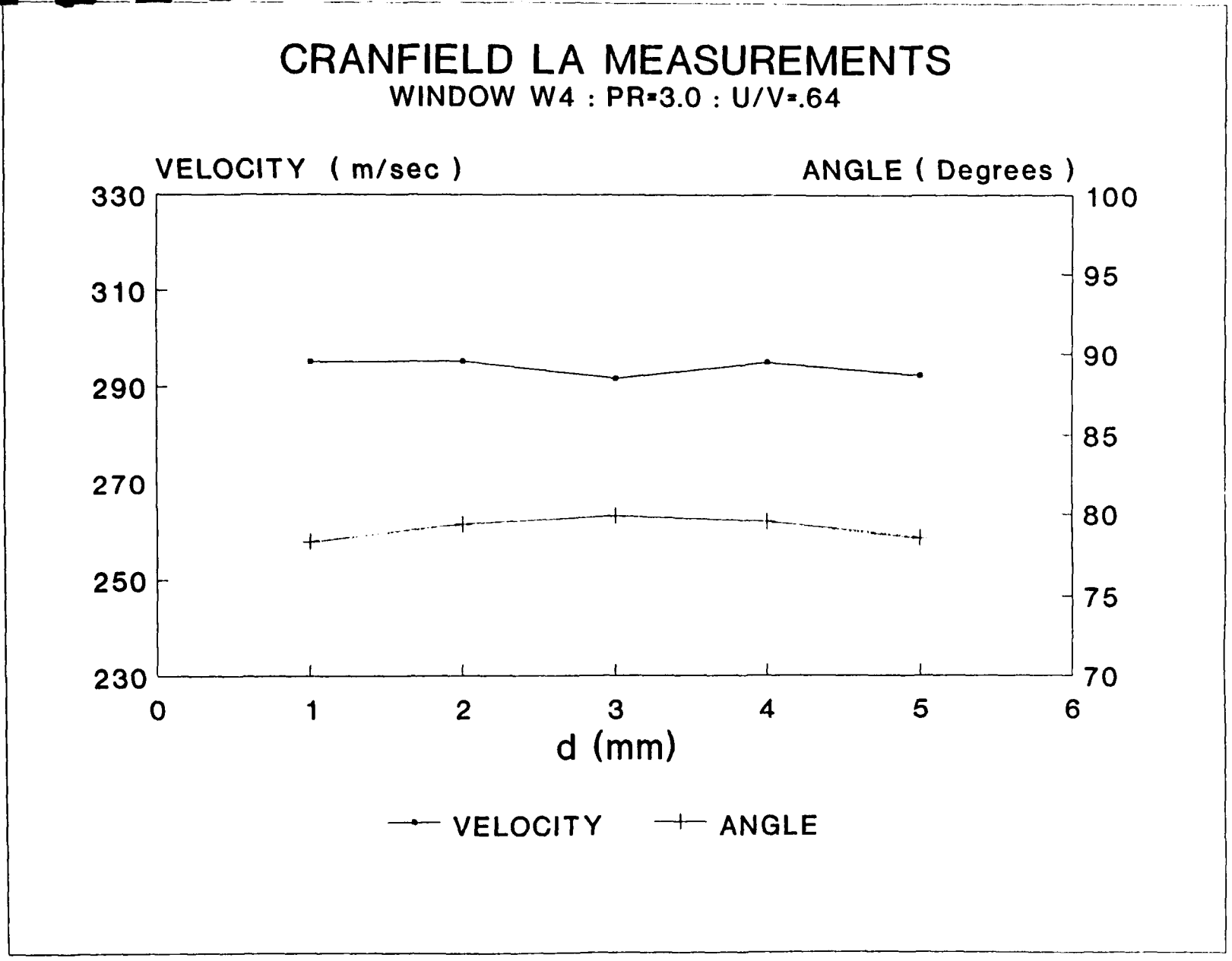

Fig 49 - Laser Anemometry Measurements between NGV and Rotor. (Window W4, PR=3.0, U/V=.64)

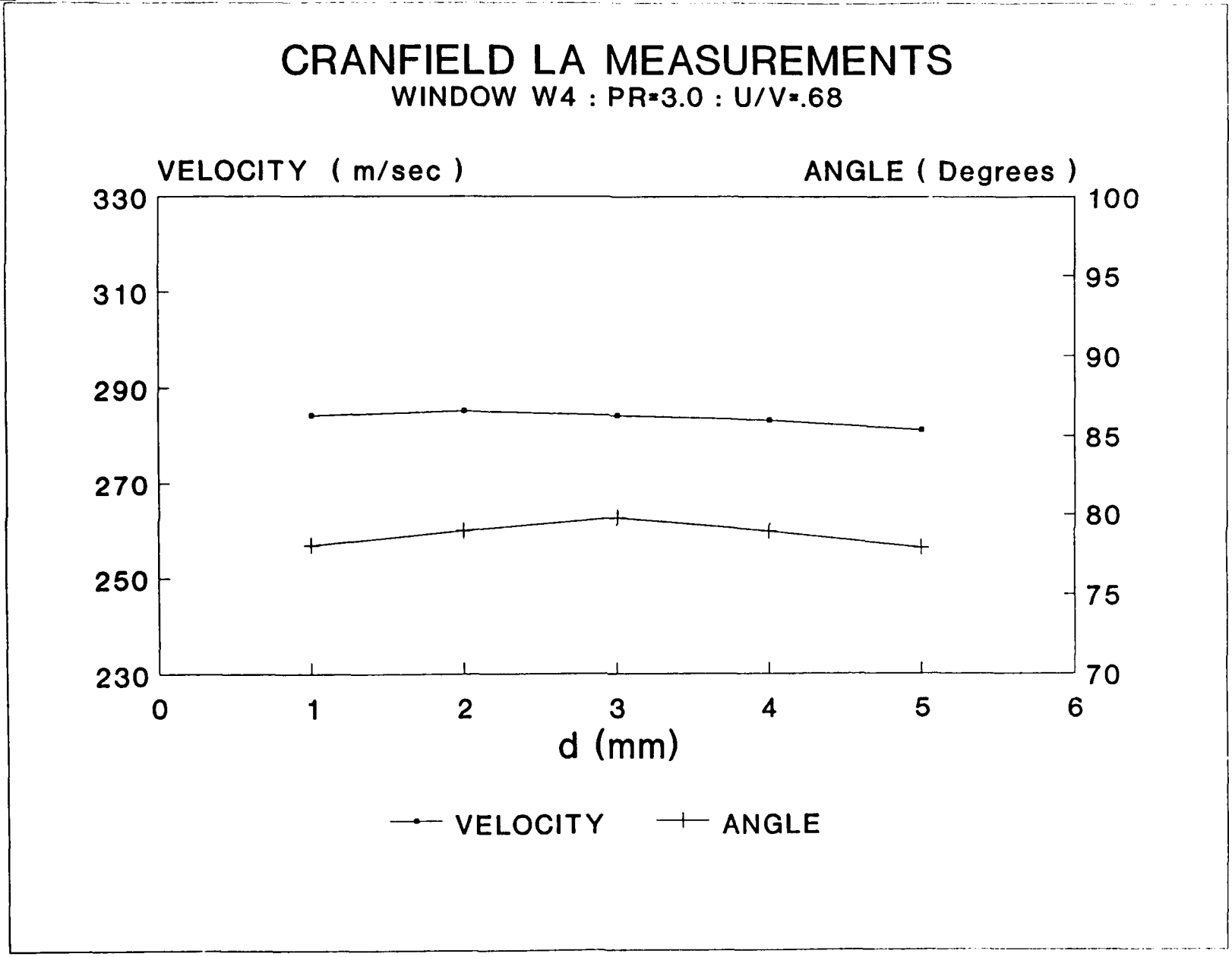

Fig 50 - Laser Anemometry Measurements between NGV and Rotor. (Window W4, PR=3.0, U/V=.68)

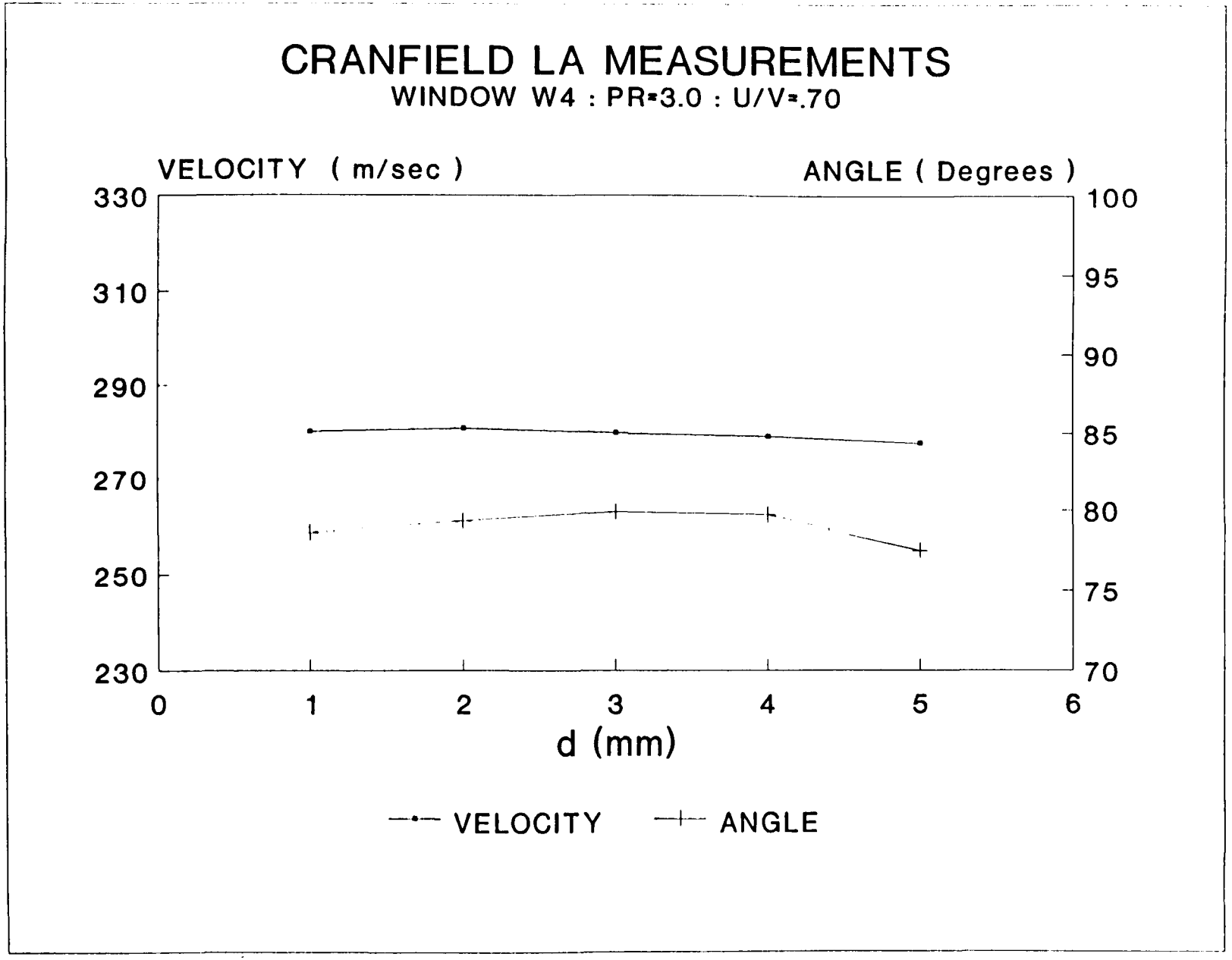

Fig 51 - Laser Anemometry Measurements between NGV and Rotor. (Window W4, PR=3.0, U/V=.70)

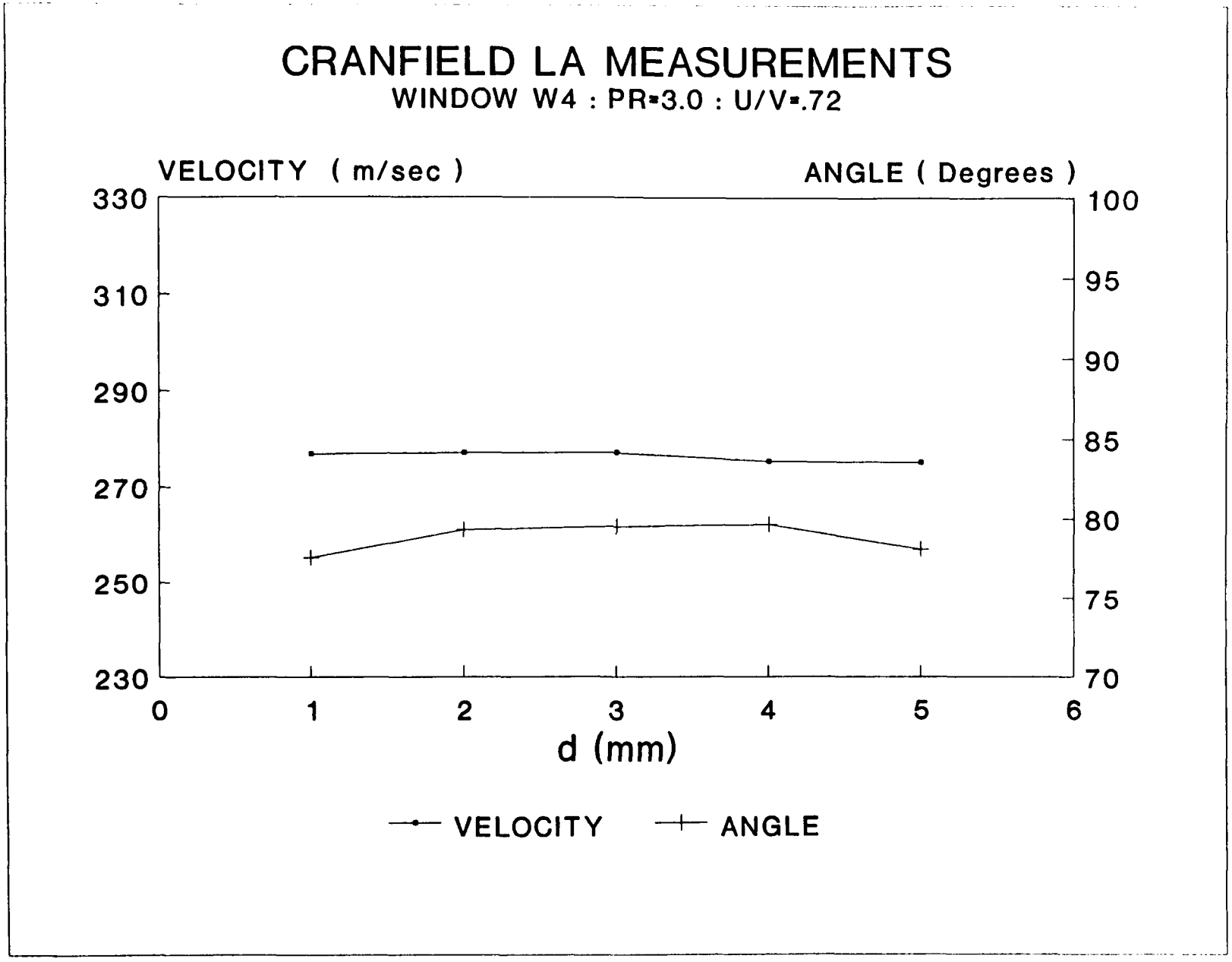

Fig 52 - Laser Anemometry Measurements between NGV and Rotor. (Window W4, PR=3.0, U/V=.72)

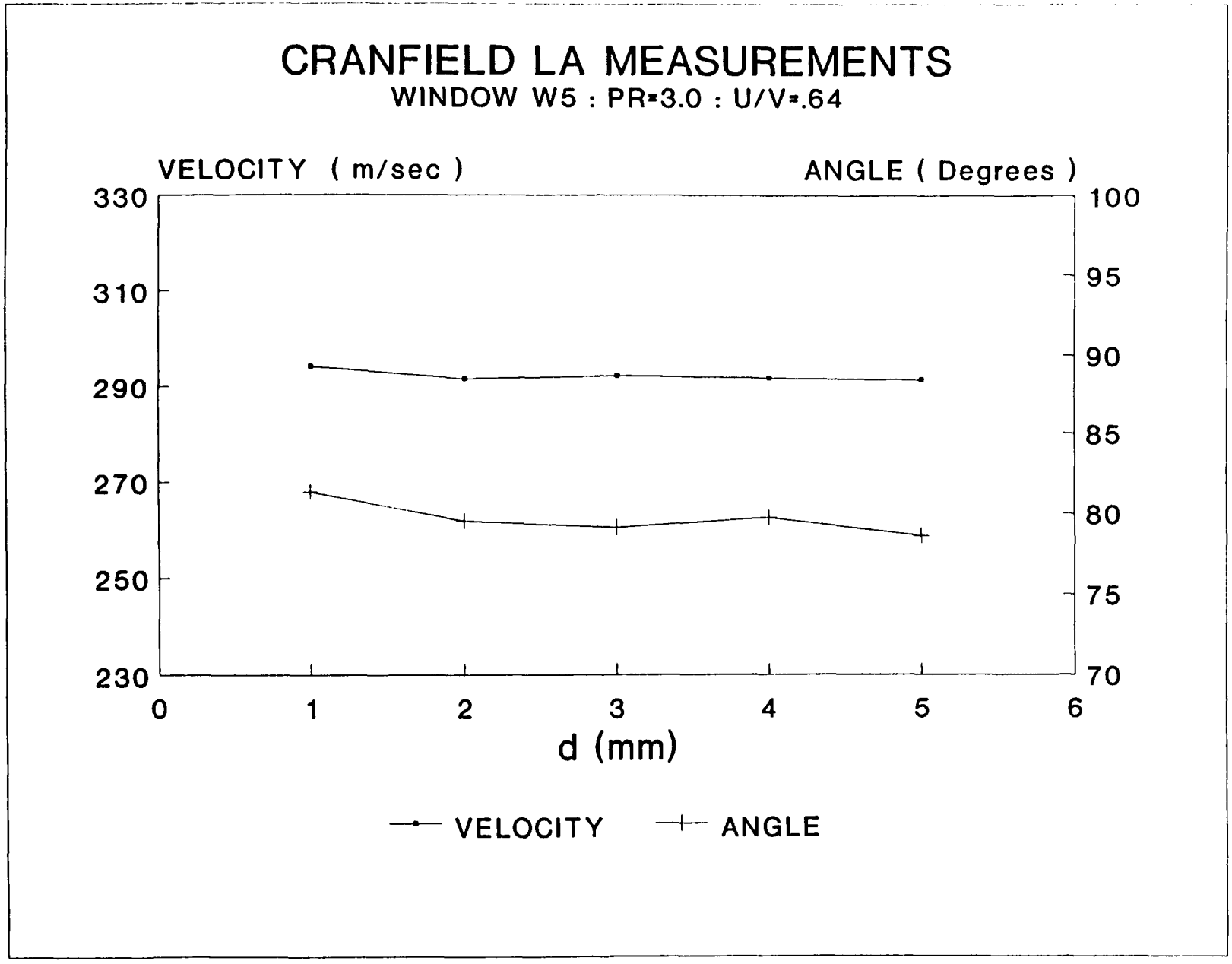

Fig 53 - Laser Anemometry Measurements between NGV and Rotor. (Window W5, PR=3.0, U/V=.64)

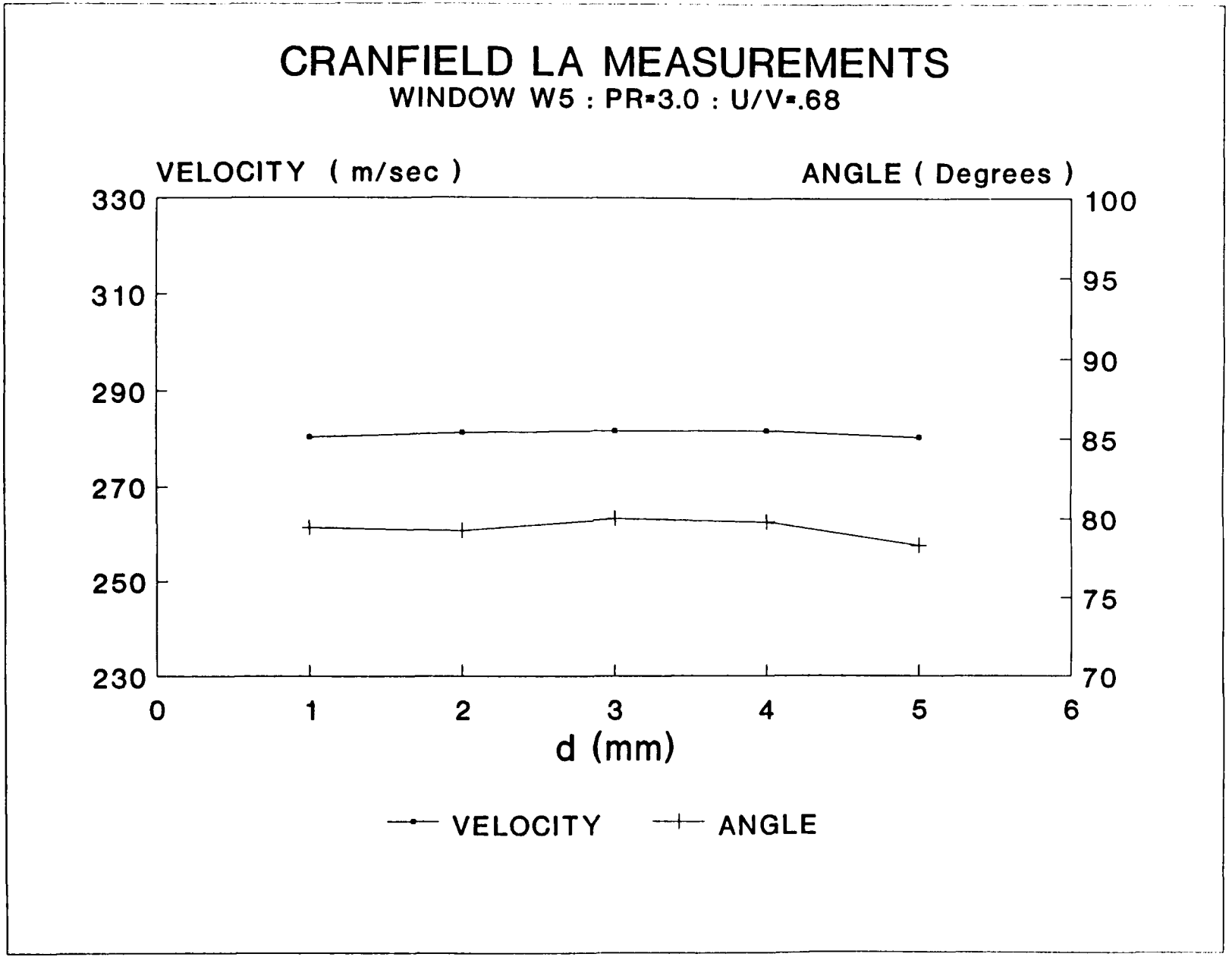

Fig 54 - Laser Anemometry Measurements between NGV and Rotor. (Window W5, PR=3.0, U/V=.68)

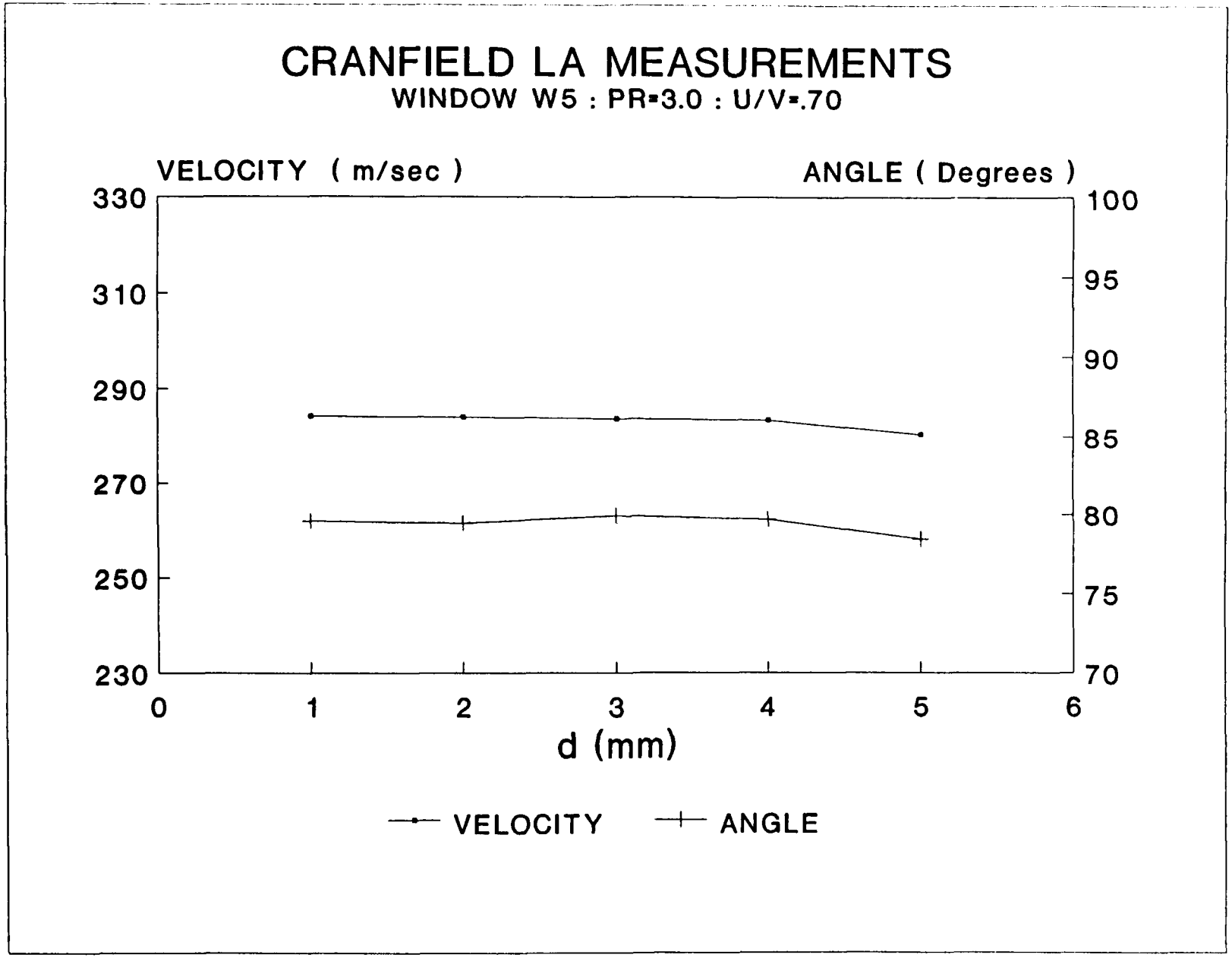

Fig 55 - Laser Anemometry Measurements between NGV and Rotor. (Window W5, PR=3.0, U/V=.70)

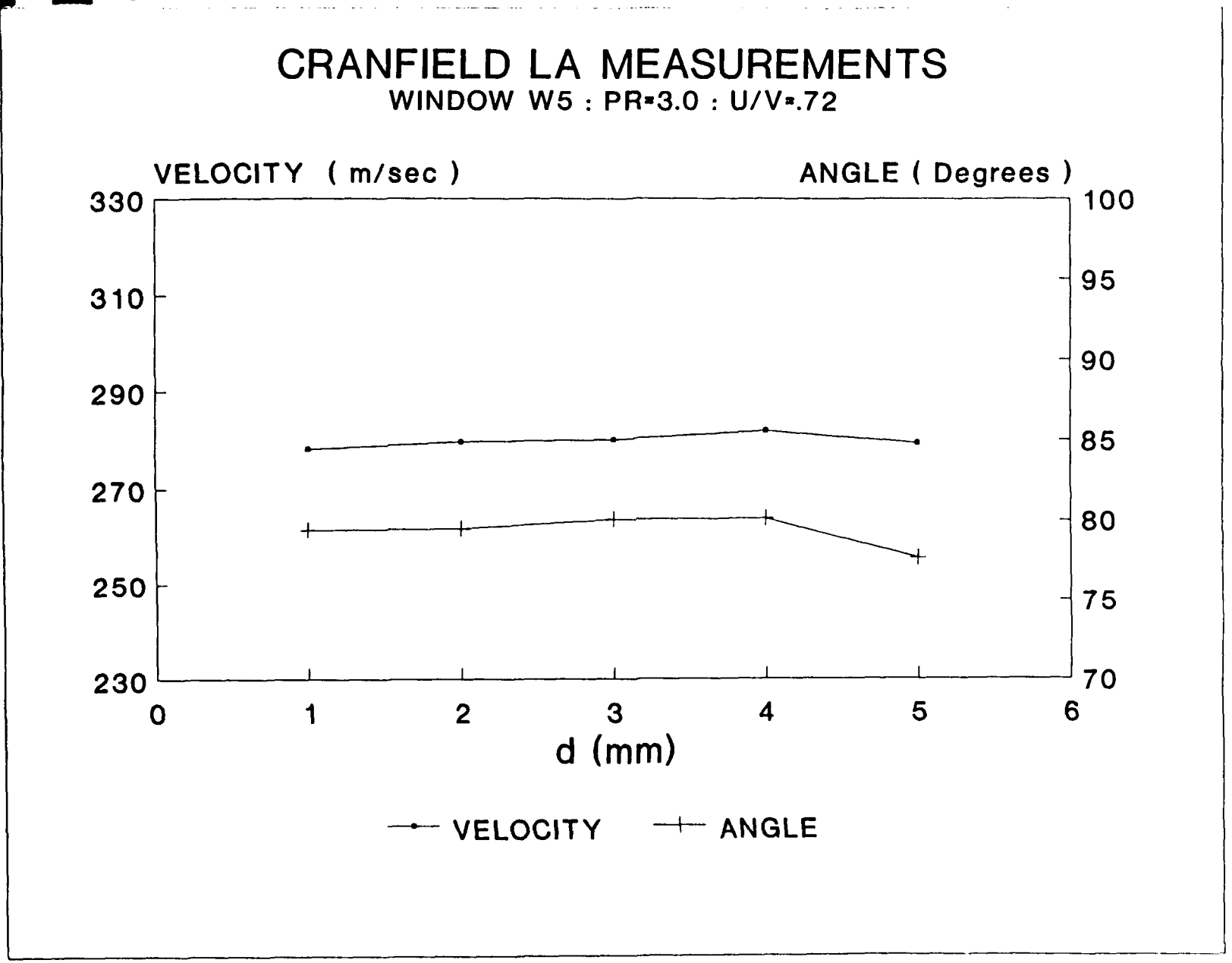

Fig 56 - Laser Anemometry Measurements between NGV and Rotor. (Window W5, PR=3.0, U/V=.72)

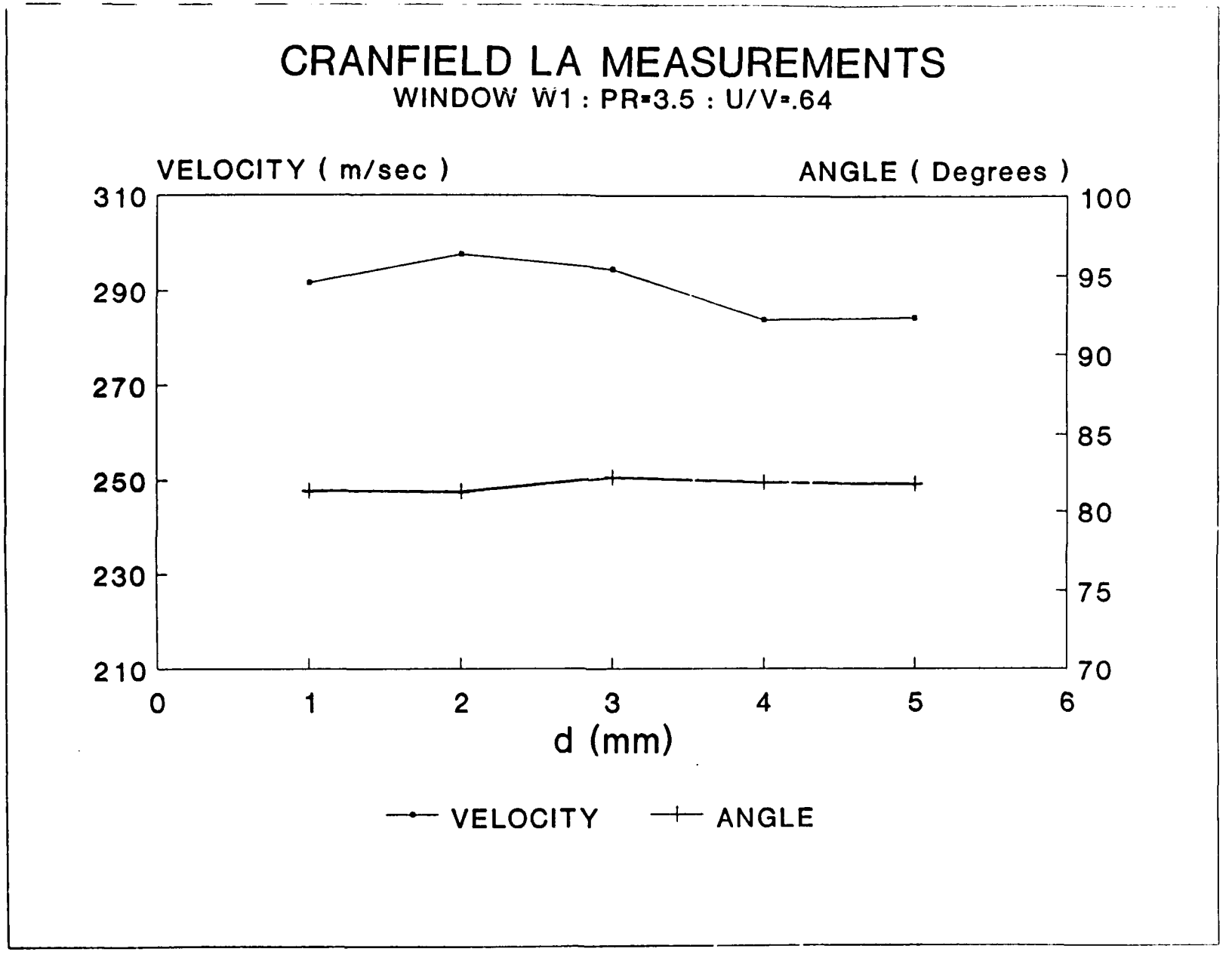

Fig 57 - Laser Anemometry Measurements between NGV and Rotor (Window W1, PR = 3.5, U/V = .64)

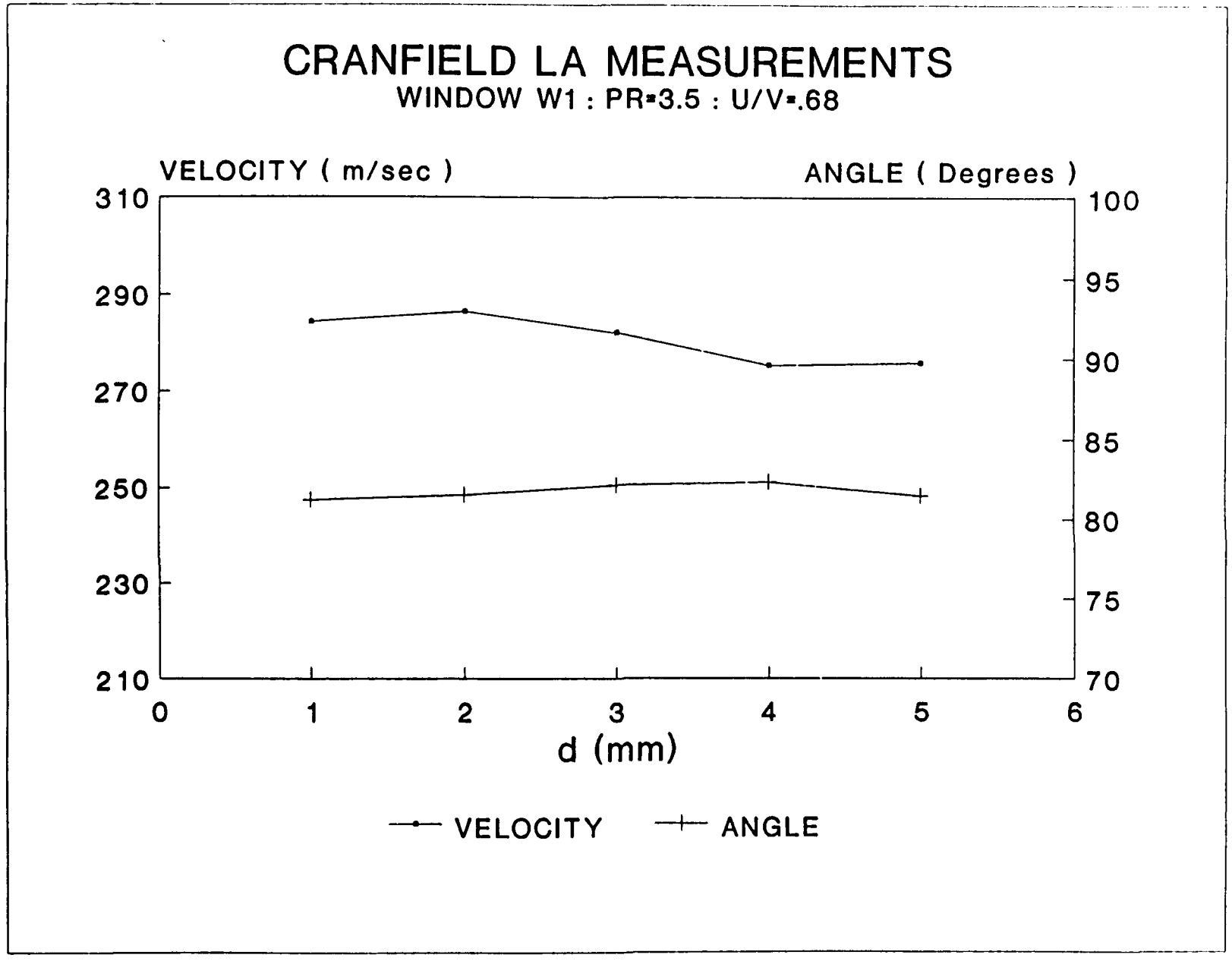

Fig 58 - Laser Anemometry Measurements between NGV and Rotor (Window W1, PR = 3.5, U/V = .68)

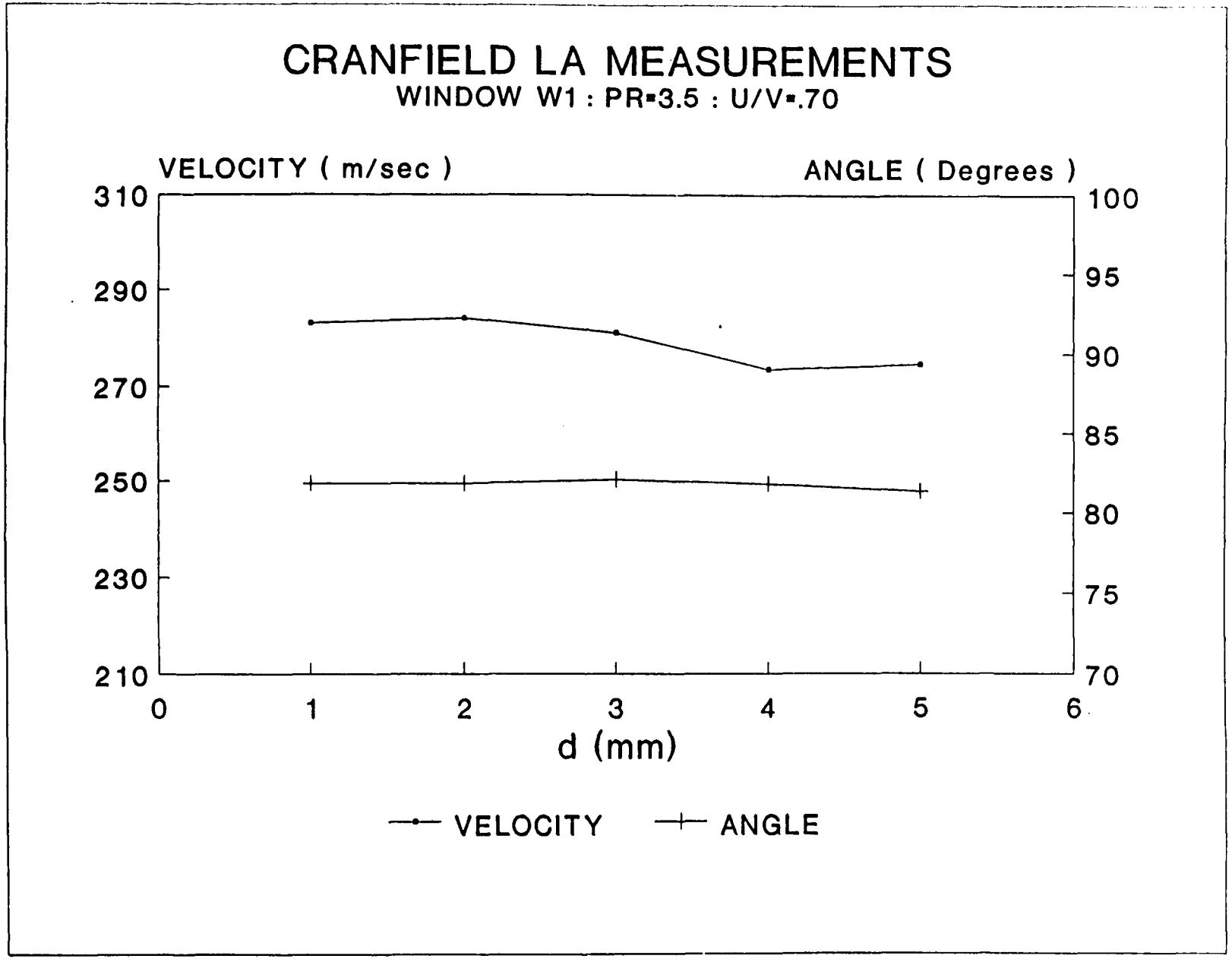

Fig 59 - Laser Anemometry Measurements between NGV and Rotor (Window W1, PR = 3.5, U/V = .70)

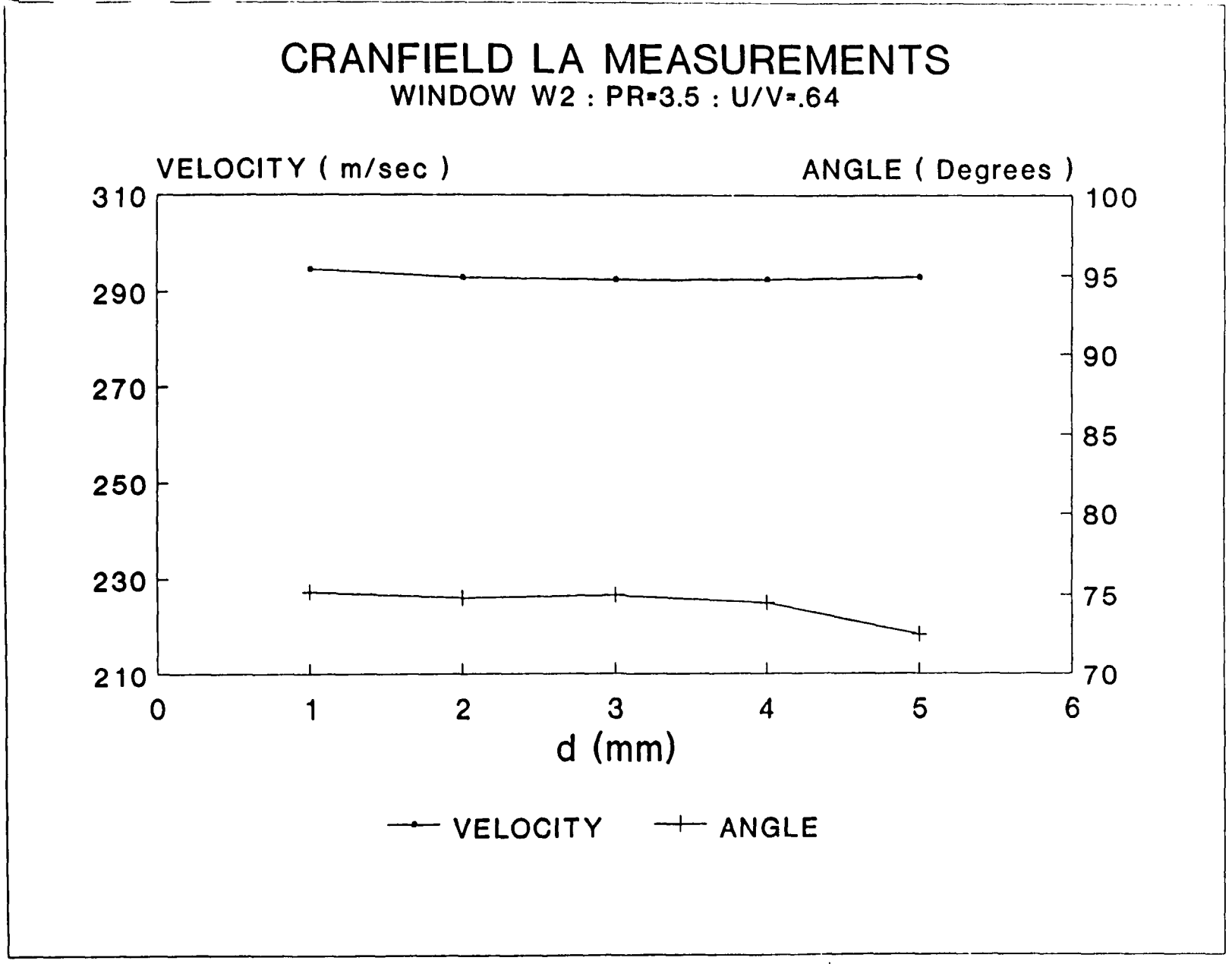

Fig 60 - Laser Anemometry Measurements between NGV and Rotor. (Window W2, PR=3.5, U/V=.64)

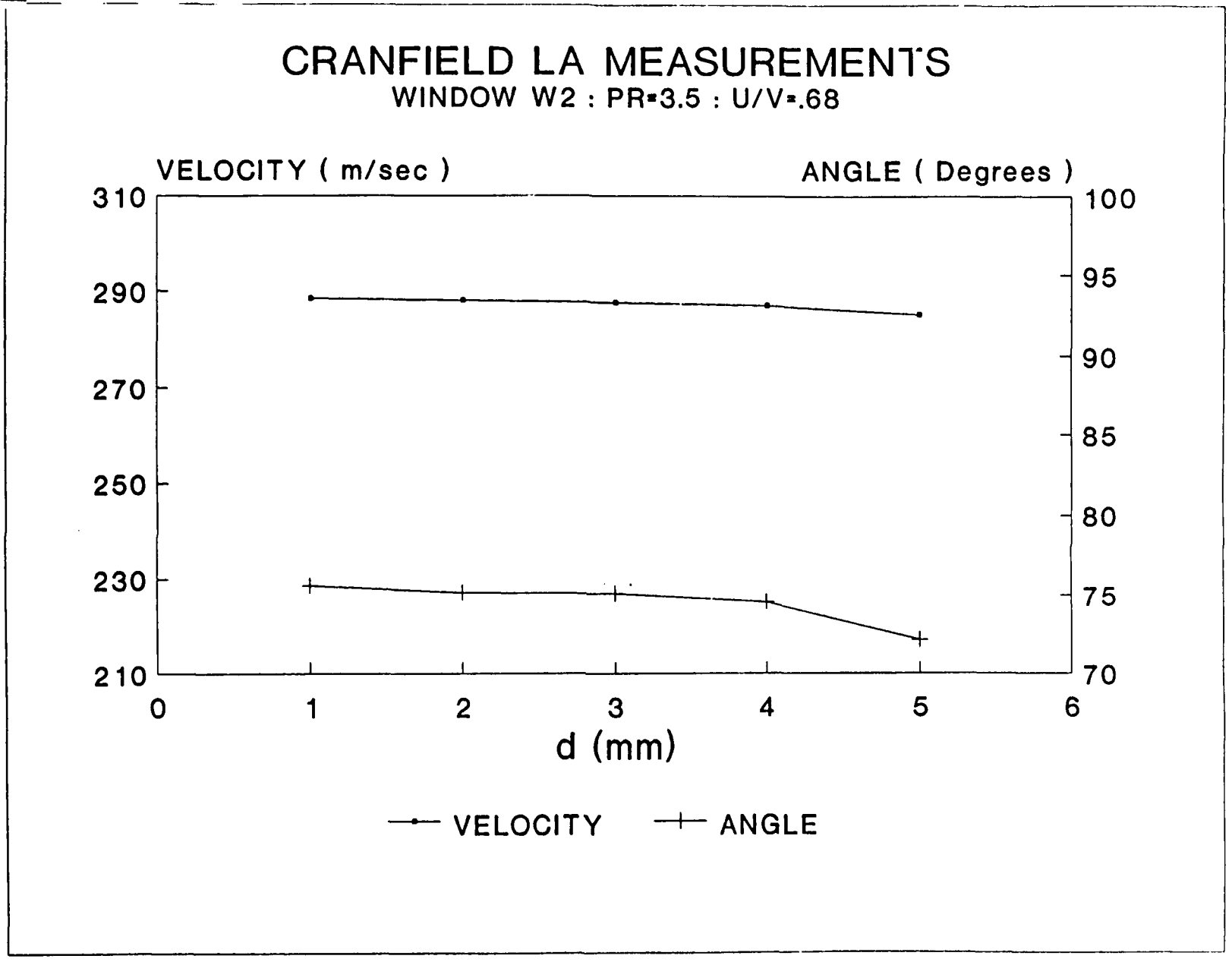

Fig 61 - Laser Anemometry Measurements between NGV and Rotor. (Window W2, PR=3.5, U/V=.68)

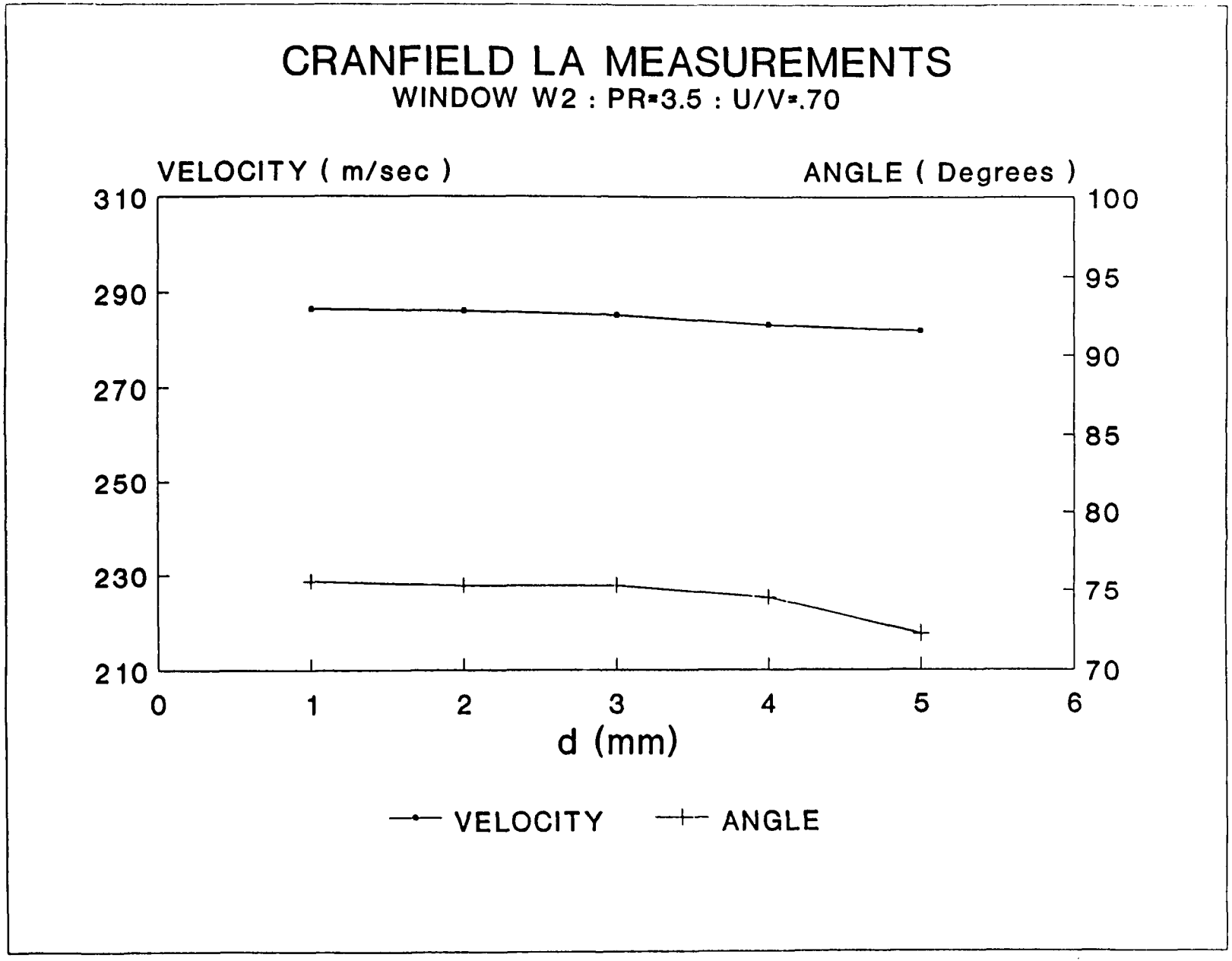

Fig 62 - Laser Anemometry Measurements between NGV and Rotor. (Window W2, PR=3.5, U/V=.70)

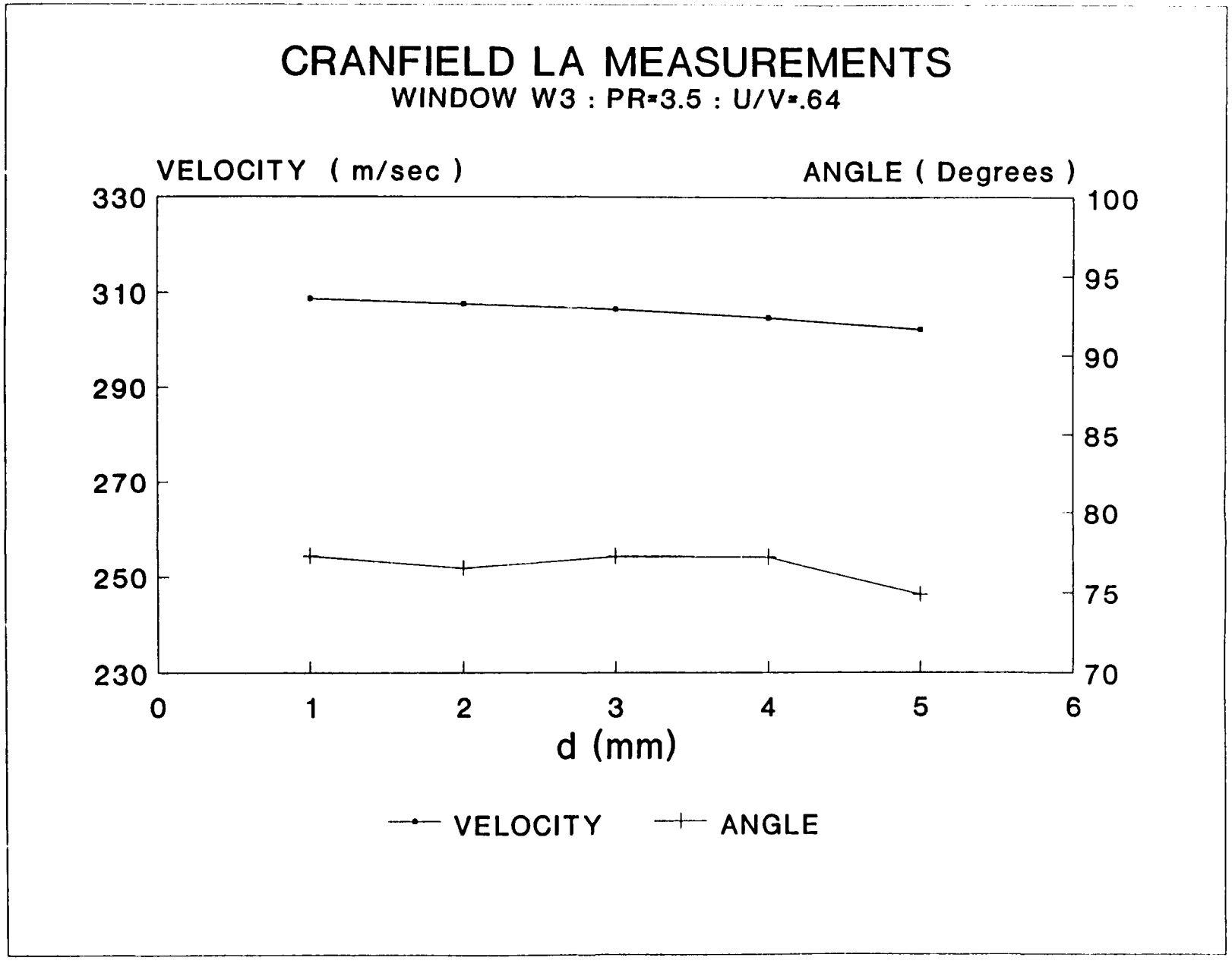

Fig 63 - Laser Anemometry Measurements between NGV and Rotor . (Window W3, PR=3.5, U/V=.64)

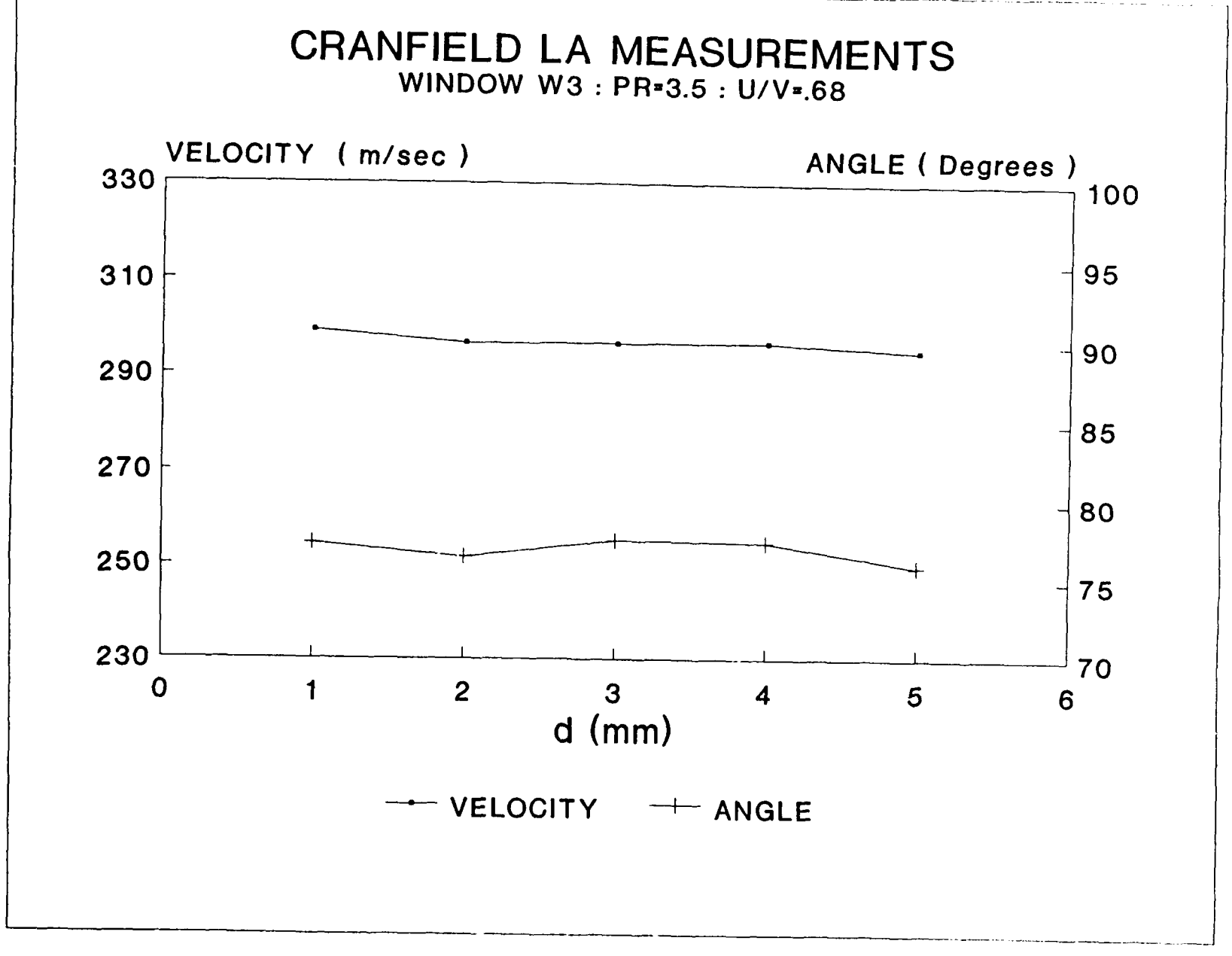

Fig 64 - Laser Anemometry Measurements between NGV and Rotor. (Window W3, PR=3.5, U/V=.68)

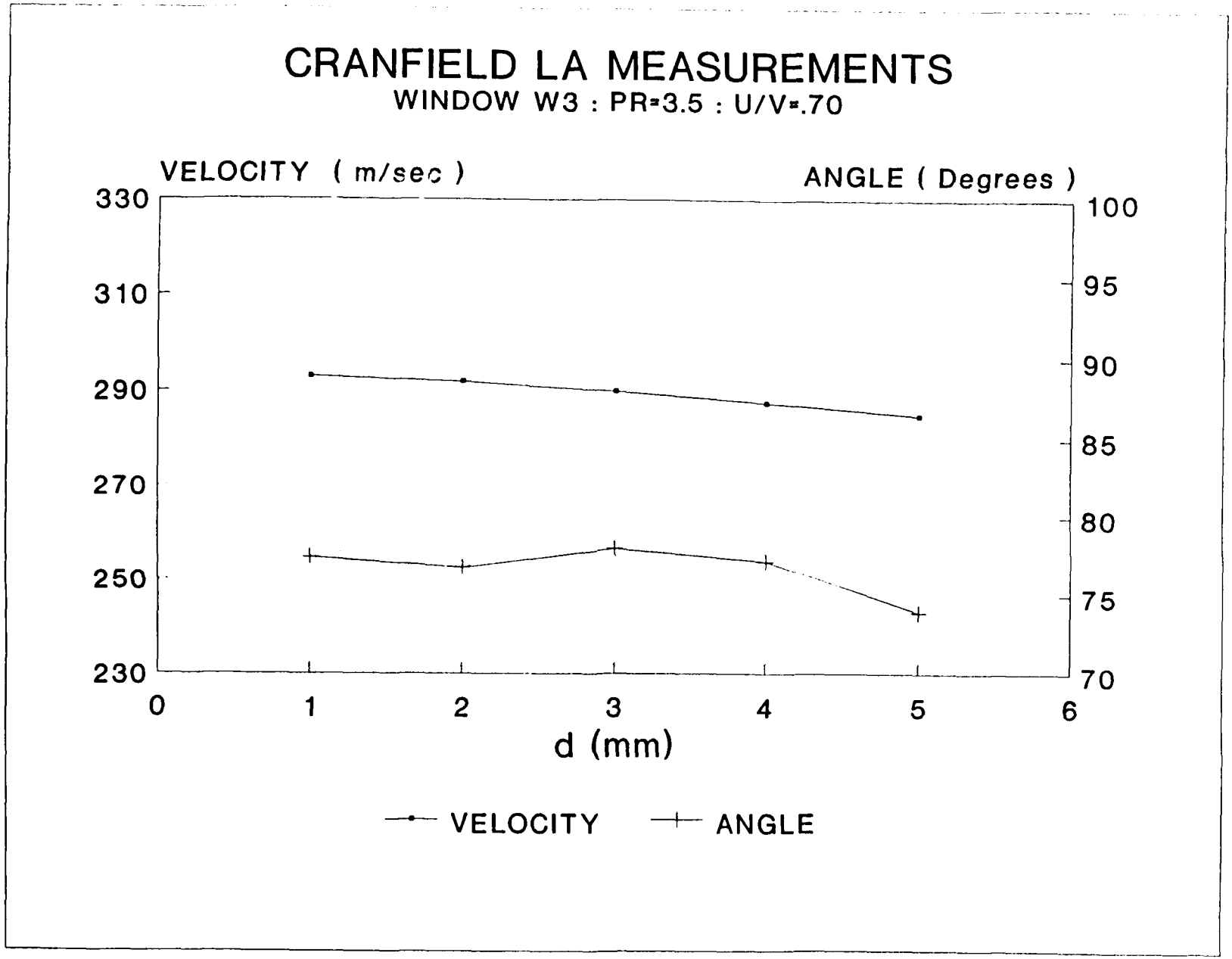

Fig 65 - Laser Anemometry Measurements between NGV and Rotor. (Window W3, PR=3.5, U/V=.70)

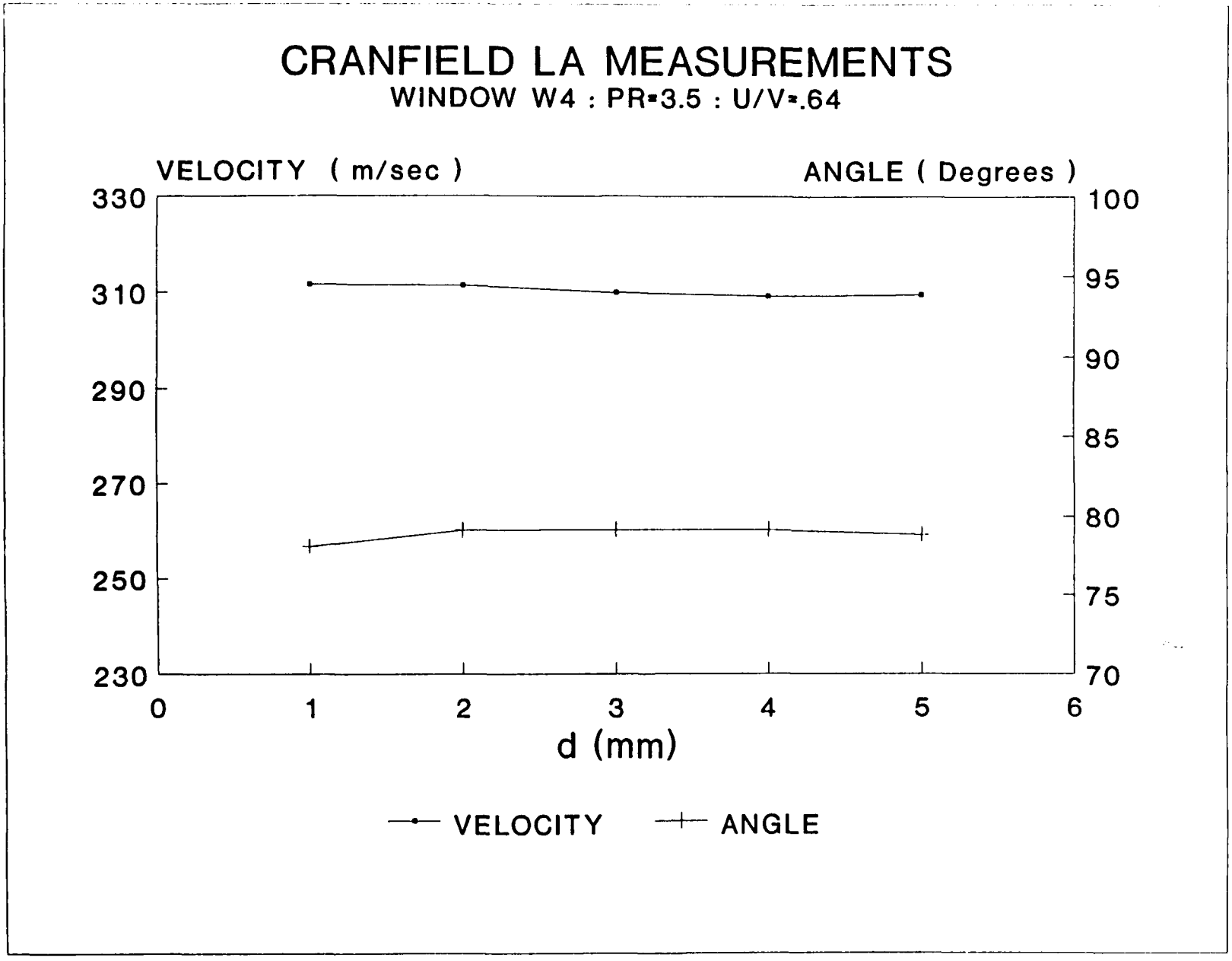

Fig 66 - Laser Anemometry Measurements between NGV and Rotor. (Window W4, PR=3.5, U/V=.64)

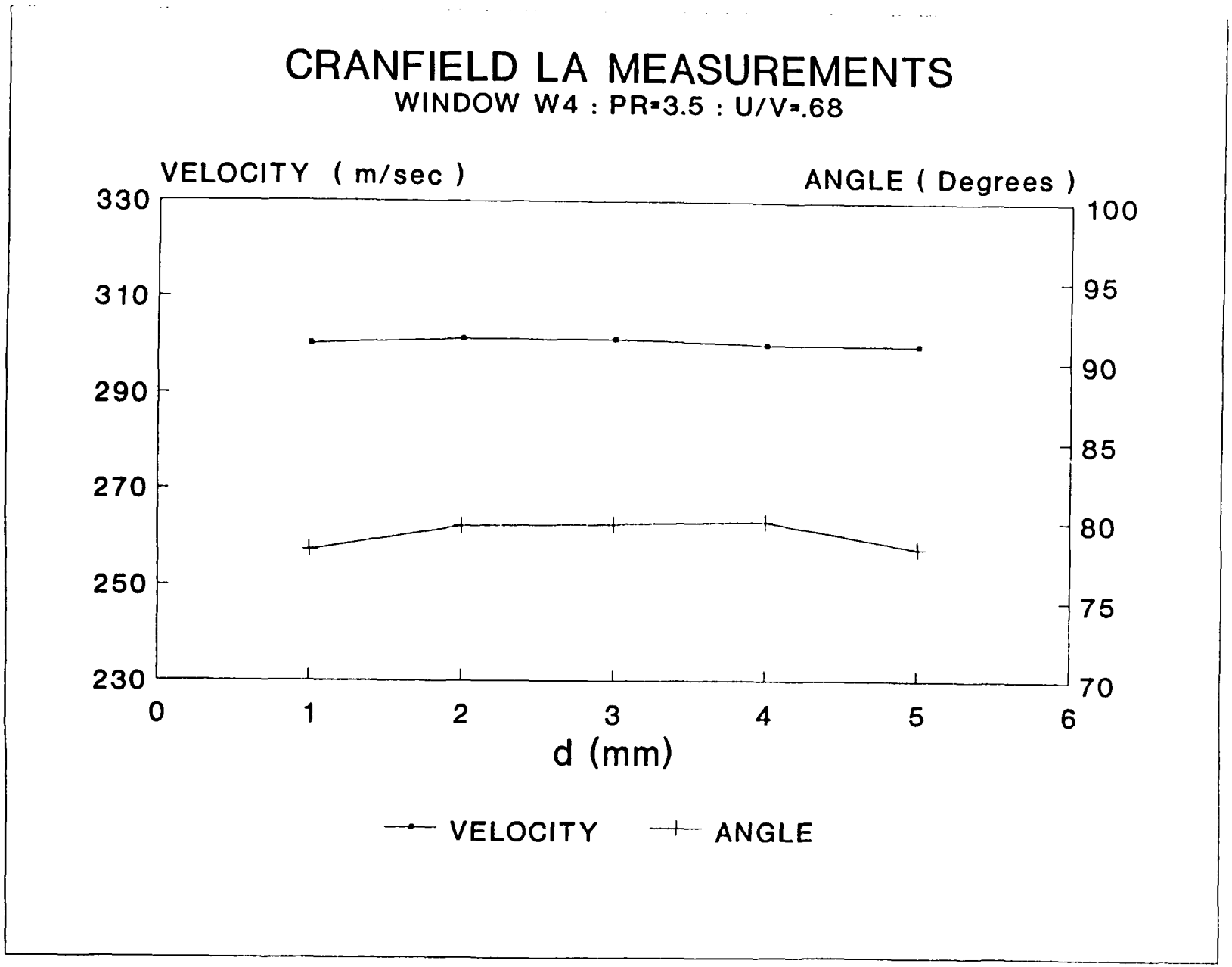

Fig 67 - Laser Anemometry Measurements between NGV and Rotor. (Window W4, PR=3.5, U/V=.68)

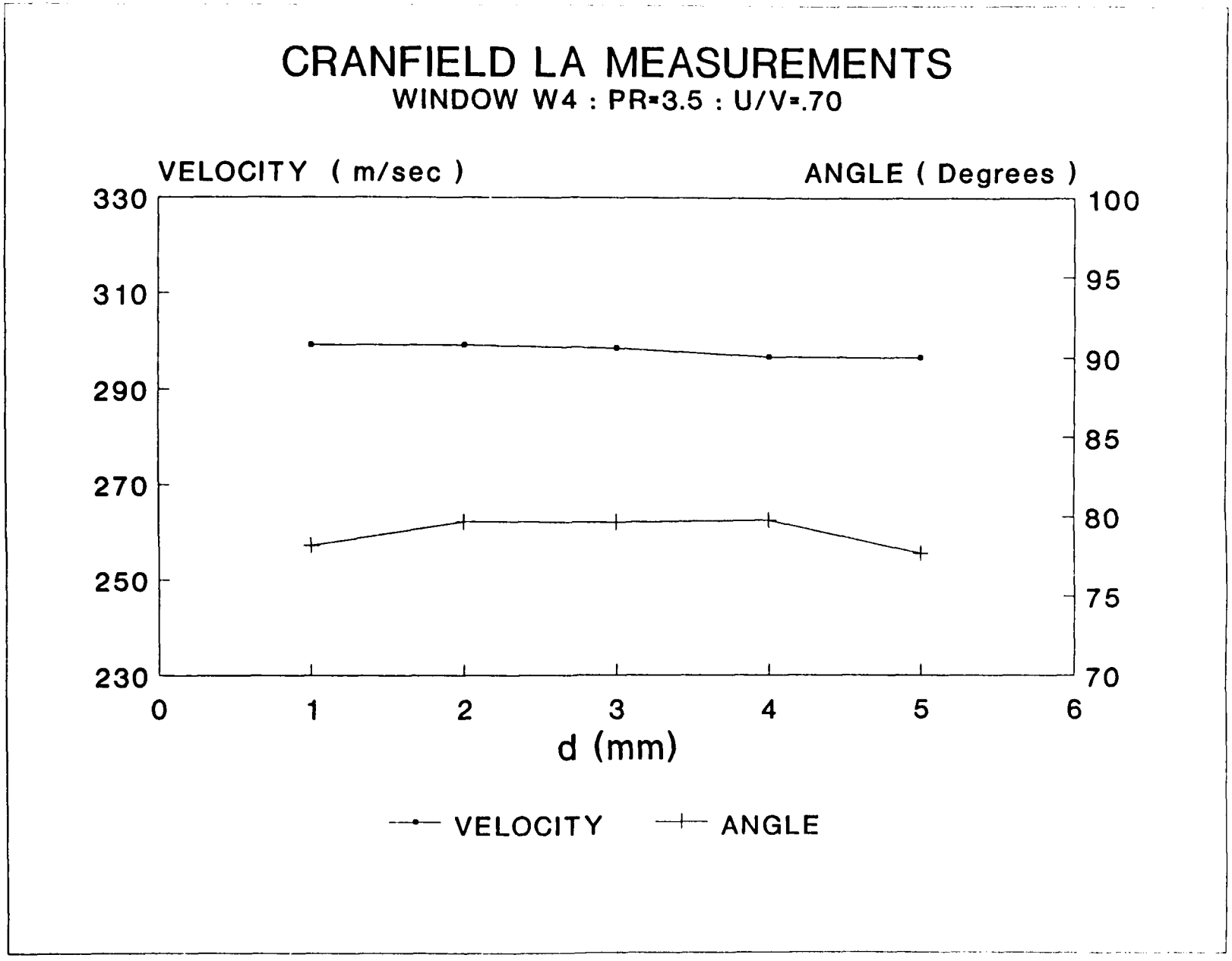

Fig 68 - Laser Anemometry Measurements between NGV and Rotor. (Window W4, PR=3.5, U/V=.70)

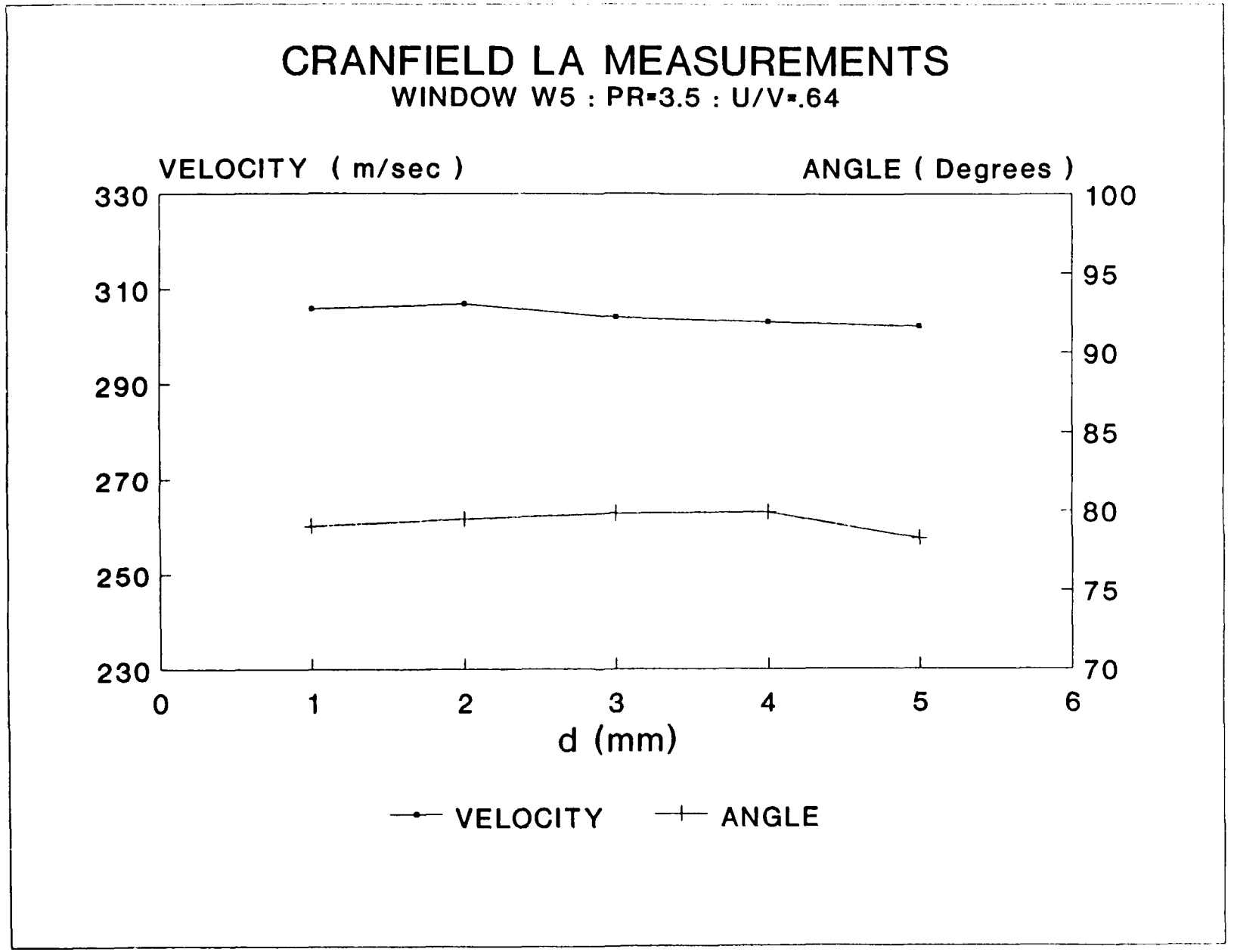

Fig 69 - Laser Anemometry Measurements between NGV and Rotor. (Window W5, PR=3.5, U/V=.64)

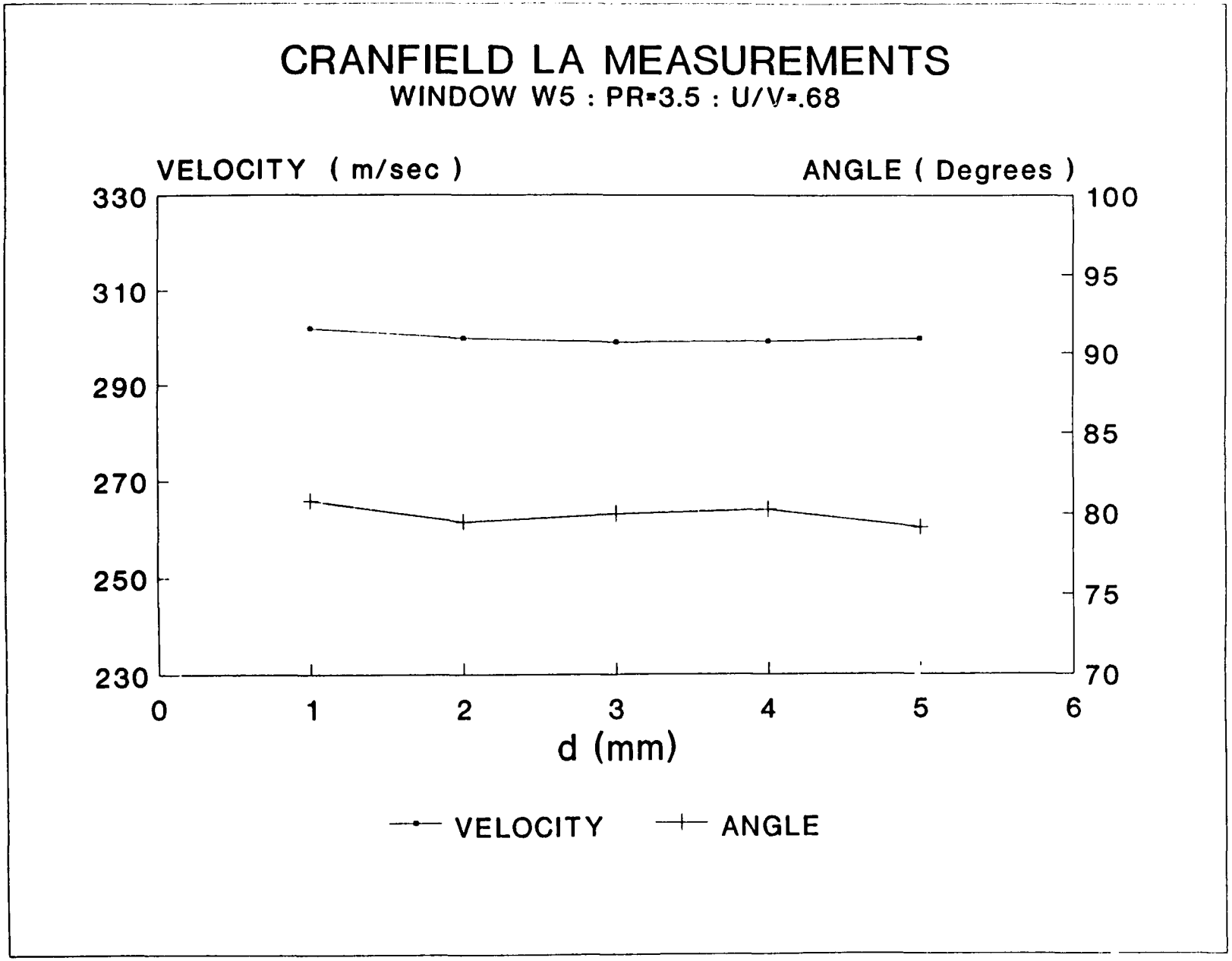

Fig 70 - Laser Anemometry Measurements between NGV and Rotor. (Window W5, PR=3.5, U/V=.68)

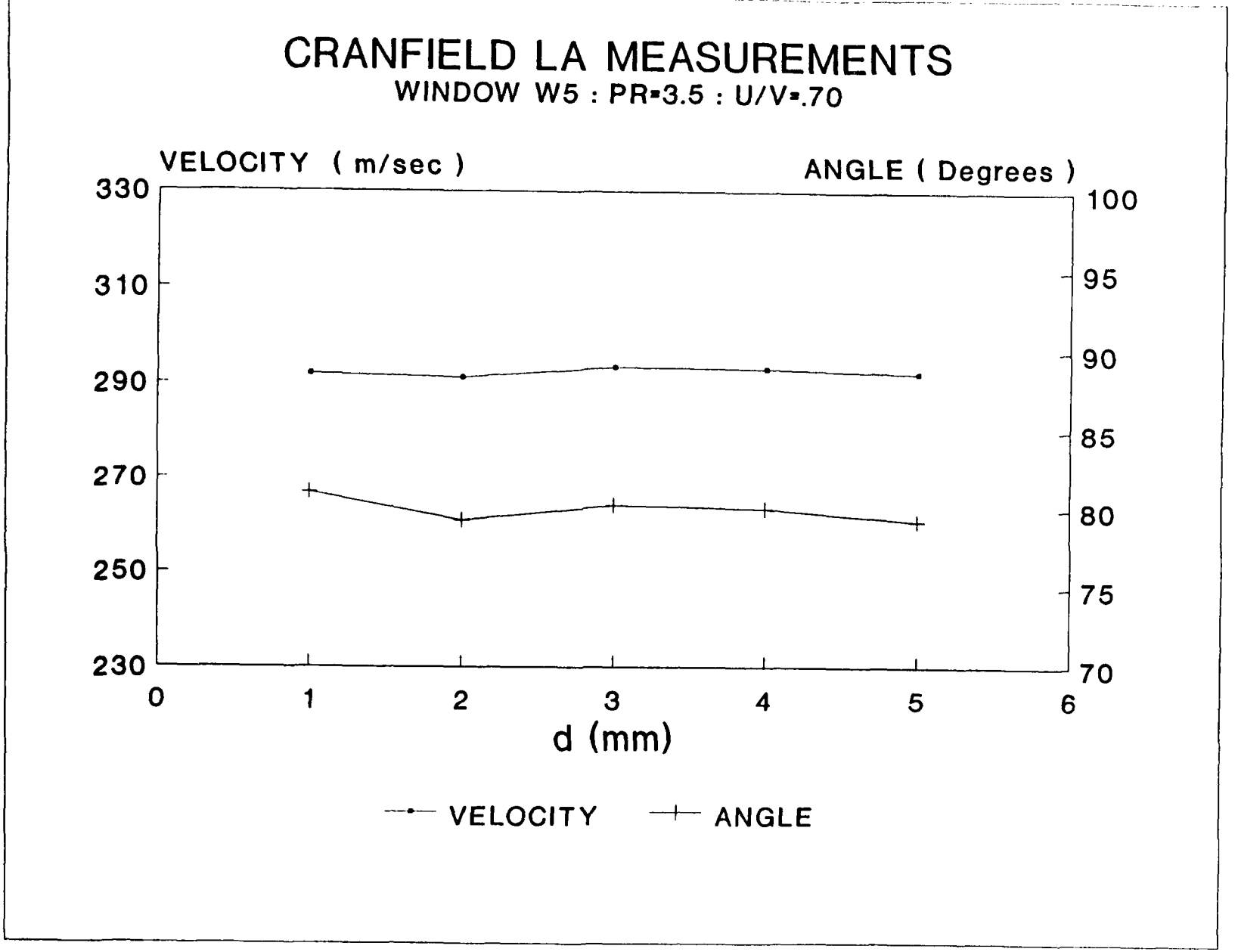

Fig 71 - Laser Anemometry Measurements between NGV and Rotor. (Window W5, PR=3.5, U/V=.70)

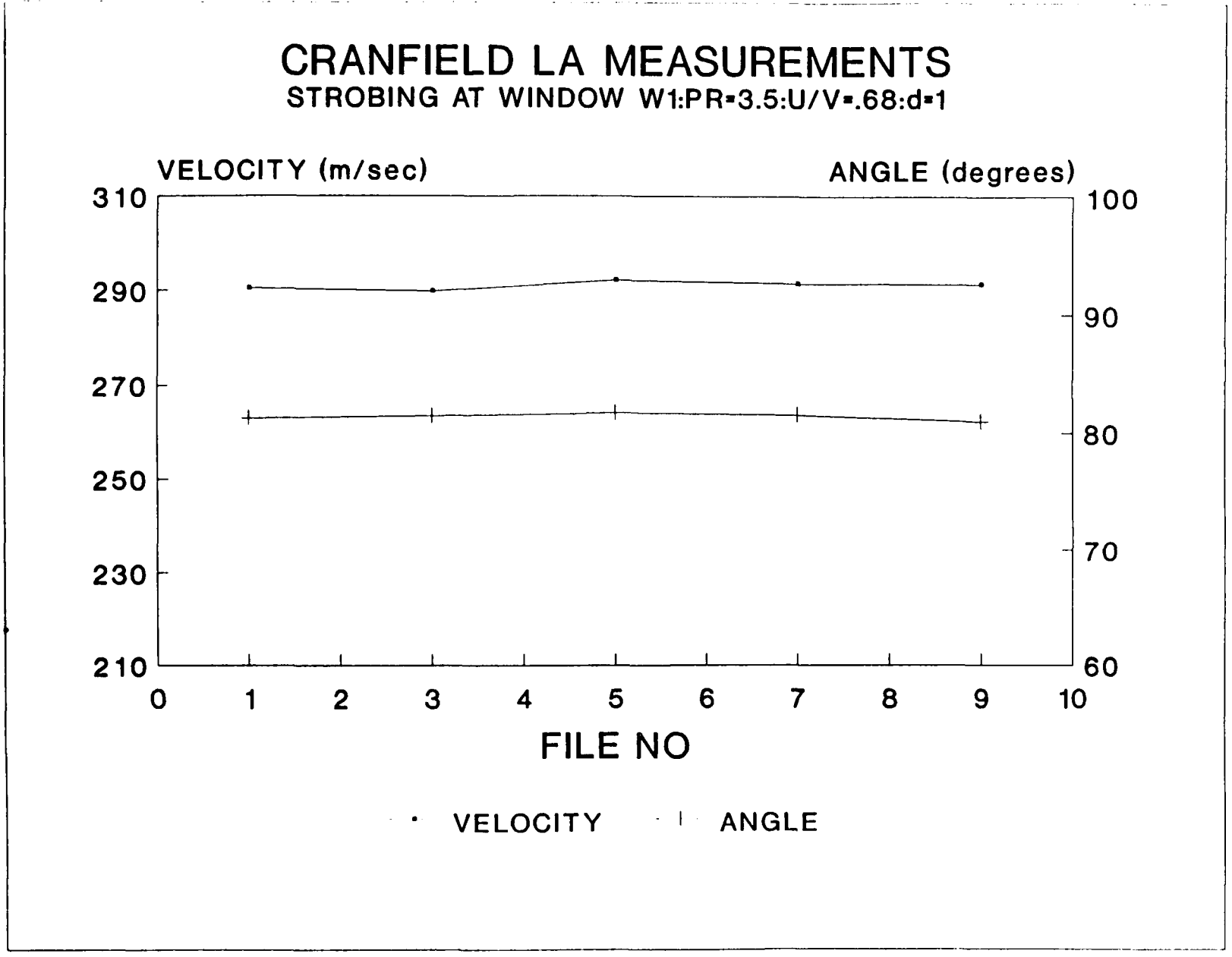

Fig 72 - Blade Strobed Results from between NGV and Rotor. (Window W1, PR=3.5, U/V=.68, d=1)

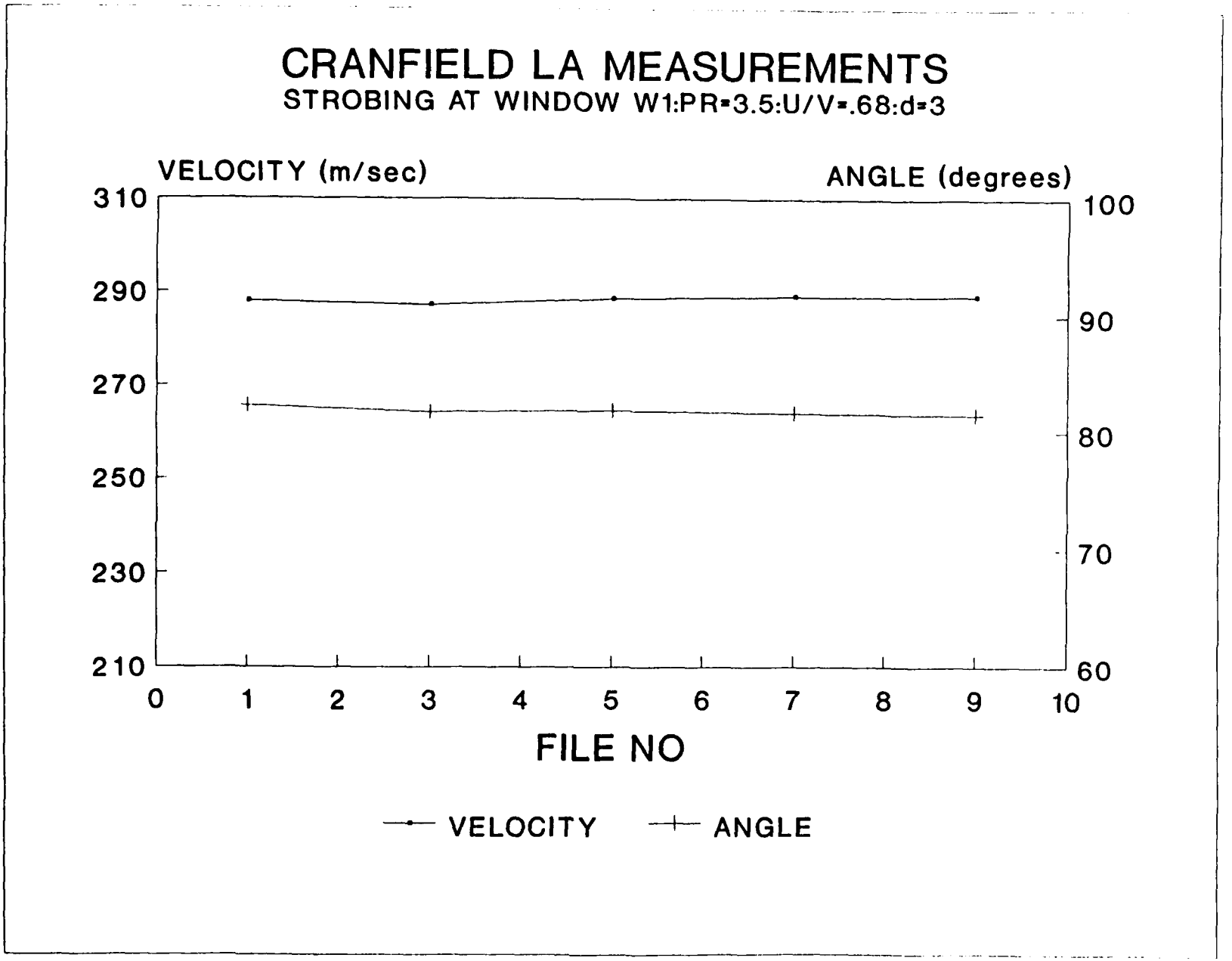

Fig 73 - Blade Strobed Results from between NGV and Rotor. (Window W1, PR=3.5, U/V=.68, d=3)

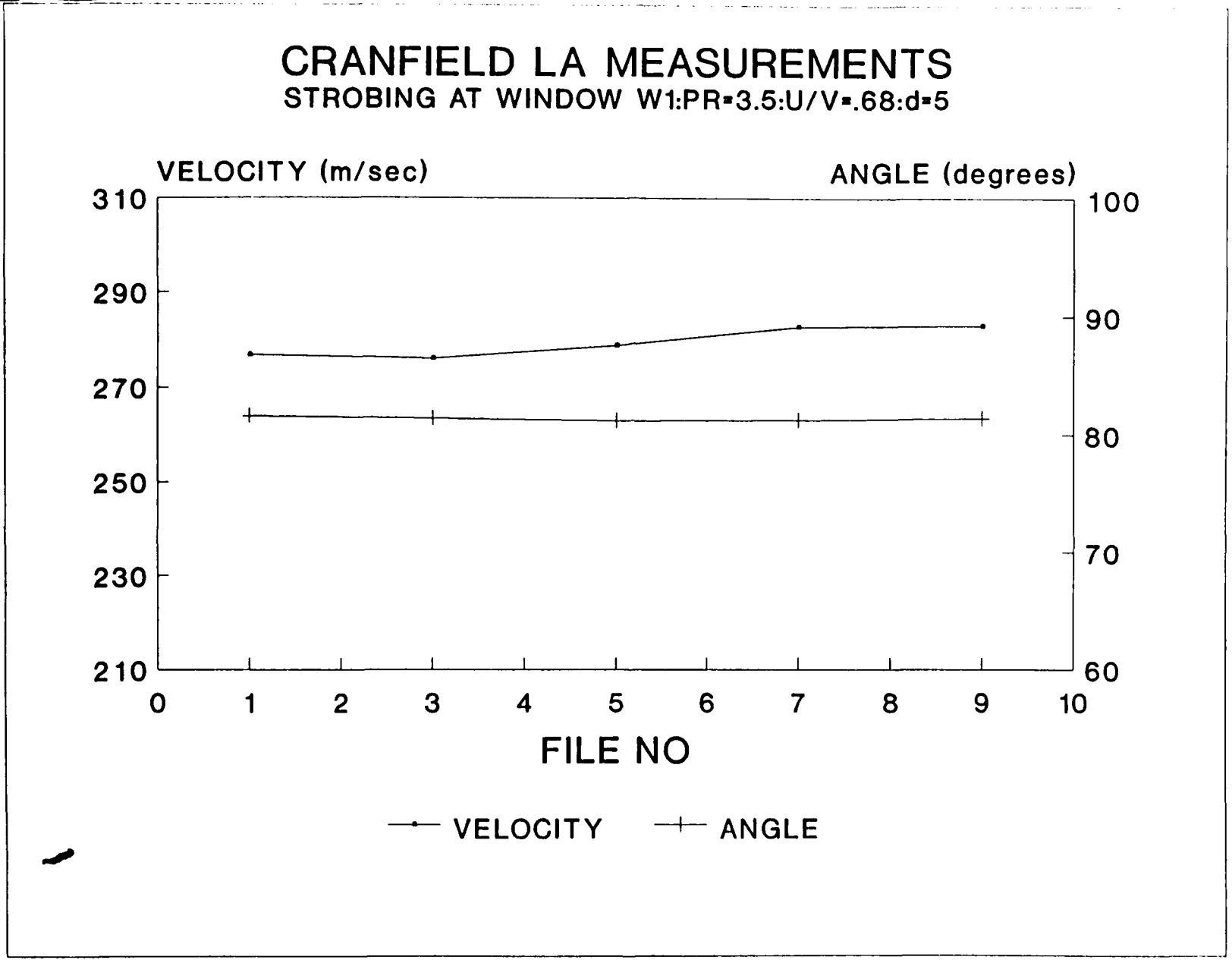

Fig 74 - Blade Strobed Results from between NGV and Rotor. (Window W1, PR=3.5, U/V=.68, d=5)

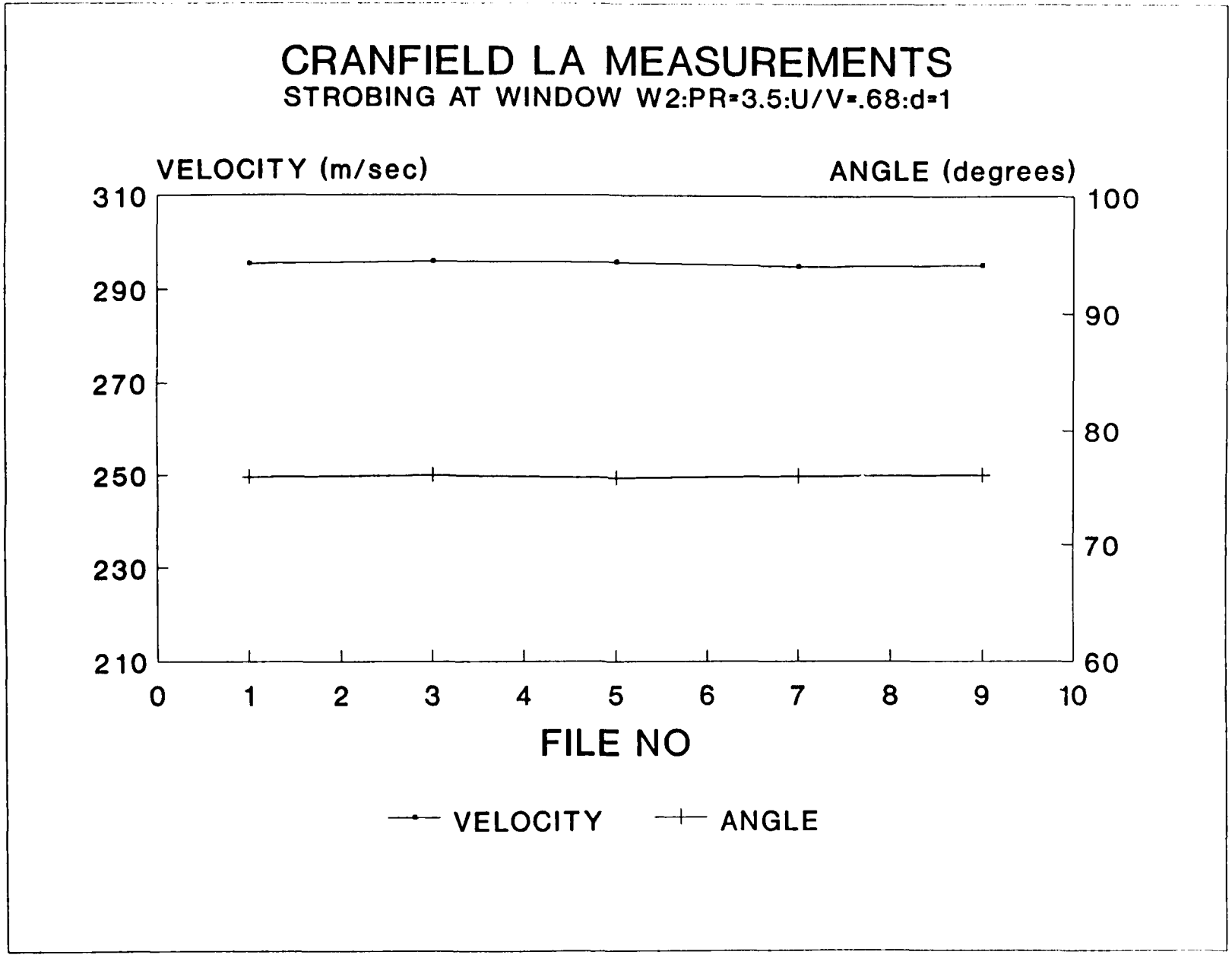

Fig 75 - Blade Strobed Results from between NGV and Rotor. (Window W2, PR=3.5, U/V=.68, d=1)

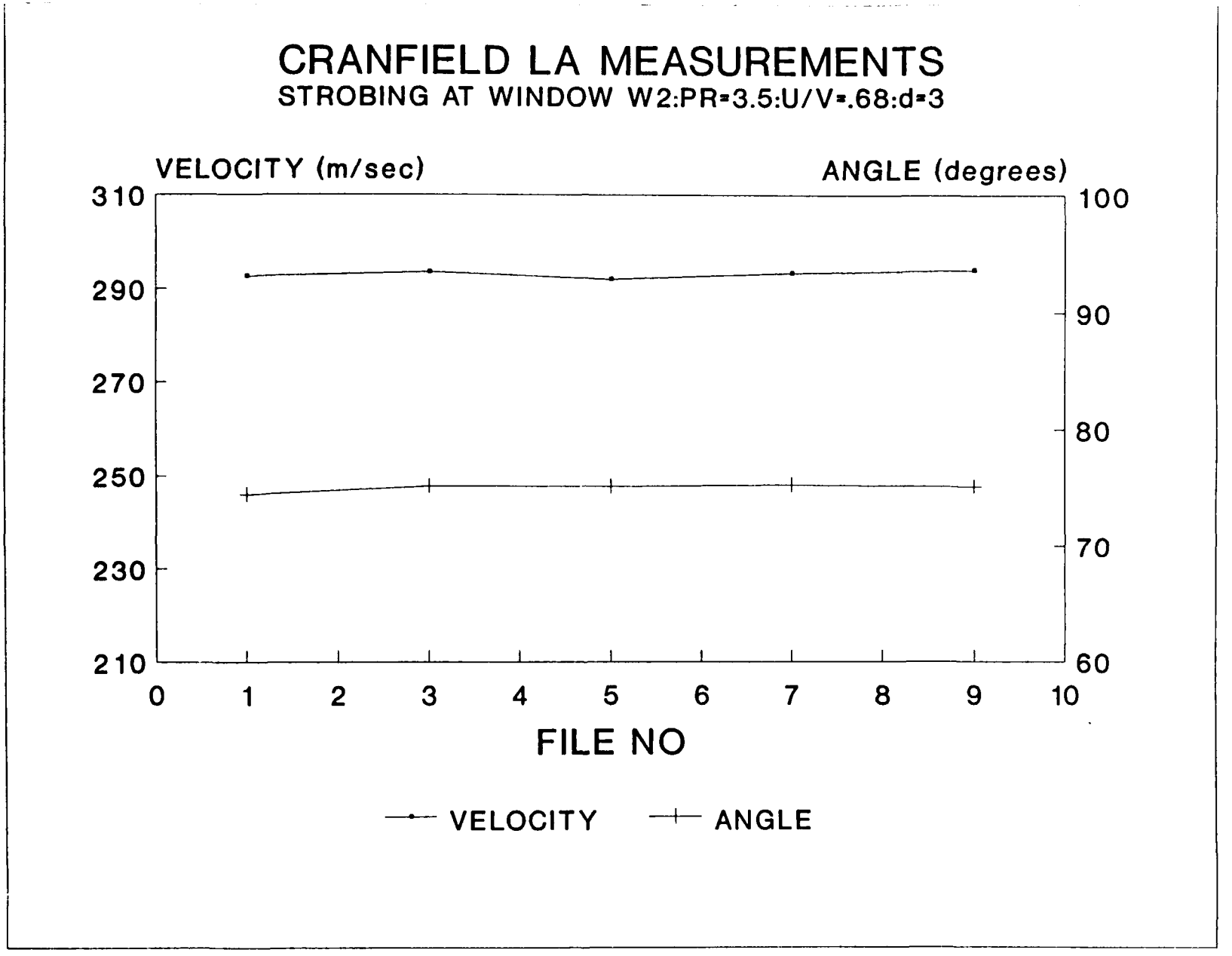

Fig 76 - Blade Strobed Results from between NGV and Rotor. (Window W2, PR=3.5, U/V=.68, d=3)

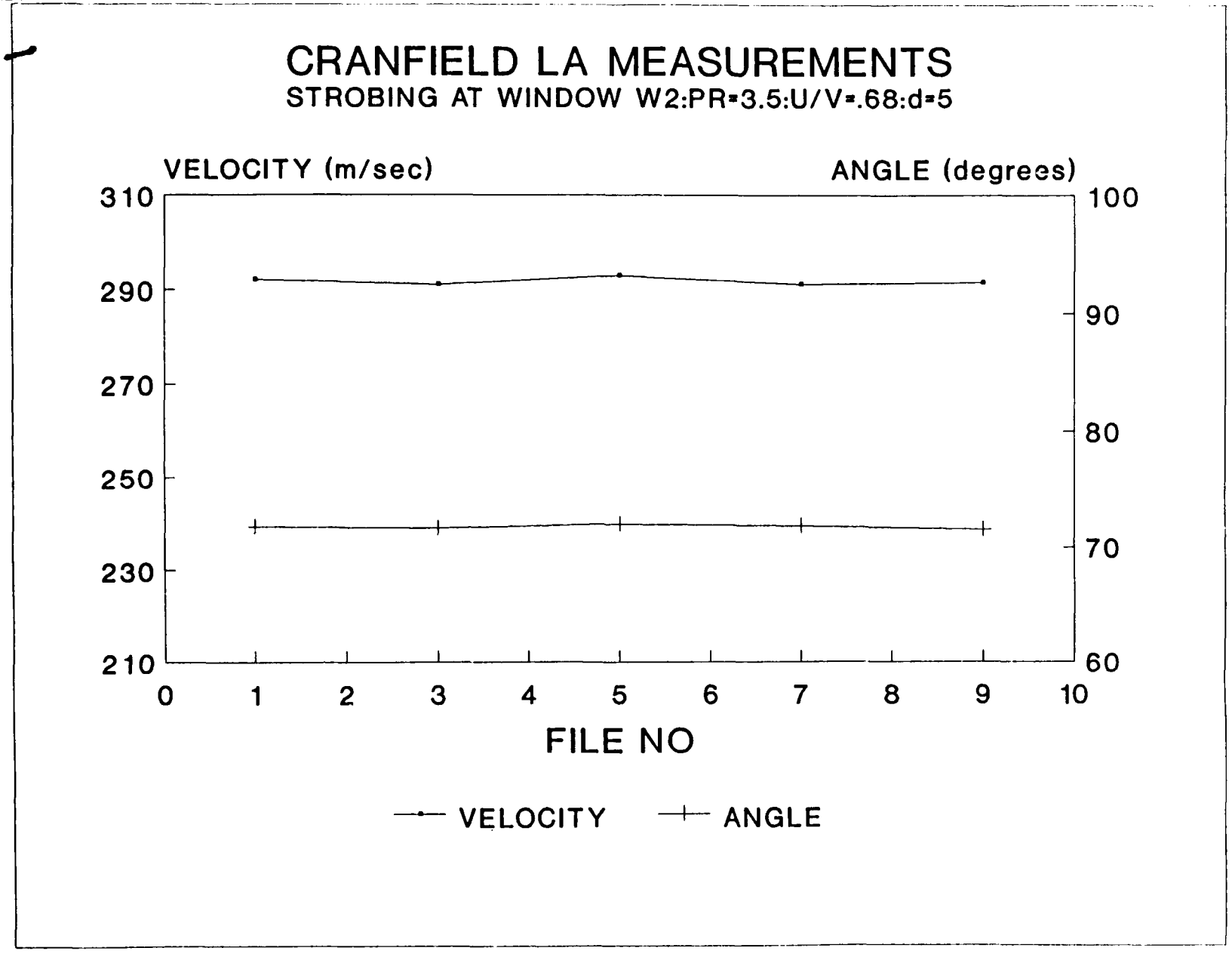

Fig 77 - Blade Strobed Results from between NGV and Rotor. (Window W2, PR=3.5, U/V=.68, d=5)

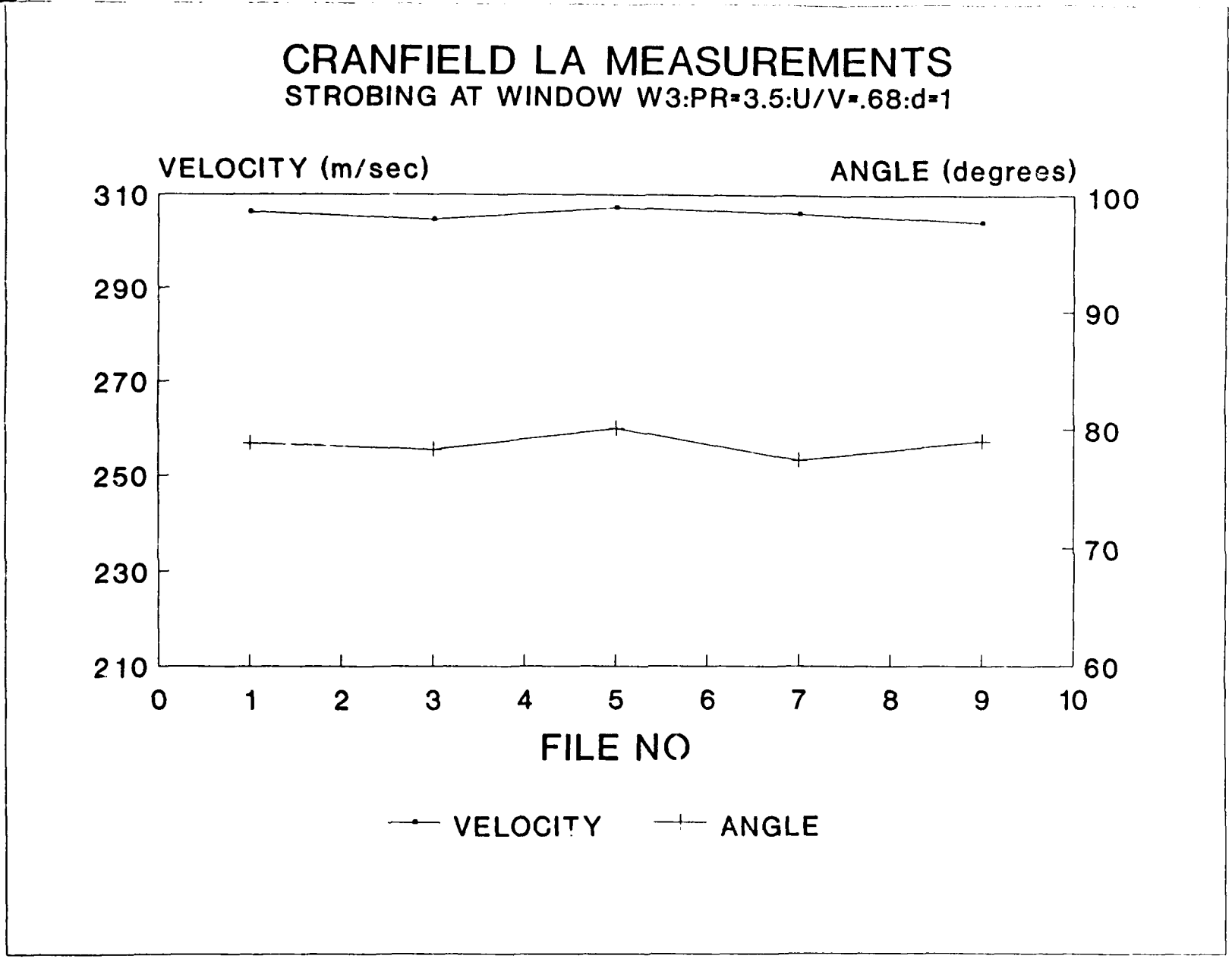

Fig 78 - Blade Strobed Results from between NGV and Rotor. (Window W3, PR=3.5, U/V=.68, d=1)

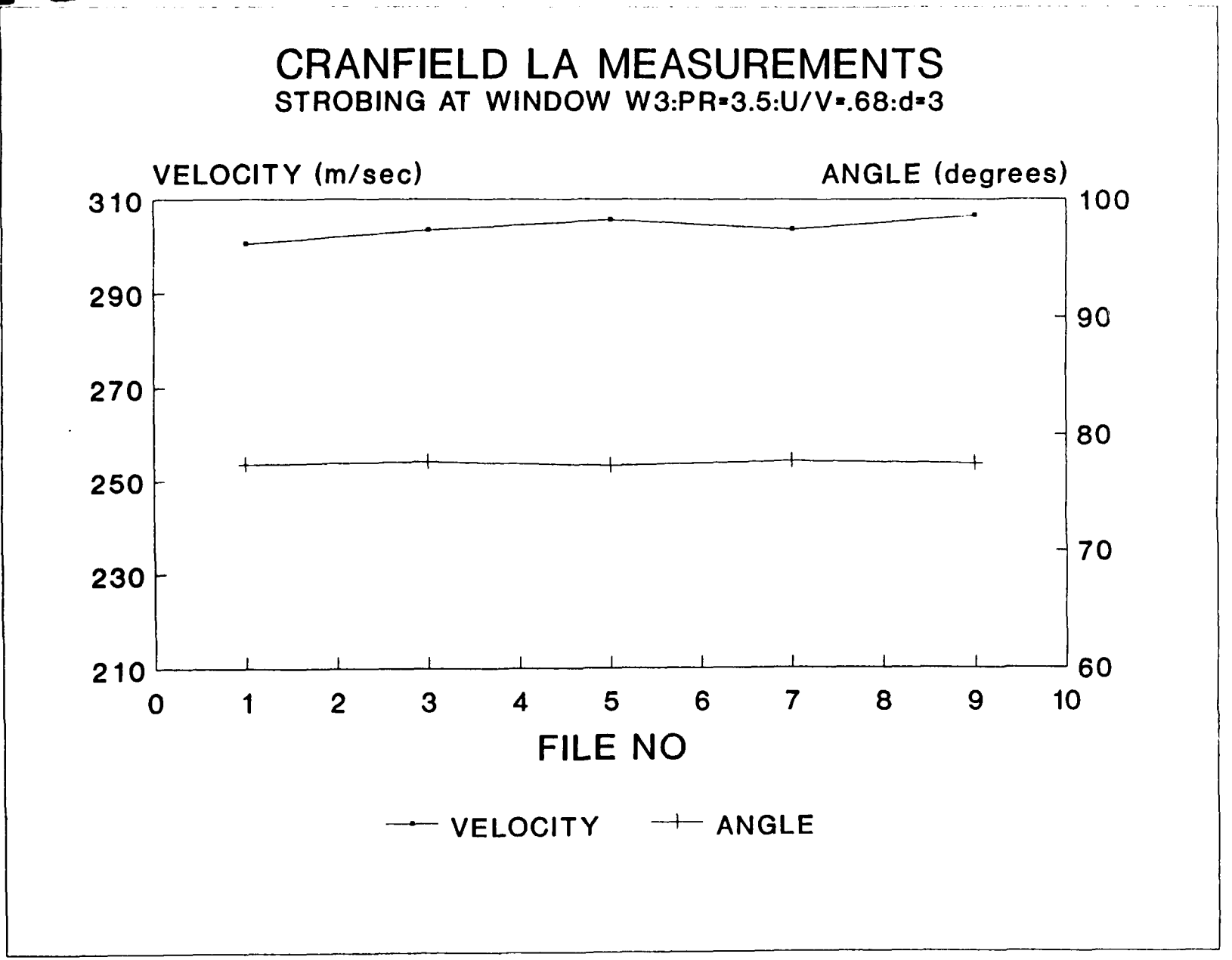

Fig 79 - Blade Strobed Results from between NGV and Rotor. (Window W3, PR=3.5, U/V=.68, d=3)

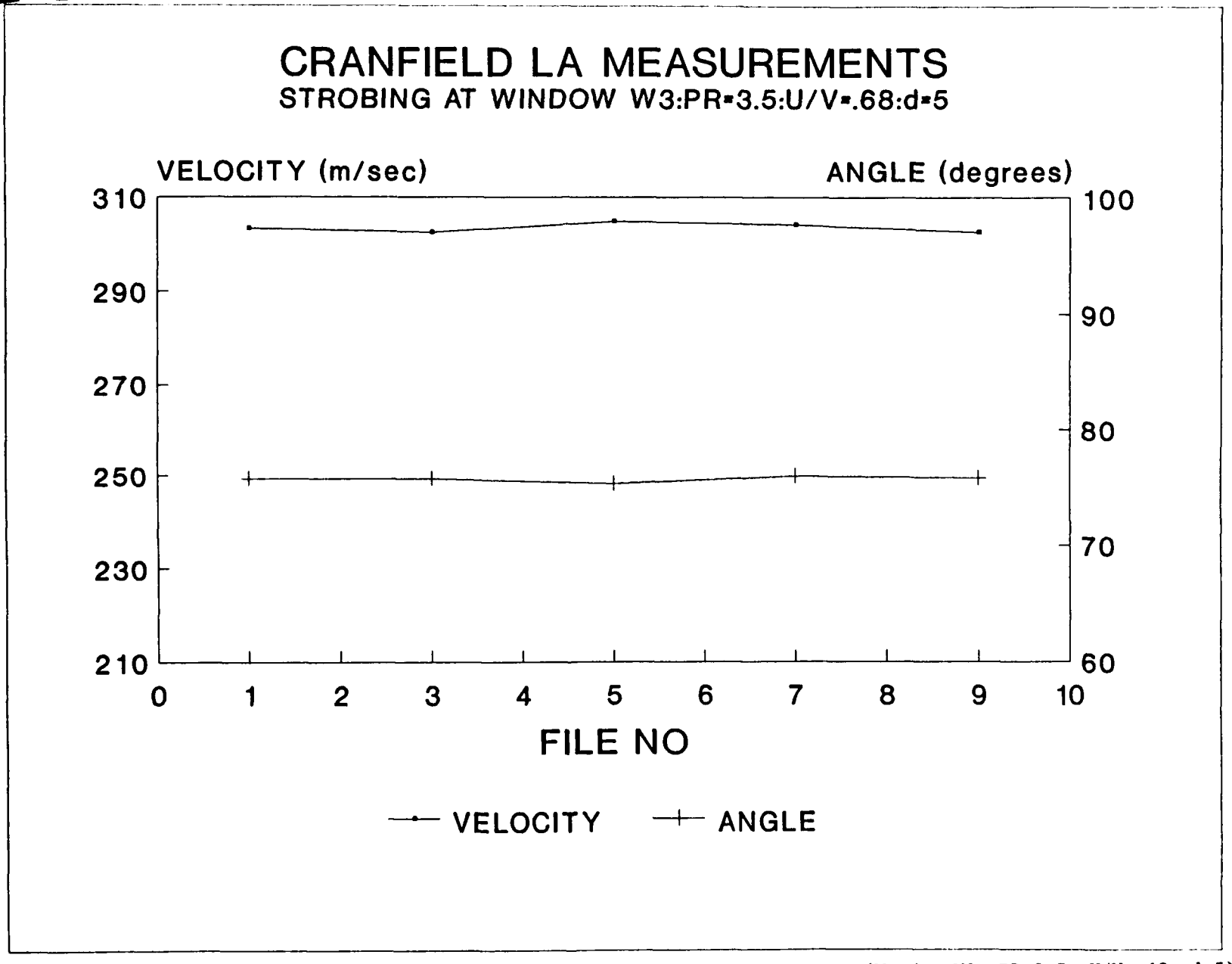

Fig 80 - Blade Strobed Results from between NGV and Rotor. (Window W3, PR=3.5, U/V=.68, d=5)

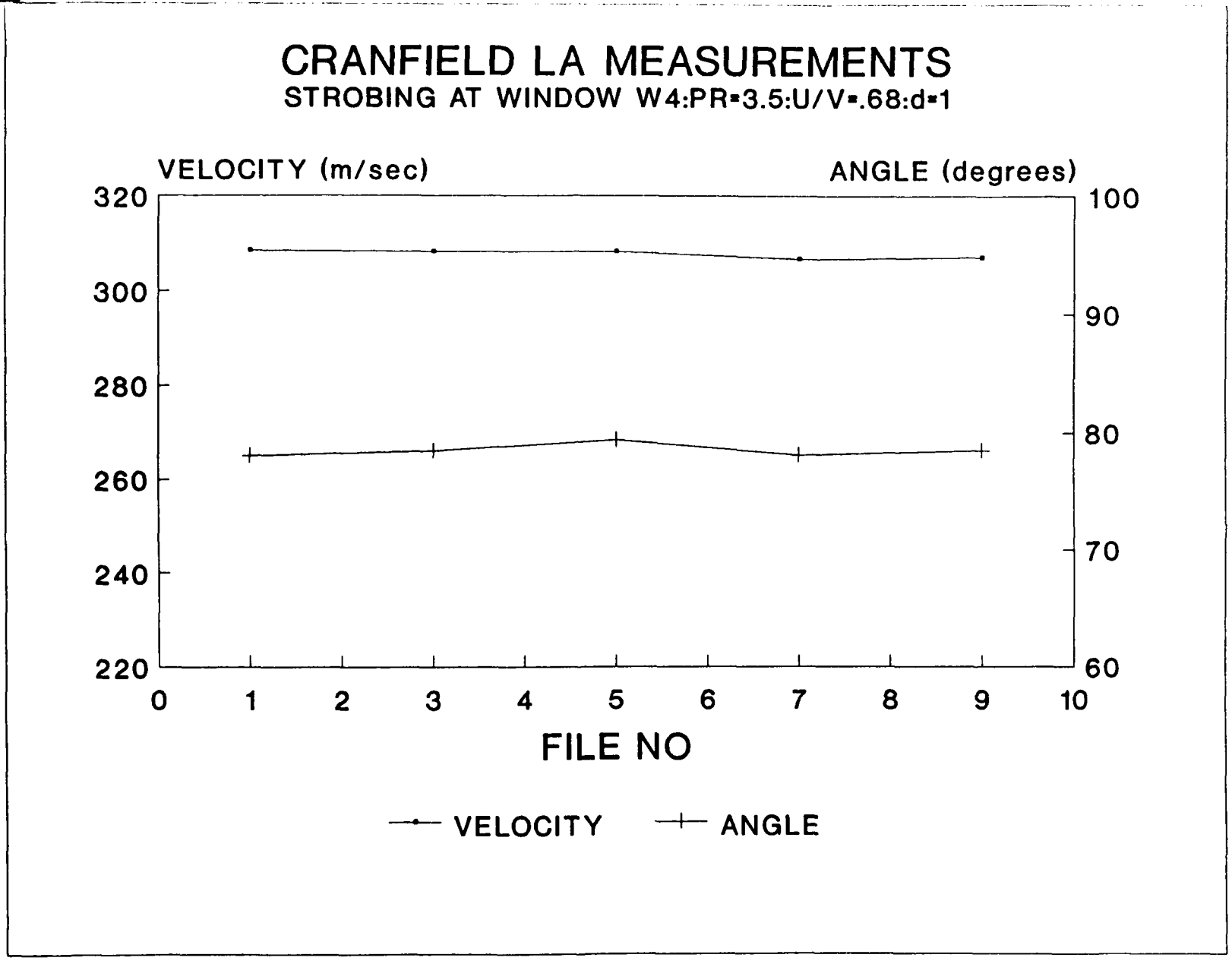

Fig 81 - Blade Strobed Results from between NGV and Rotor. (Window W4, PR=3.5, U/V=.68, d=1)

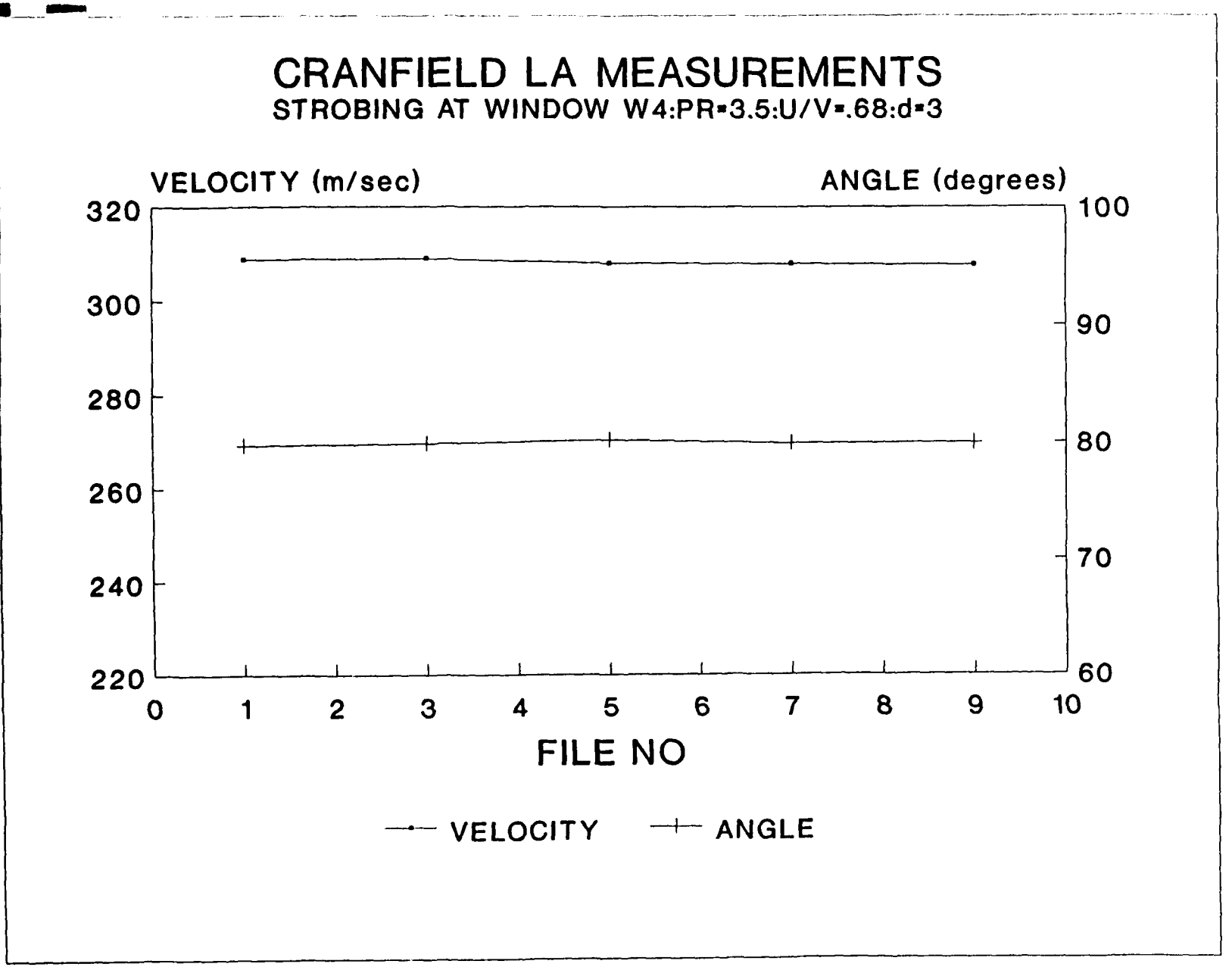

Fig 82 - Blade Strobed Results from between NGV and Rotor. (Window W4, PR=3.5, U/V=.68, d=3)

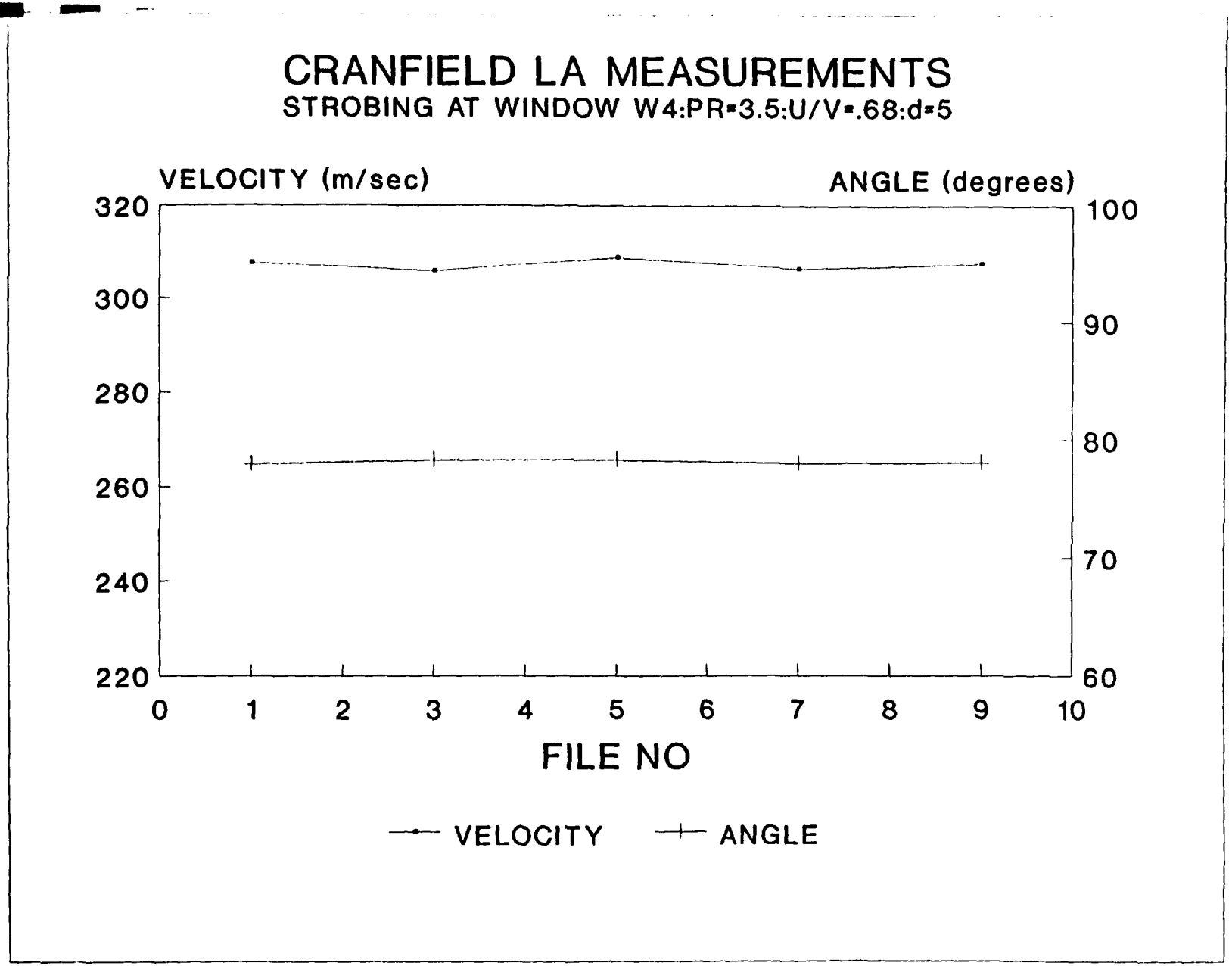

Fig 83 - Blade Strobed Results from between NGV and Rotor. (Window W4, PR=3.5, U/V= 68, d=5)

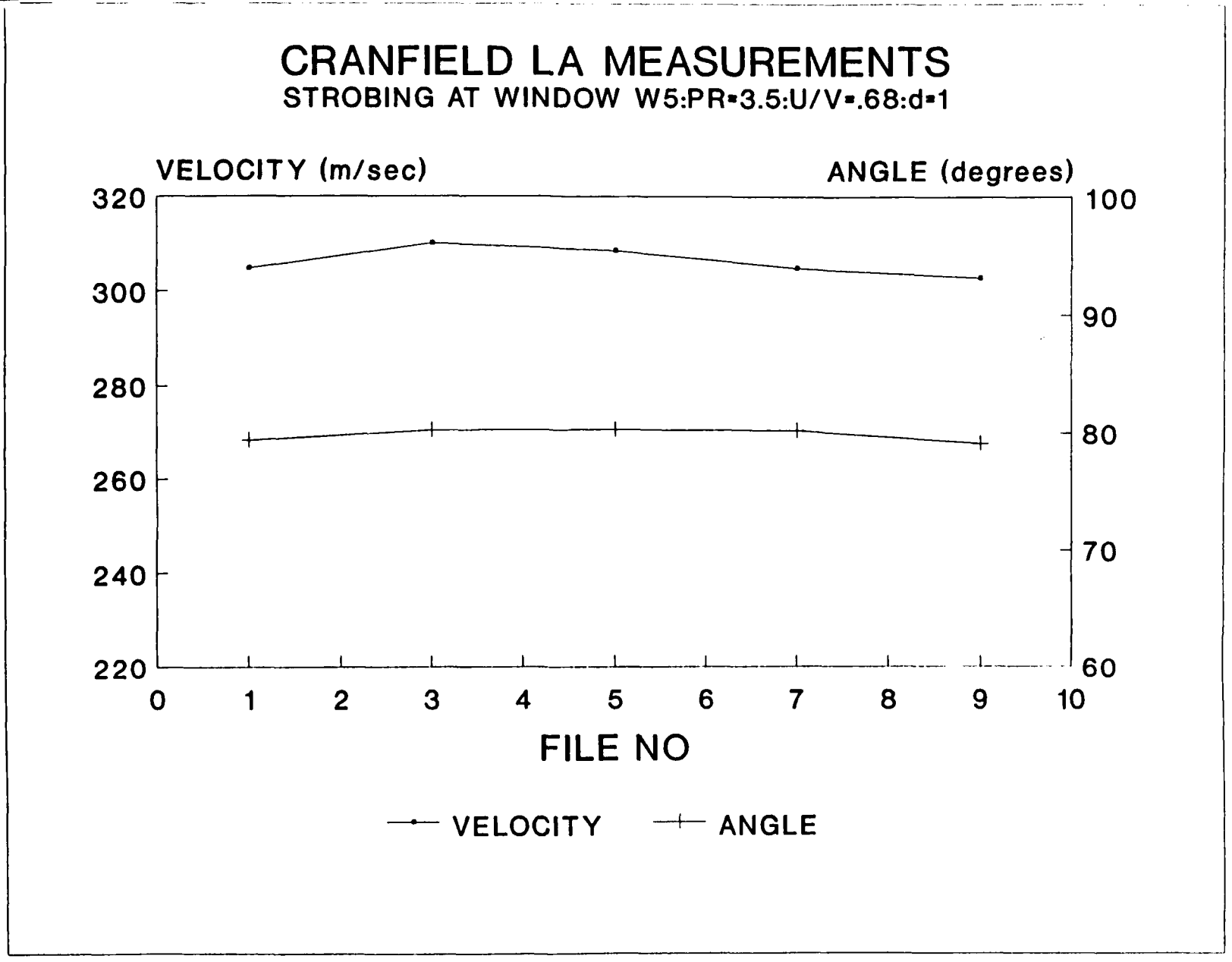

Fig 84 - Blade Strobed Results from between NGV and Rotor. (Window W5, PR=3, U/V=.68, d=1)

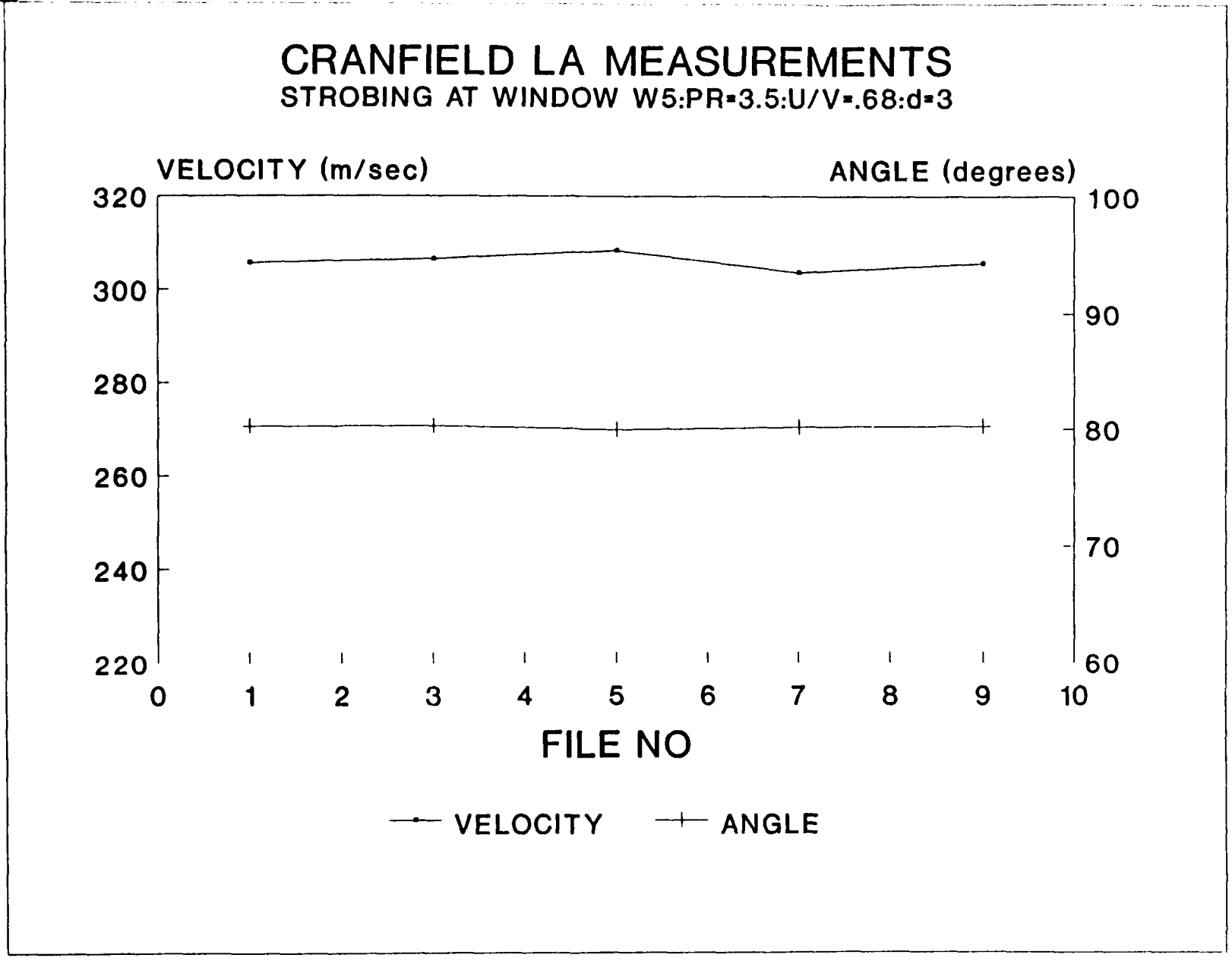

Fig 85 - Blade Strobed Results from between NGV and Rotor. (Window W5, PR=3, U/V=.68, d=3)

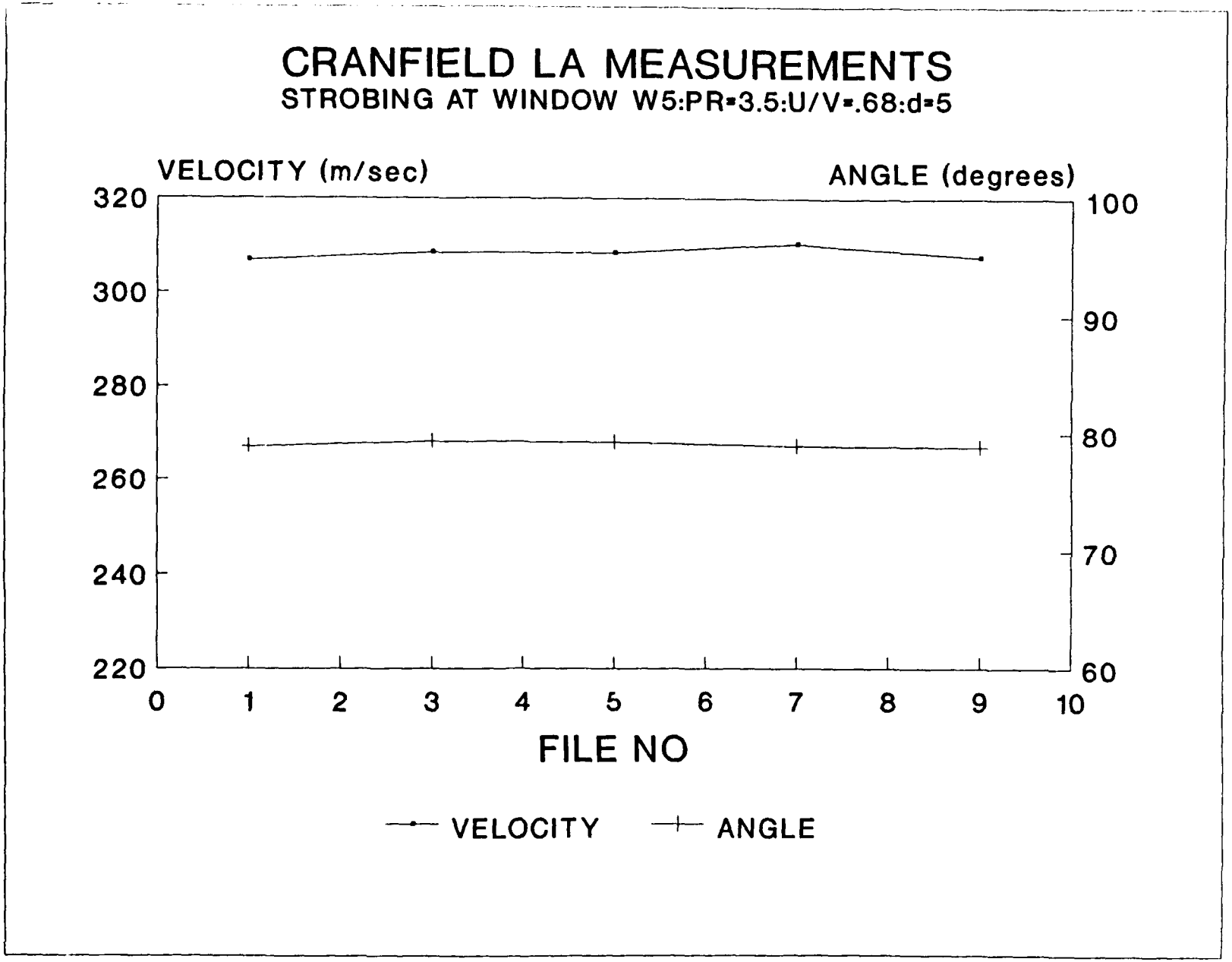

Fig 86 - Blade Strobed Results from between NGV and Rotor. (Window W5, PR=3, U/V=.68, d=5)

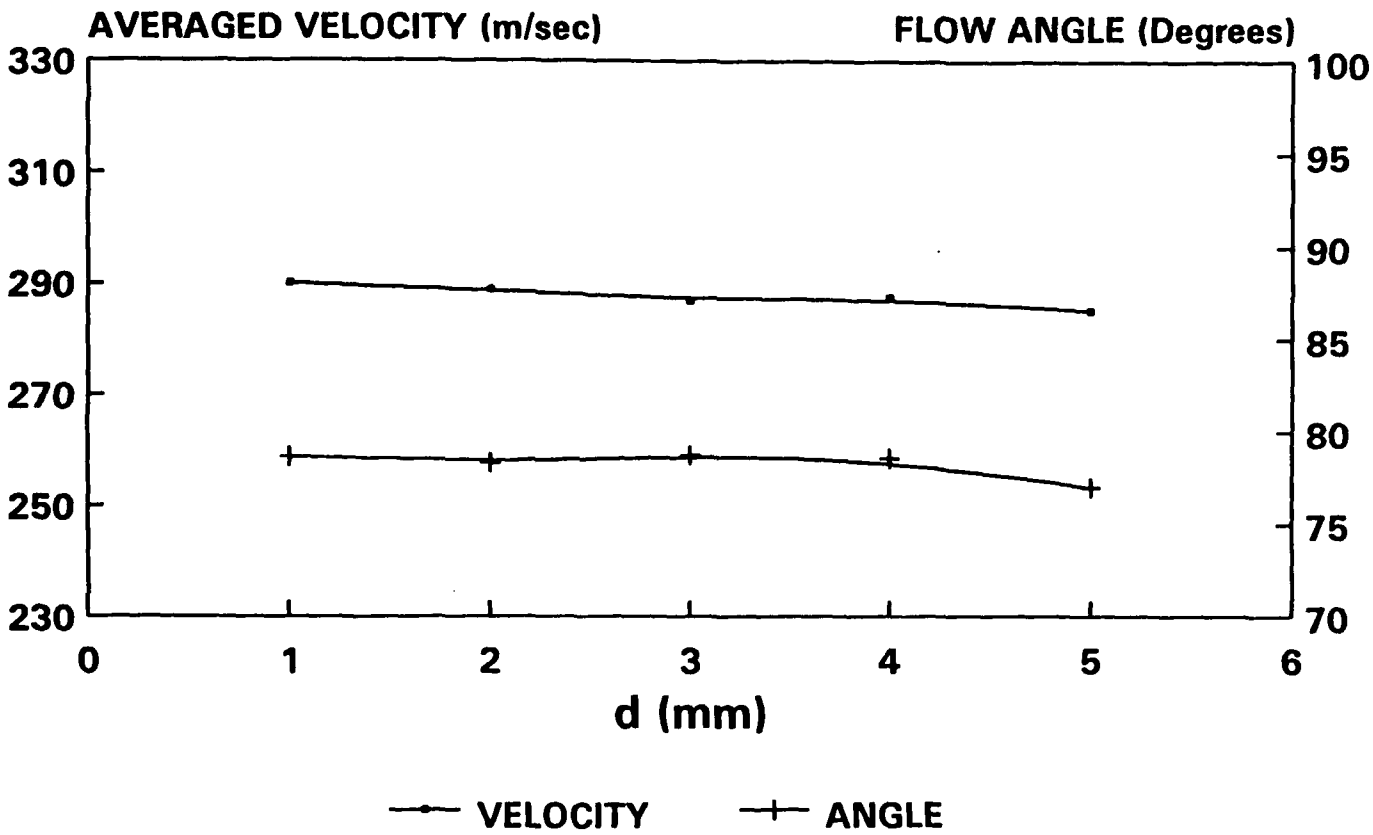

Fig 87 Pitchwise averaged results between NGV and Rotor (PR=3.0, U/V=0.64)

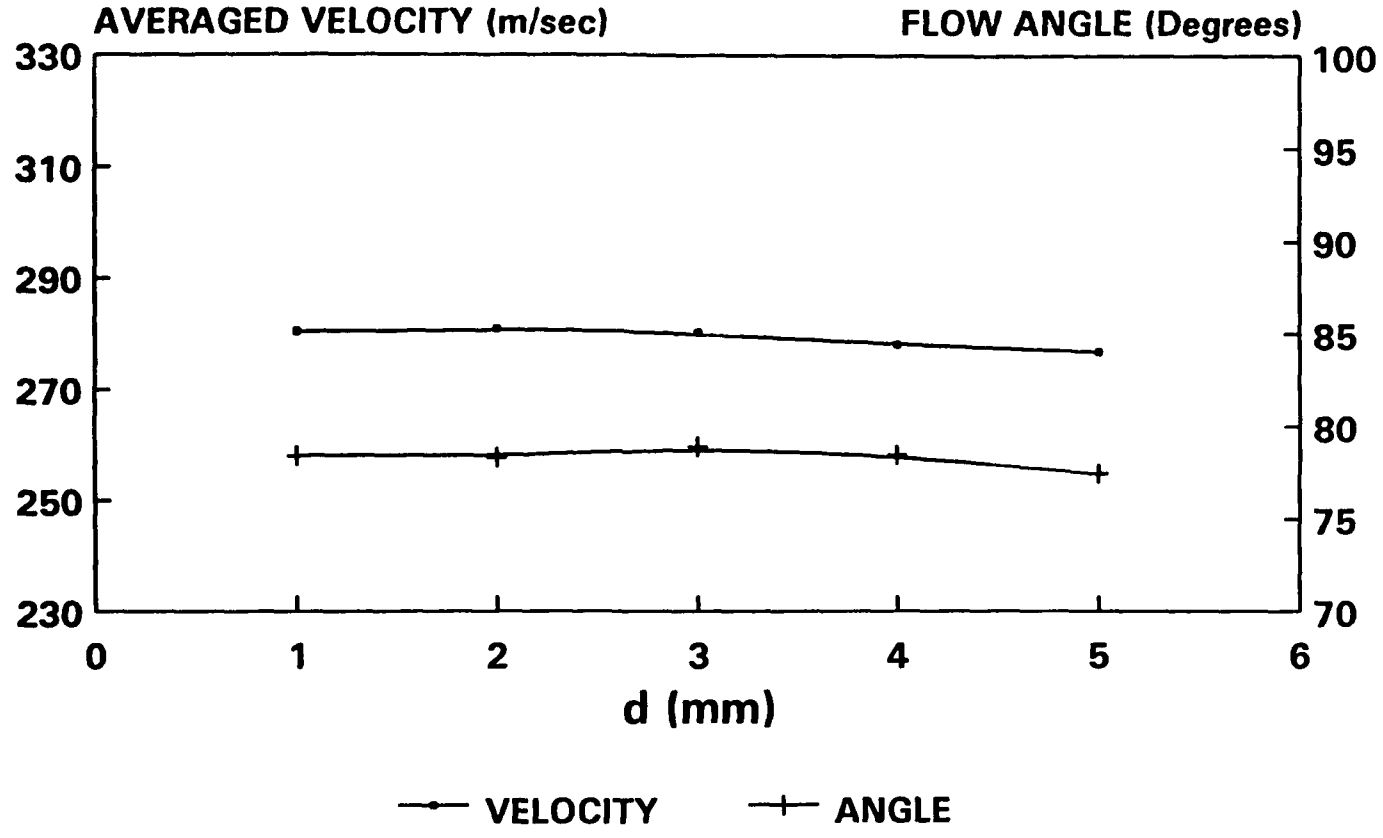

Fig 88 Pitchwise averaged results between NGV and Rotor (PR=3.0, U/V=0.68)

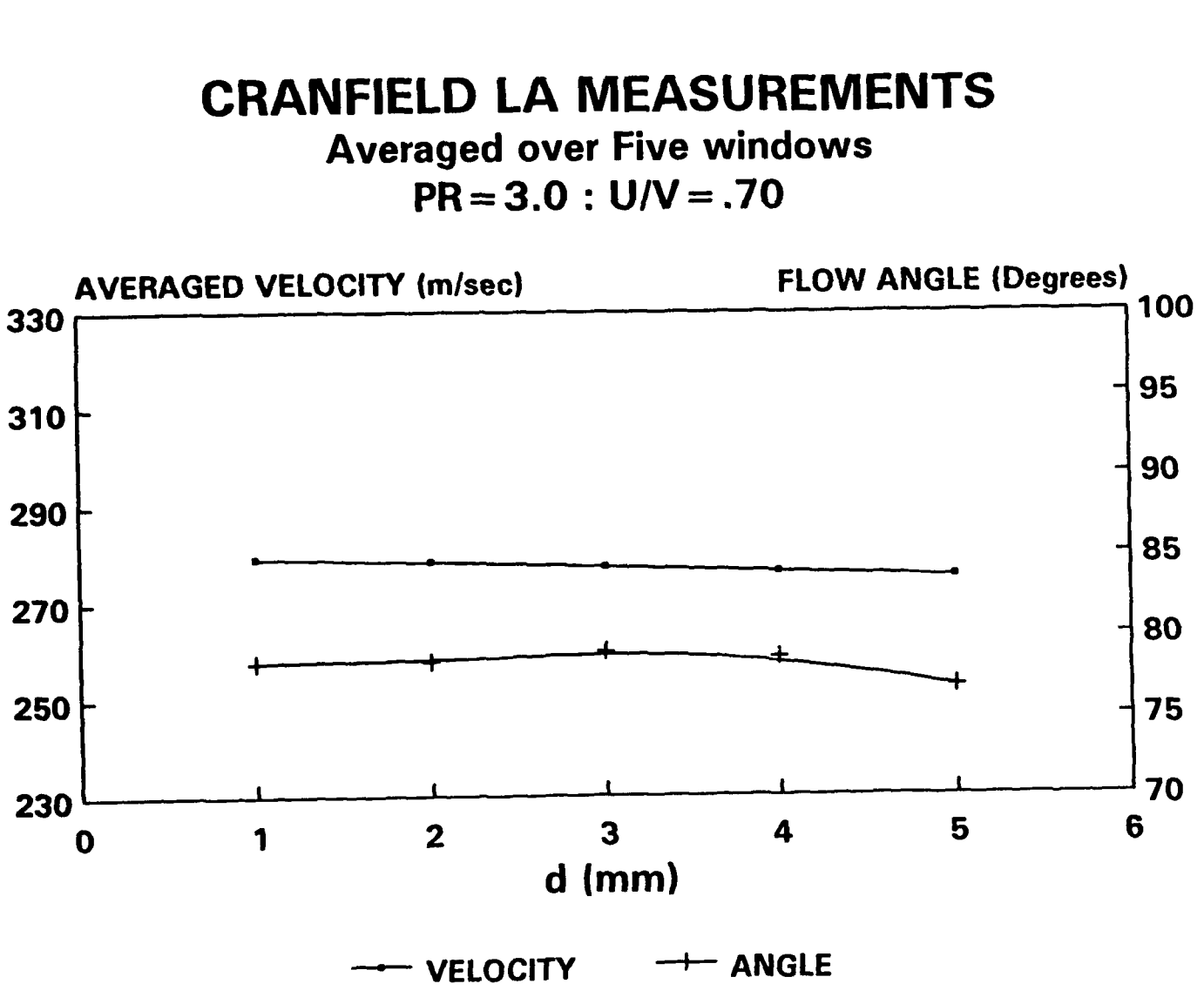

Fig 89 Pitchwise averaged results between NGV and Rotor (PR=3.0, U/V=0.70)

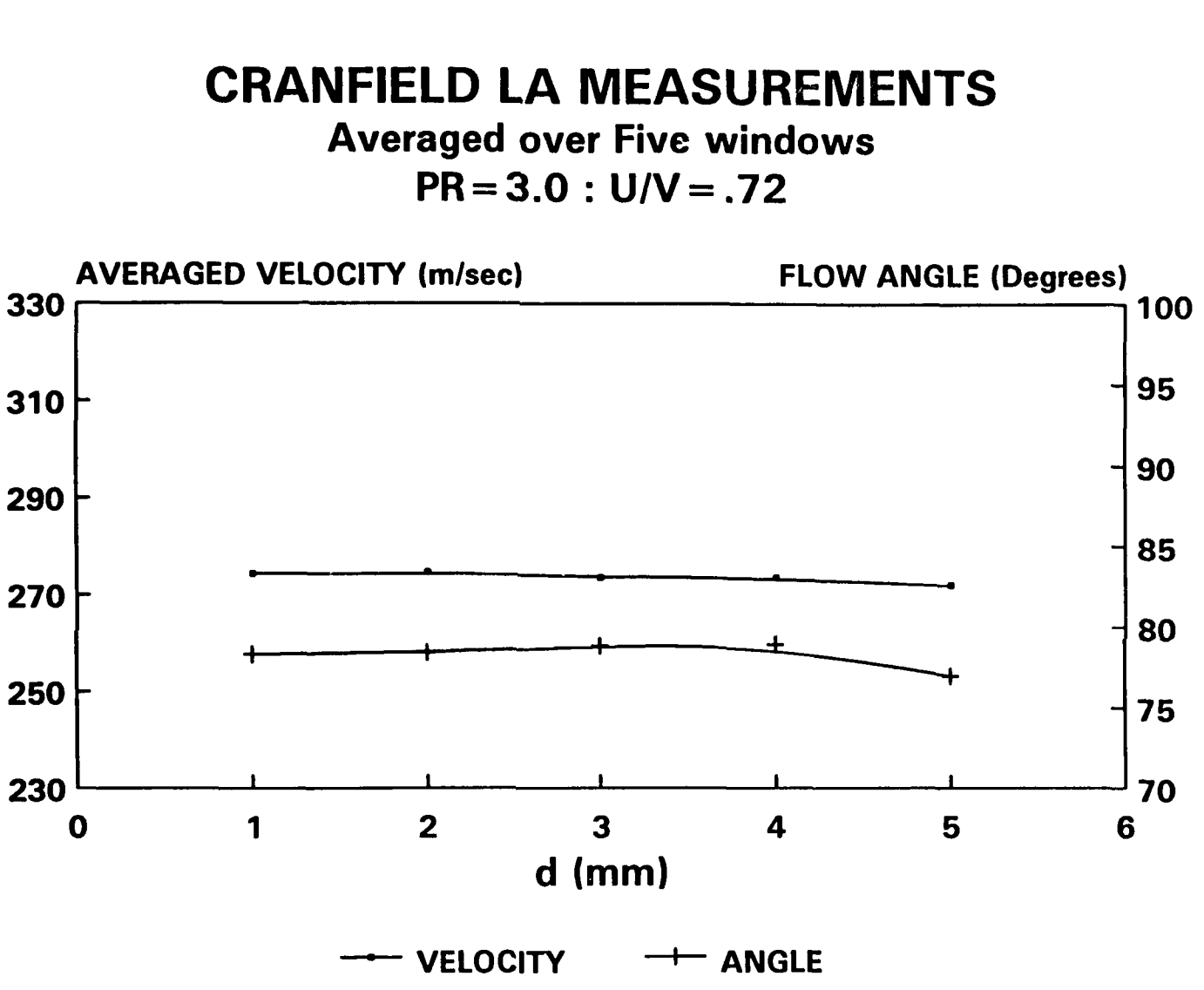

Fig 90 Pitchwise averaged results between NGV and Rotor (PR=3.0, U/V=0.72)

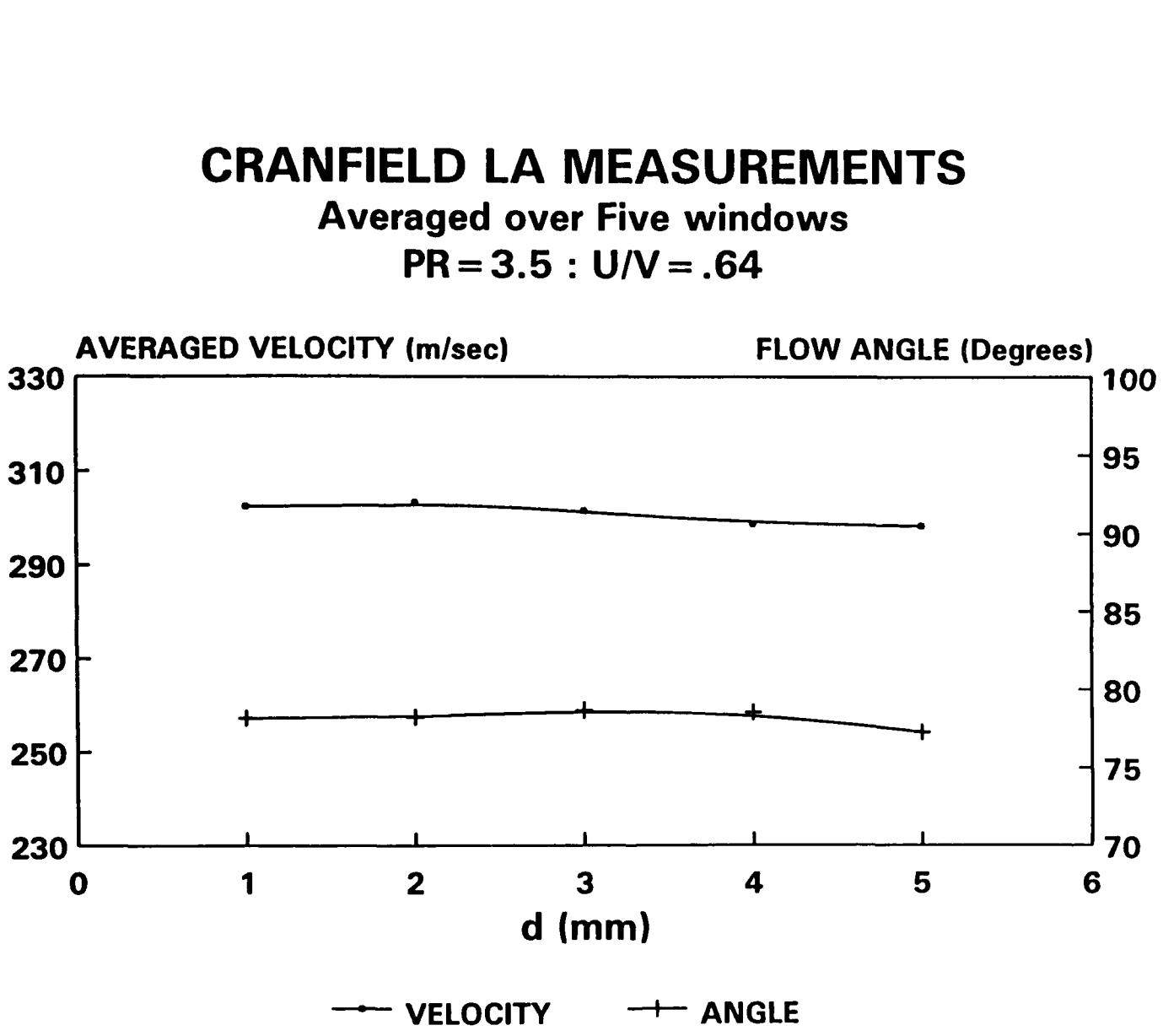

Fig 91 Pitchwise averaged results between NGV and Rotor (PR=3.5, U/V=0.6 4)

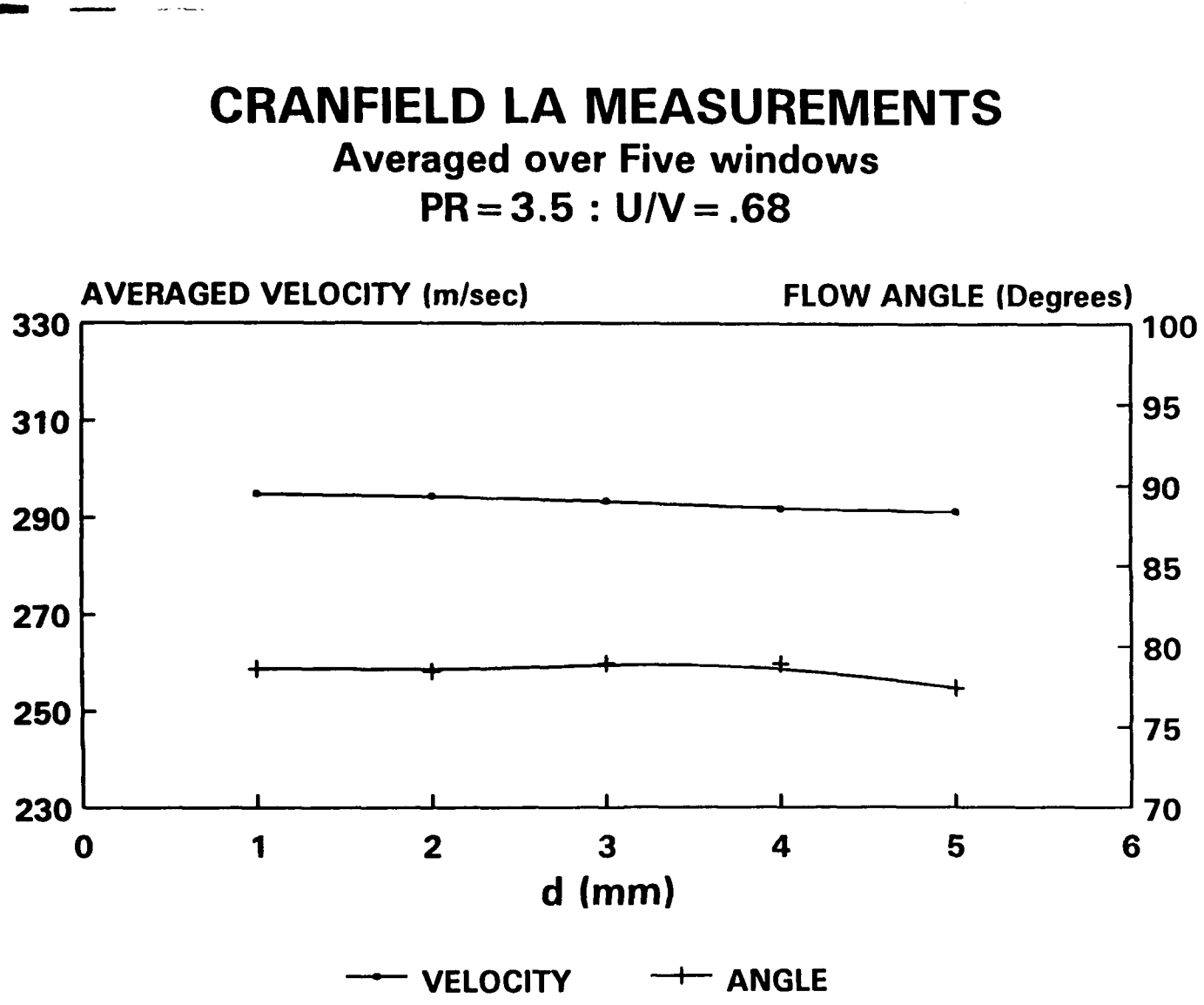

Fig 92 Pitchwise averaged results between NGV and Rotor (PR=3.5, U/V=0.68)

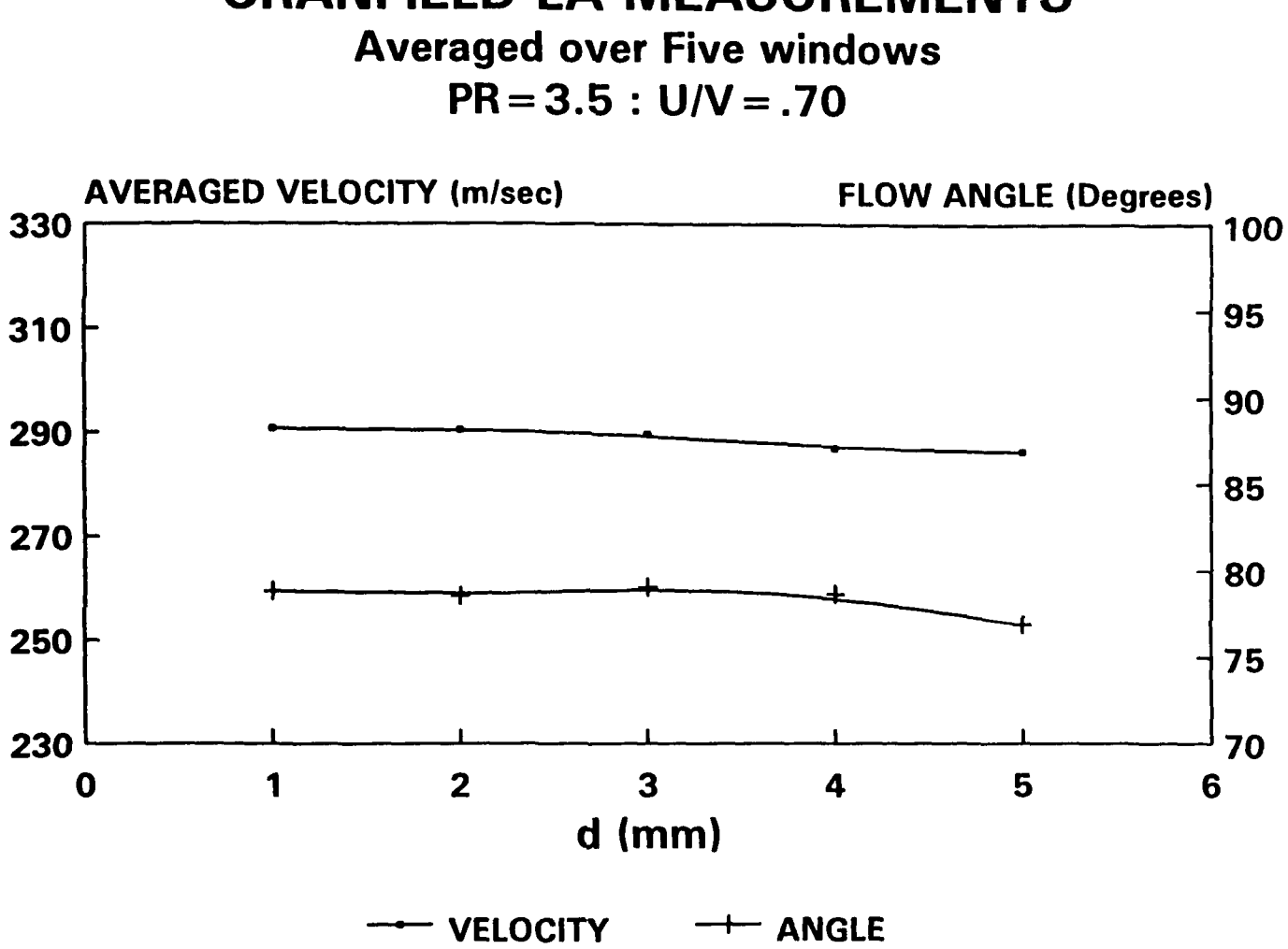

Fig 93 Pitchwise averaged results between NGV and Rotor (PR=3.5, U/V=0.70)

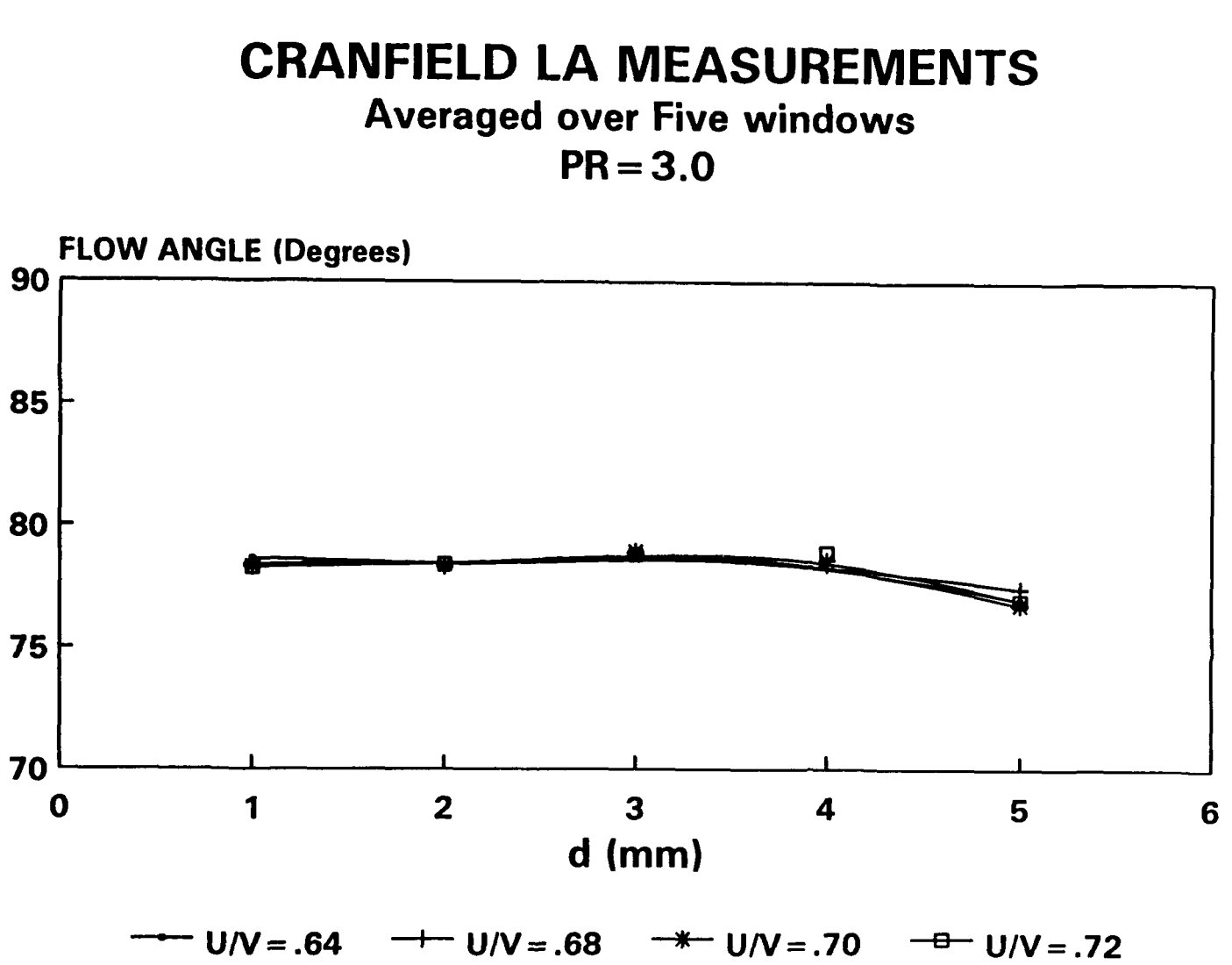

Fig 94 Pitchwise averaged results between NGV and Rotor for PR=3.0

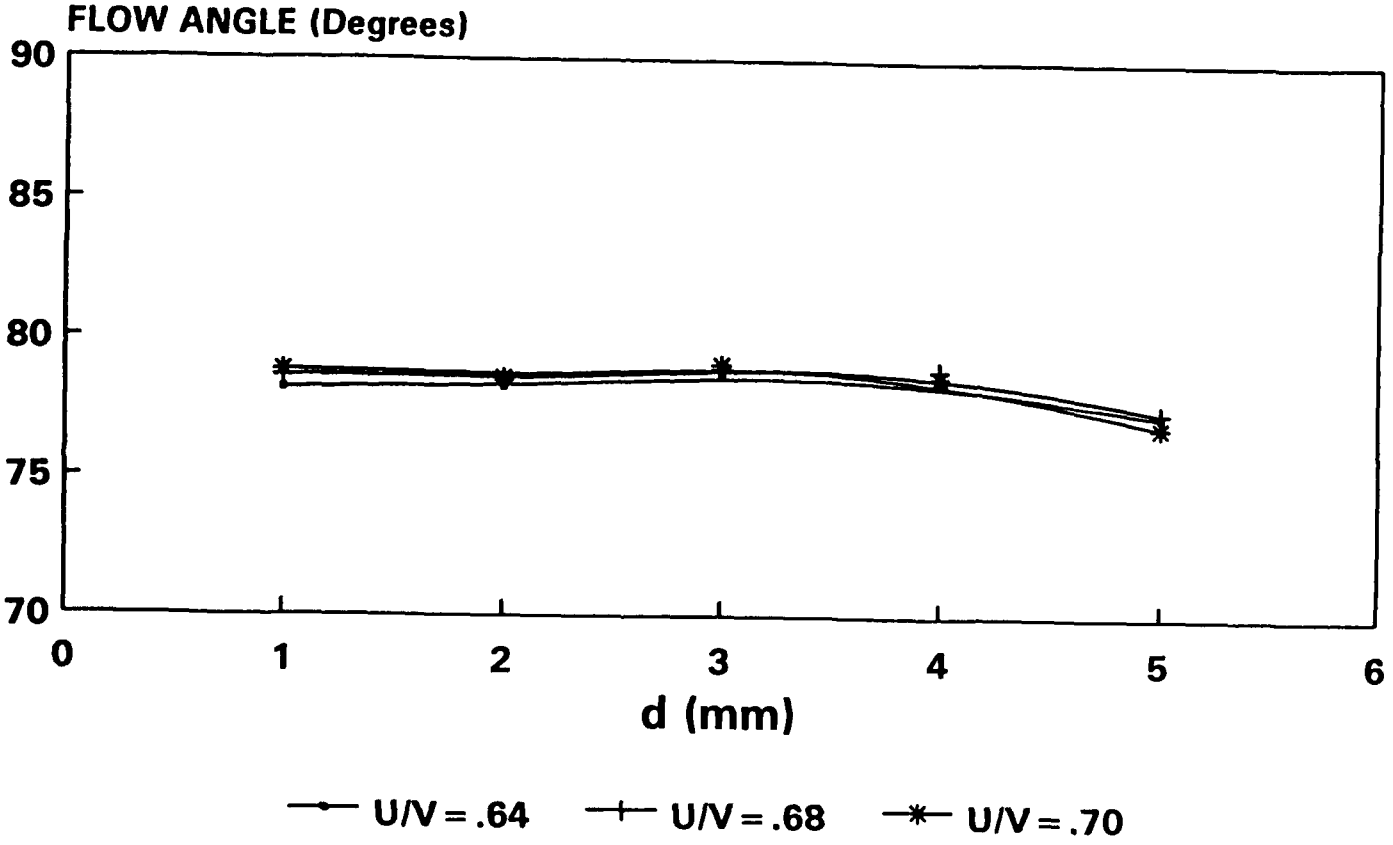

Fig 95 Pitchwise averaged results between NGV and Rotor for PR=3.5

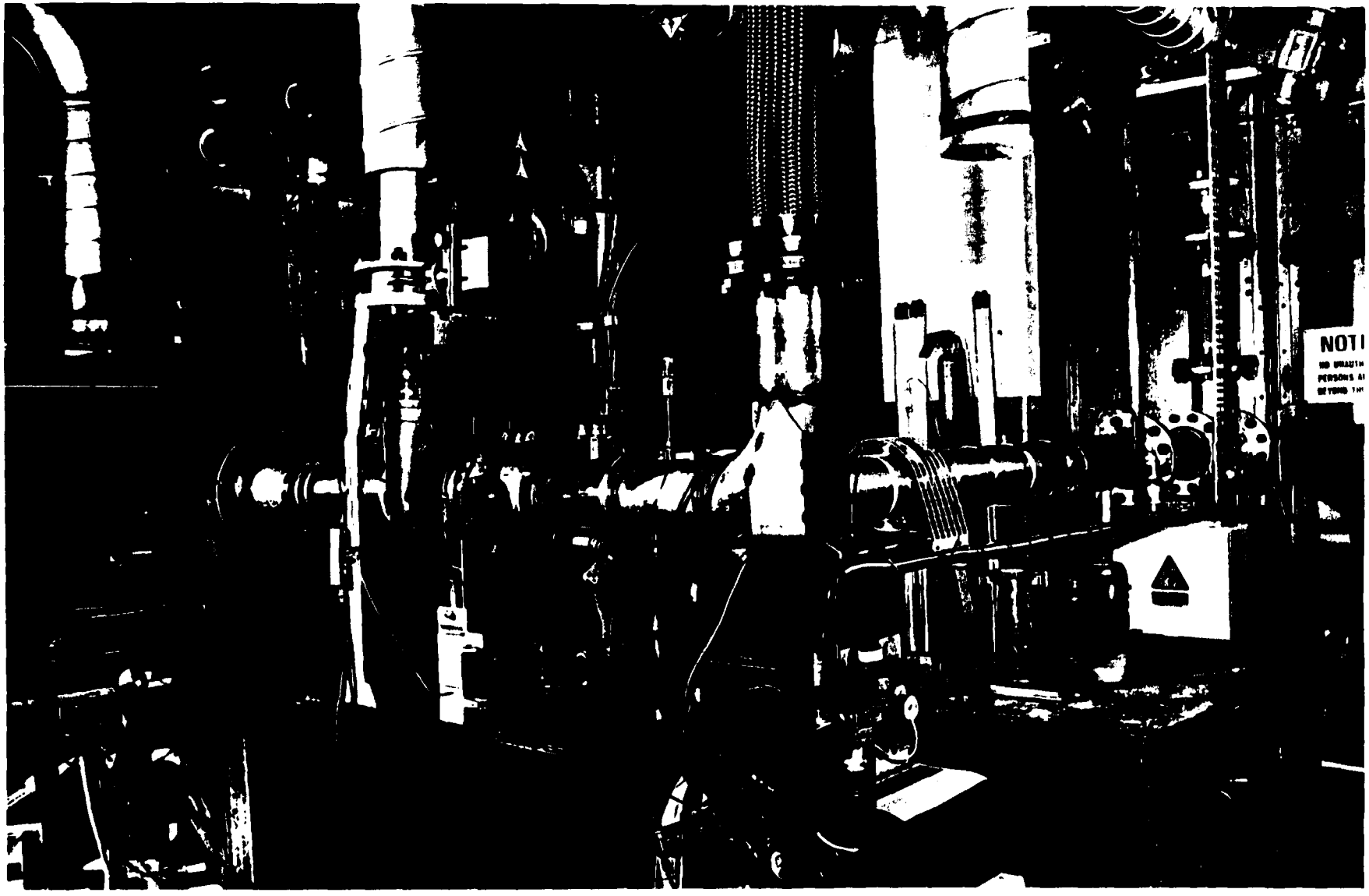

PLATE A - The Rig Assembly

PLATE B - The Cone Assembly

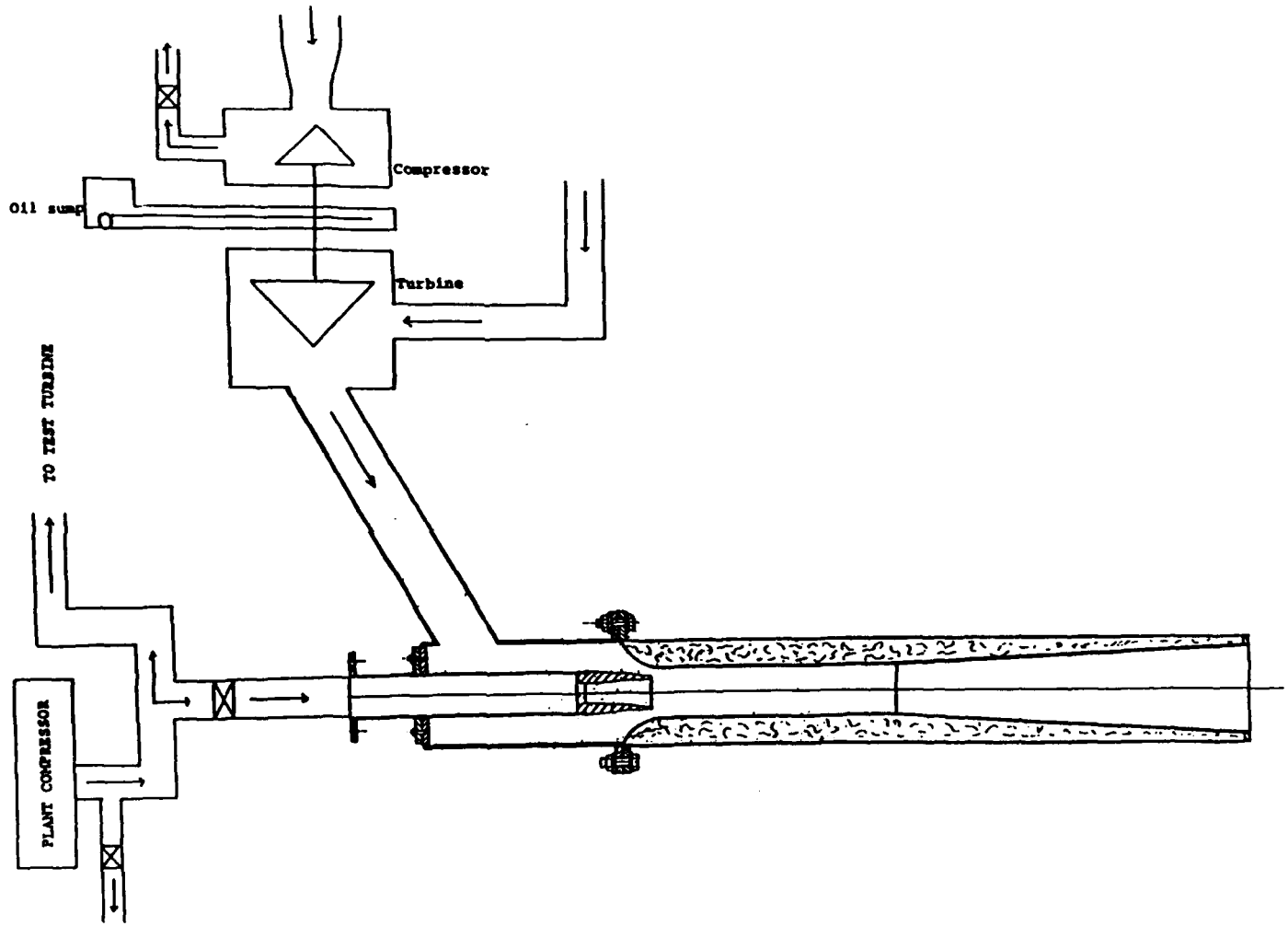

APPENDIX A : EJECTOR DESIGN ASSEMBLY

APPENDIX B

TURBOMACH TURBOCHARGER

INSTRUMENTATION AND PERFORMANCE CALCULATION USING TURBOMACH PROGRAM

1. MEASURED QUANTITIES

1.1	Atmospheric pressure	(in of Hg)
1.2	Venturitube upstream pressure	(psi)
1.3	Venturitube upstream temperature	(C°)
1.4	Venturitube differential	(in of Hg)
1.5	Turbine inlet temperature	(C°)
1.6	Turbine outlet temperature	(C°)
1.7	Turbine inlet total pressure	(psi)
1.8	Turbine outlet static pressure	(psi)
1.9	Belmouth depression	(mm of H_2O)
1.10	Speed	(rps)

2. NOMENCLATURE

P_1	Atmospheric pressure	(in of Hg)
P_2	Turbine inlet total pressure	(psi)
P_4	Turbine outlet static pressure	(psi)
P_3	Venturitube differential (h)	(in of Hg)
P_5	Venturitube upstream pressure	(psi)
T_1	Turbine inlet total temperature	(C°)
T_3	Turbine outlet total temperature	(C°)
T_5	Venturitube upstream temperature	(C°)
NA	Rotation speed	(rps)

3. DATA CONVERSION

$T_2 = T_1 - T_3$

$P_1 = P_1 * 0.491$ (psi)

$T_1 = T_1 + 273.15$ (A)

$T_3 = T_3 + 273.15$ (A)

$P_3 = P_3 * 13.6$ (in of H_2O)

4. CALCULATION OF Cp AND $(\gamma - 1) / \gamma$, (C,G)

$T = (T_1 + T_3) / 2$

$X = (T - 1125) / 875$

$C = ((((.0128 * X) - .007)*X - .0214)*X + .0371)*X + .278$

$G = 1.0 / 14.588 / C$

5. PERFORMANCE CALCULATION

5.1 VOLUME FLOW

FROM BS1042

$L = 359.1 * C_d * Z * d^2 * E * \sqrt{h} * \sqrt{W}$

where

L = Actual flow (lb/hr)

C_d = Coefficient of discharge = 0.986

Z = 1.0

$E = 1/\sqrt{(1.0 - m^2)}$

5.4 ROTATION SPEED

NA = Rotation speed (rps)

NC = Non dimensional speed (rps)

NC = NA / Sqrt (T_1 + 273.15)

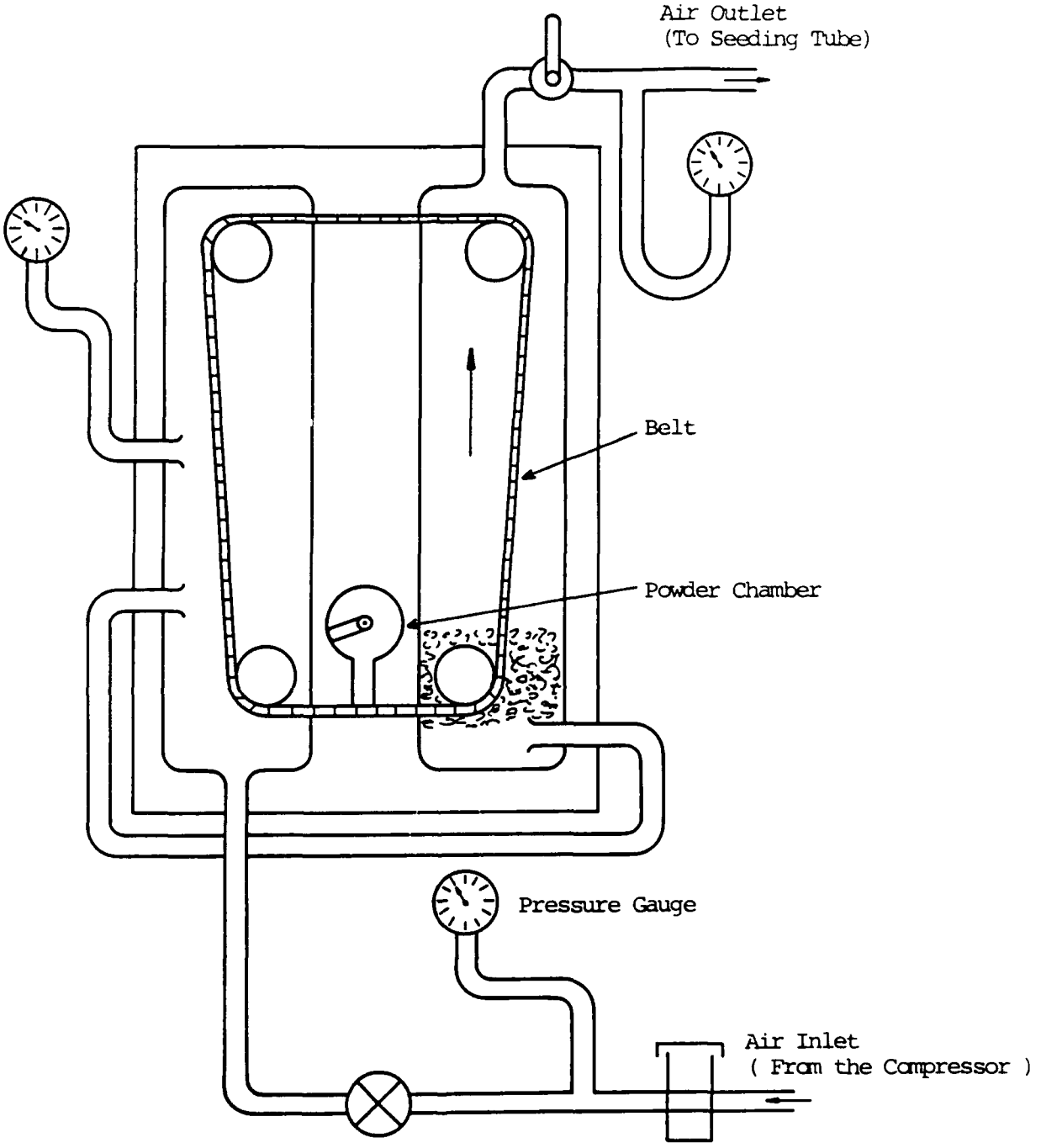

APPENDIX C : FLOW DIAGRAM FOR SOLID SEEDER